TECHNISCHE UNIVERSITÄT DARMSTADT

GEORG SPEYER HAUS
INSTITUT FÜR TUMORBIOLOGIE
UND EXPERIMENTELLE THERAPIE

Targeting FUBP1

in Hepatocellular Carcinoma

Vom Fachbereich Biologie der Technischen Universität Darmstadt

zur

Erlangung des akademischen Grades

eines Doctor rerum naturalium

genehmigte Dissertation von

M.Sc. Sabrina Khageh Hosseini, geb. Ploog

aus Hamburg

1. Referent/ Referentin: Prof. Dr. B. Süß

2. Referent/Referentin: Prof. Dr. M. Zörnig

3. Referent/Referentin: Prof. Dr. C. Cardoso

Tag der Einreichung: 01.07.14

Tag der mündlichen Prüfung: 12.09.14

Darmstadt 2014

D 17

Nothing is impossible, the word itself says “I’m possible” (Audrey Hepburn)

TABLE OF CONTENTS

Zusammenfassung

In unserem Labor wurden funktionelle „Yeast-survival-screens“ zur Identifikation neuer anti-apoptotischer Onkogene durchgeführt. Als Ausgangsmaterial der Identifikation dienten cDNA-Bibliotheken, welche aus Tumorgeweben hergestellt worden waren. Das „far upstream element binding protein 1“ (FUBP1) wurde im Laufe eines solchen Screens als anti-apoptotisches Onkoprotein detektiert.

Zu diesem Zeitpunkt war FUBP1 bereits als transkriptioneller Regulator des *c-myc*-Onkogens beschrieben. Die Tatsache, dass FUBP1 offensichtlich anti-apoptotische Eigenschaften aufweist, veranlasste uns dazu, immunhistochemische Expressionsanalysen von FUBP1 in verschiedenen Tumorgeweben durchzuführen. Anhand dieser Analyse konnte gezeigt werden, dass 83% (90 / 109) aller untersuchten hepatozellulären Karzinom (HCC)-Proben eine starke nukleäre Färbung für FUBP1 aufwiesen, während das Protein in gesunden Lebergeweben nicht nachzuweisen war. Des Weiteren konnte in *in vitro* Experimenten gezeigt werden, dass ein stabiler *FUBP1* knock-down in der humanen HCC-Zelllinie Hep3B eine deutlich verminderte Proliferation sowie die Sensitivierung der Zellen gegenüber apoptotischer Stimuli zur Folge hatte. In einem anschließenden Maus-Xenograft Transplantations-Experiment führte der stabile *FUBP1* knock-down in den verwendeten Hep3B Zellen zu einem deutlich verminderten Tumorwachstum im Vergleich zu den kontrollimplantierten Wildtyp-Zellen. Diese Daten etablierten FUBP1 als wichtiges, im HCC stark überexprimiertes Onkoprotein, welches das Tumorwachstum durch direkte und indirekte Inhibition von Zellzyklusinhibitoren und anti-apoptotischer Zielgene reguliert.

Auf Grundlage dieser Ergebnisse wurde die Hypothese aufgestellt, dass die Inhibition von FUBP1 im hepatozellularem Karzinom zu einem therapeutischen Nutzen für die Patienten führen könnte. Daher war die Identifikation und Validierung neuer FUBP1-inhibierender Substanzen das Ziel dieser Dissertation. Zu diesem Zweck wurde eine rekombinante Expression von FUBP1 in *E. coli* durchgeführt und das Protein über einen 3-stufigen Prozess aufgereinigt. Um die Funktionalität des rekombinanten Proteins nachzuweisen, wurden Bindungsstudien mit FUBP1 und dessen Ziel-DNA-Sequenz „*FUSEp21*“ mit Hilfe der sogenannten „surface plasmone resonance (SPR)“ Methode durchgeführt. Der durch dieses Experiment durchgeführte Nachweis einer spezifische Bindung ermöglichte es, das rekombinante Protein, sowie das *FUSEp21* Oligonukleotid

für weitere Experimente zu verwenden. Das Screening von 16.000 potentiell inhibitorischen Substanzen wurde mit Hilfe des AlphaScreen® Interaktions-Verdrängungsassays durchgeführt. Nach bioinformatischer Evaluation wurden solche Substanzen als „Hit“ bewertet, welche das Interaktionssignal von FUBP1 und *FUSEp21* zu mindestens 70% verminderten. Eine der gefunden Hit-Substanzen war Camptothecin (CPT), dessen inhibitorisches Potential in einem zweiten, unabhängigen SPR-Test bestätigt wurde, bevor weitere *in vitro*-Tests folgten. Die Behandlung unterschiedlicher HCC-Zelllinien (Hep3B, HuH7 und HepG2) mit CPT führte zu einer Sensitivierung gegenüber apoptotischen Stimuli. Besonders die Kombination von Camptothecin mit Mitomycin C bewirkte eine signifikante, synergistische Steigerung der Apoptoserate in Hep3B Zellen. Des Weiteren wurde eine reduzierte Zellexpansion sowie eine verminderte mitochondriale Aktivität in CPT-behandelten Hep3B Zellen nachgewiesen. Zudem hatte die Behandlung mit CPT in allen drei untersuchten HCC-Zelllinien eine signifikante Steigerung des *p21*-mRNA Levels zur Folge, welches ein bekanntes Zielgen von FUBP1 darstellt und dessen Expression von FUBP1 inhibiert wird.

Diese Daten legen nahe, dass CPT zusätzlich zu seinem bekannten anti-Tumor Wirkungsmechanismus, der Topoisomerase I Inhibition, auch mit der FUBP1 Funktion in HCC Zellen interferieren könnte. Um diesen Verdacht zu erhärten, wurden weitere Topoisomerase-I-Inhibitoren wie NSC 725776, NSC 724998 und das Camptothecinderivat 7-Ethyl-10-Hydroxycamptothecin auf eine mögliche FUBP1-Inhibition hin untersucht. Durch SPR-Messungen konnte gezeigt werden, dass alle getesteten Topoisomerase-I-Inhibitoren auch die Bindung von FUBP1 an *FUSEp21* inhibieren können. Des Weiteren zeigt die Behandlung verschiedener HCC Zelllinien die gleichen Effekte, die auch durch die Behandlung mit Camptothecin sichtbar wurden.

Insgesamt zeigen die *in vitro*-Experimente mit der FUBP1-Inhibition nicht nur eine bisher unbekannte Funktion der untersuchten Topoisomeraseinhibitoren, sondern auch deren pro-apoptotische Wirkung in verschiedenen HCC-Zelllinien nach Kombination mit unterschiedlichen Chemotherapeutika wie Mitomycin C.

Um die Wirkung von CPT auf einen etablierten Xenograft-Tumor untersuchen zu können der nach subkutaner Injektion einer humanen HCC-Zelllinie entstand, wurden Maus-Xenograft-Transplantations-Experimente mit dem CPT-Derivat Irinotecan durchgeführt. Alle mit Irinotecan und Irinotecan plus Mitomycin C behandelten Tiere zeigten eine 100%-ige Tumorremission.

Zusammenfassend unterstützen die Daten, die während dieser Dissertation erhoben wurden, die Annahme dass FUBP1 ein geeignetes Ziel in der HCC-Therapie darstellt. Des Weiteren konnte durch unterschiedliche zelluläre Experimente eine neue potentielle HCC-Therapie entwickelt werden, die im *in vivo* Mausmodell zu einer 100%-igen Tumorremission führte.

Als Weiterführung dieses Projektes wurde eine investigative Pilotstudie in zwei Patienten mit intermedian klassifiziertem HCC gestartet, die über eine transarterielle Chemoembolisation mit einer Kombination aus CPT und Mitomycin C behandelt werden.

Summary

In previous studies performed in our laboratory, *FUBP1* was isolated in a functional yeast survival screen of tumor-derived cDNA libraries for the identification of anti-apoptotic oncogenes. Because FUBP1, which had previously been described as a transcriptional regulator of the important proto-oncogene *c-myc*, at the same time protects cells from apoptosis, the expression of FUBP1 in tumors was analyzed by immunohistochemistry. A strong nuclear staining for *FUBP1* was found in 83% (90 / 109) of the analysed hepatocelluar carcinoma, whereas FUBP1 was not detected in normal liver cells. Furthermore, a stable knockdown of *FUBP1* in the HCC cell line Hep3B strongly reduced tumor growth in a xenograft transplantation mouse model, and we could show decreased proliferation and increased sensitivity to apoptosis for these cells *in vitro*. This data established FUBP1 as an important oncoprotein overexpressed in hepatocellular carcinoma, which induces tumor propagation by direct or indirect regulation of cell cycle inhibitors and pro-apoptotic target genes [1].

On the basis of these results, we hypothesize that the inhibition of FUBP1 may result in a therapeutic benefit for HCC patients. The goal of this thesis was to inhibit the function of FUBP1 as a transcriptional regulator by novel identified small molecule inhibitors.

For this purpose, I expressed and purified recombinant FUBP1 in *E. coli* and confirmed its functionality in surface plasmon resonance (SPR) binding studies. The protein was used for an AlphaScreen interaction-displacement assay to identify small molecules (including FDA-approved drugs) that were able to disrupt or prevent the binding of FUBP1 to its single stranded target sequence *FUSEp21*. After bioinformatical evaluation and a subsequent re-evaluation of the identified “hit-compounds” in a second binding-interference-assay (SPR), one of the identified inhibitors, camptothecin (CPT), was further tested for its therapeutic potential in *in vitro* (HCC cell lines) and *in vivo* (mouse xenograft transplantation experiments) preclinical studies

Upon treatment of the HCC cell line Hep3B with CPT, reduced cell expansion and cell viability were observed. Furthermore, treatment of Hep3B, HuH7 and HepG2 cells with CPT resulted in a sensitizing effect towards apoptotic stimuli, best seen in the combinatorial treatment of Hep3B cells with CPT and mitomycin C, which led to a significant, synergistic increase in cell death rates

To confirm the inhibitory effect of CPT on FUBP1 activity, the expression pattern of the FUBP1 target gene *p21* (repressed by FUBP1) was monitored using qRT-PCR. When treated with CPT, mRNA expression of the cell cycle inhibitor *p21* increased significantly, whereas FUBP1 protein level remained stable, suggesting that CPT in addition to its known function as a topoisiomerase I inhibitor indeed interferes with FUBP1 function in Hep3B, HuH7 and HepG2 cells.

Besides CPT, other topoisomerase I inhibitors like NSC 725776, NSC 724998 and CPT derivate 7-ethyl-10-hydroxycamptothecin (the active part of the clinically used irinotecan) were tested for their potential as FUBP1 inhibitors. In all experiments performed these substances showed similar results to CPT treatment, consolidating the effects of CPT on FUBP1 in HCC cells.

Finally, a xenograft transplantation experiment demonstrated that a combinatorial treatment of established HCC tumors with irinotecan and mitomycin C led to complete tumor remission in 100% of the treated mice.

Taken together, the data collected in this study does not only strengthen the role of FUBP1 as a potential therapeutic target in primary HCC, but also led to the evaluation of its novel potent inhibitor camptothecin. Moreover, the results of this thesis initiated a pilot study in patients with intermediate stage HCC using transarterial chemoembolization with a combination of CPT and mitomycin C.

1 Introduction

1.1 Far Upstream Element Binding Protein 1

The far upstream element binding protein 1 (FUBP1) was first identified as a regulator of the proto-oncogene *c-myc.* FUBP1 binds to the single stranded, non-coding DNA strand of the *far upstream element* (*FUSE*), which is located 1.5 kb upstream of the *c-myc* promotor. It was shown that the binding of FUBP1 to *FUSE* is required for maximal *c-myc* transcription upon interaction of FUBP1 with the TFIIH subunit of the transcriptional machinery [2]. Duncan et al. analyzed the primary FUBP1 amino acid sequence and the predicted secondary structure and confirmed that FUBP1 acts as a transcriptional activator of *c-myc* expression by binding to single stranded *FUSE* [3]. The FUBP1 interacting repressor FIR counteracts the binding of FUBP1 to *FUSE*. FIR can bind to both, FUBP1 and TFIIH, which leads to FUBP1 release and subsequent downregulation of TFIIH activity [4].

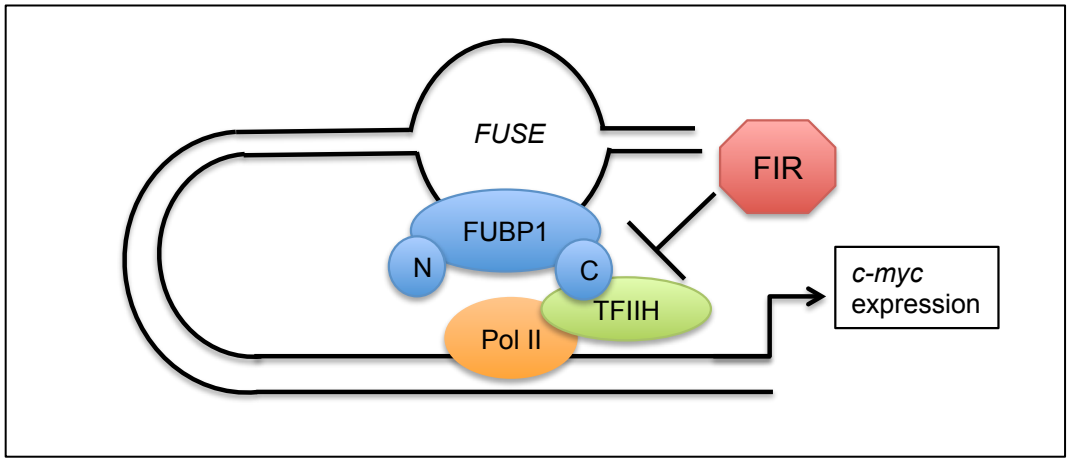

Figure 1: Generally accepted model of *c-myc* transcriptional peak activation via FUBP1. Upon basal *c-myc* transcription, torsional stress occurs due to DNA unwinding, leading to unwinding and melting of the *FUSE* double strand. FUBP1 can bind to both the unwinded anti-sense *FUSE* strand and the p89 subunit of TFIIH, causing a promoter loop formation and increased *c-myc* transcription. The subsequent FUBP1 inactivation is promoted by FIR, which binds as a homodimer to FUBP1, and eventually displaces FUBP1 from *FUSE*.

1.1.1 FUBP1 Structure

The human *FUBP1* gene encodes a 644-amino acid long protein, which consists of three domains: The N-terminal transcriptional repression domain, the central DNA binding domain, and the C-terminal transcriptional activation domain [3, 5].

The N-terminus is composed of the amino acids 1-106 and it represses the activity of the C-terminal domain. Therefore it has been suggested, that FUBP1 folds into an enclosed conformation in an inactive state and undergoes a conformational change upon activation of the protein [5].

The central domain, represented by amino acids 107-447, is composed of four K-homology (KH) motifs, each mediating ssDNA and ssRNA binding [3]. The KH-domains 1 to 3 are followed by an adjacent amphiphatic helix. KH3 and KH4 are sufficient for *FUSE* binding. To elucidate which bases of the *FUSE* motif were predominantly important for the binding of KH3 and KH4, 10-mer *FUSE* oligonucleotides were used to determine the bases responsible for the interaction with FUBP1. It could be shown, that the GXXG motifs in KH3 and KH4 domains bound to either the ss 5'-dTTTT (KH3) or 5'-dATTC (KH4) of the *FUSE* oligonucleotides, *in vitro* [6].

The C-terminal domain consists of amino acids 448-644 and inherits three tyrosine rich motifs (YM). These motifs were shown to be important for the physical interaction between the FUBP1 C-terminus and transcription factor TFIIH [4]. FUBP1 binding stimulates the 3'-5' helicase activity of the p89/XBP/ERCC3 subunit of the transcription factor TFIIH, which mediates *c-myc* promoter melting [7].

Additionally, FUBP1 itself possesses a 3'-5' helicase activity and is known as helicase V. Its helicase activity is probably mediated by the arginine-glycine-glycine (RGG) motifs at the C-terminus. These motifs are highly conserved among several proteins with helicase activities, e.g. nucleolin and the Ras-GAP SH3 binding protein [8]. The helicase activity of FUBP1 might play a role in the unwinding of the DNA duplex around *FUSE* to sustain *c-myc* activity [9].

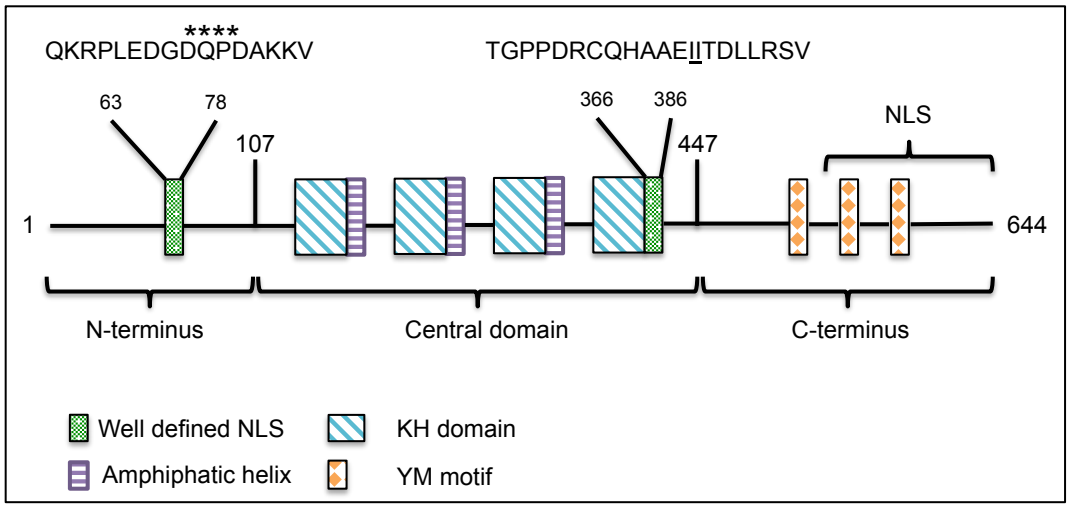

Figure 2: Schematic structure of human FUBP1 protein. Adapted from Zhang et al. 2013 [11]. FUBP1 consists of three domains: 1. The N-terminal repression domain (aa 1-106), 2. The central DNA binding domain (aa 107-447), and 3. The C-terminal activation domain (aa 448 -644). The well defined NLS, localized at the N-terminus, and the central domain are depicted in green. The two isoleucins at position 378 and 379 are important for the FUBP1 localization. The caspase cleavage site, DPQD [10], is labeled with asterisks.

1.1.2 FUBP1 Family Members

The *FUBP1* gene is highly conserved in eukaryotes, showing over 90% similarity among mammals [11]. Two FUBP1 homologs were found, upon screening of a human skeletal muscle library: FUBP2 (also known as KHSRP) and FUBP3 [12]. The *FUBP1* gene is located at chromosome 1p31.1, whereas *FUBP2* and *3* are located at 19p13.3 and 9q34.11, respectively [13].

Sequence homology and the common structural features such as the KH domains would suggest an analogous function of the family members. Nevertheless, FUBP1 is the only family member with confirmed helicase activity [9], and whereas FUBP1 is best known as a DNA binding protein, FUBP2 is better known for its RNA binding potential and has mostly been studied for its role in mRNA stability regulation (for review see [14]). FUBP3 is less well studied than the other two family members. Apart from its initial binding to *c-myc FUSE* before replacement by FUBP1 (for details see 1.1.3) it is assumed to cooperate with FUBP2 in RNA binding [15].

1.1.3 Transcriptional Regulation by FUBP1-FUSE-FIR

FUBP1 binds to single stranded *FUSE* sequence located on the non-coding DNA strand. A systematic evolution of binding partners by a SELEX assay indicated that FUBP1 interacts with *FUSE* with a low stringency. *In vitro* binding of 29-mers consisting of partial *FUSE* sequence to FUBP1-linked KH domains revealed the minimal DNA binding sequence required for full length FUBP1: TTGTa$(N)_{4/5}$ TYGTa$(N)_{4/5}$ TYGTa$(N)_{4/5}$ KTGY (Y=T or C, K= T or G). Every KH-domain recognizes the binding sequences with a weak preference for an “A” at the fifth position [7]. Binding of FUBP1 to *FUSE* is not sufficient for *c-myc* activation, but is needed to coordinate additional cis-elements and their corresponding transcription factors to promote optimal *c-myc* transcription [16].

FUBP1 binds to *FUSE* DNA and at the same time to the basal transcription factor TFIIH, causing a promoter loop. Furthermore, FUBP1 and TFIIH not only interact with each other, but also with the FUBP1 Interacting Repressor (FIR) [16]. FIR is a 542 amino-acid long protein, with two RNA recognition motifs in the central domain [4, 16] and a U2AF (splicing factor; U2 auxiliary factor) homology motif at the c-terminus (UHM) [17]. The UHM mediates protein-protein interactions. FIR binds as a homo-dimer to *FUSE* via its UHM at the C-terminus and its two RNA recognition motifs [17]. This interaction might in turn be responsible for the interaction between the N-terminal part of FIR and TFIIH, which eventually leads to the inhibition of TFIIH activity [4, 16].

In 2008, Levens et al. suggested the following model for the *c-myc* peak transcription involving FUBP1. First, upon basal *c-myc* expression via RNA polymerase II, *FUSE* becomes exposed due to chromatin remodeling and melts because of torsional stress. Afterwards, FUBP1 and FUBP3 recognize the single-stranded *FUSE* motif and bind to it. Initially, FUBP3 interacts with *FUSE*, but is replaced by FUBP1 by an unknown mechanism. Subsequently, *FUSE*-bound FUBP1 interacts with TFIIH and stimulates its helicase activity. Due to the interactions between *FUSE*, FUBP1 and TFIIH, the genomic DNA is bending and forms a promoter loop, which allows for maximal *c-myc* transcription. Finally, FIR displaces FUBP1 from *FUSE*, thereby downregulating *c-myc* expression again [18].

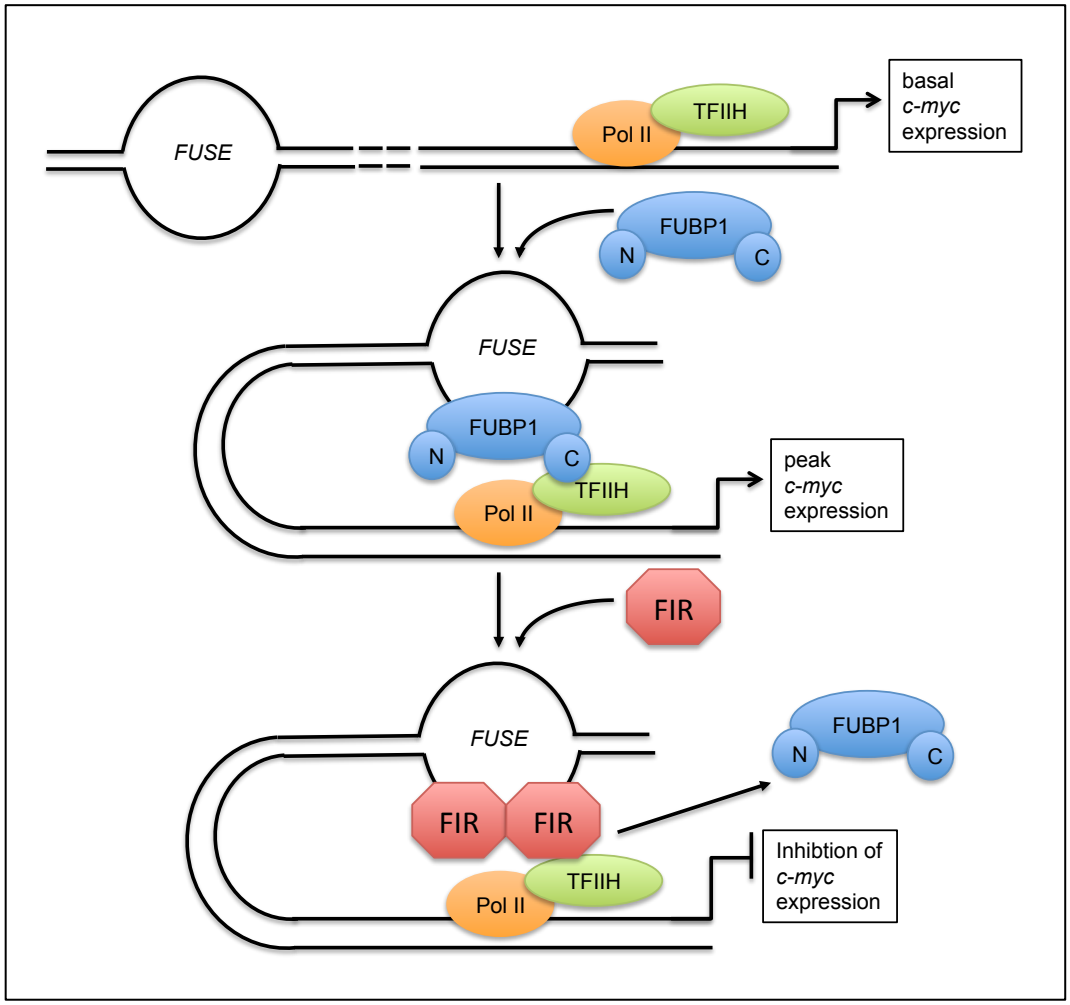

Figure 3: Three-step mechanism of *c-myc* peak expression. Due to basal transcription and the resulting torsional stress, *FUSE* melts and unwinds. FUBP1 binds simultaneously to both *FUSE* and TFIIH, which leads to a promoter loop formation and maximal *c-myc* transcription. Afterwards, FIR is recruited to the FUBP1/TFIIH/*FUSE* complex, replaces FUBP1, and stops *c-myc* transcription.

1.1.4 FUBP1 as a Cancer Biomarker

FUBP1 expression is altered in many cancer types (see Table 1, adapted from Zhang et al. [11]), and although the transcriptional up-regulation of *c-myc* is a fundamental finding of FUBP1 action in carcinogenesis, the protein also facilitates further pro-oncogenic functions independently of *c-myc* transcription. For example, FUBP1 promotes the replication of HCV, a virus, which is one of the main causes of hepatocellular carcinoma [19].

A study of Weber et al. showed that there is a correlation of elevated FUBP1 and *c-myc* levels in clear cell renal cell carcinoma (ccRCC), but not in bladder or prostate cancer, further indicating that FUBP1 facilitates additional oncogenic functions [20]. The low expression levels in normal tissue compared to the high expression in cancer cells suggest FUBP1 as a potent cancer biomarker.

Not only the overexpression of FUBP1, but also the loss of FIR plays a role in carcinogenesis [21]. In colorectal cancer patients, a splicing variant of FIR, lacking exon 2, was found. This truncated variant lacks its N-terminus and is therefore unable to inhibit FUBP1 activity. This splicing variant exhibits dominant negative effects compared to functional wildtype FIR and is only found in the colorectal cancer tissue, but not in the normal neighboring tissue, indicating a potential role in colorectal carcinogenesis [21, 22].

Table 1: Role of FUBP1 in different human malignancies; adapted from Zhang et al. 2013

Malignancy	Alterations	Downstream Target	Reference
Oligodendrioglioma	FUBP1 mutation	NA	[23]
Non-small lung cancer	FUBP1↑	*Stathmin 1*↑	[24]
Breast	FUBP1↑	NA	[25, 26]
Clear cell renal cancer	FUBP1↑	*c-myc*↑	[20]
Liver	FUBP1↑	*p21*↑, *p15*↑, *Cyclin D2*↑	[1, 27]
Liver	FUBP1↑	*Stathmin 1*↑	[27, 28]
Colon	FIR truncation	*c-myc*↑	[21, 22]
Bladder	FUBP1↑	NA	[20]
Prostate	FUBP1↑	NA	[20]

NA: not available

1.1.5 FUBP1 in Hepatocellular Carcinoma

As described before, FUBP1 was found overexpressed in many malignancies. In our laboratory we could show that FUBP1 is highly overexpressed in hepatocellular carcinoma (HCC) compared to normal liver tissue (see Figure 5). Furthermore, it was demonstrated that not the transcriptional regulation of *c-myc*, but the inhibition of molecules of the extrinsic and intrinsic apoptosis pathways like Noxa and TRAIL, as well as the inhibition of cell cycle regulators like p21 and p15, represent the important activities of FUBP1 in HCC (Figure 4) [1].

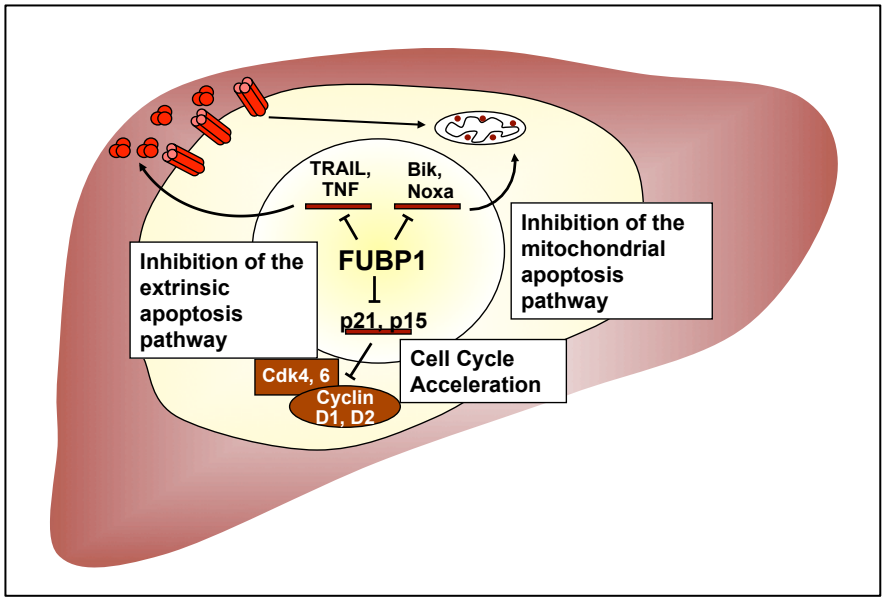

Figure 4: Model of FUBP1 function in hepatocellular carcinoma [1]. In HCC, FUBP1 inhibits important molecules of the extrinsic and intrinsic apoptosis pathway as well as cell cycle inhibitors, leading to increased proliferation, decreased apoptosis and cell cycle acceleration.

Using EMSA and luciferase activity experiments, we could show that *p21* is a direct target gene of FUBP1 in HCC. Finally, in a murine xenograft transplantation model with human Hep3B cells, we demonstrated that the knockdown of *FUBP1* impairs tumor formation compared to the control cells (see Figure 5).

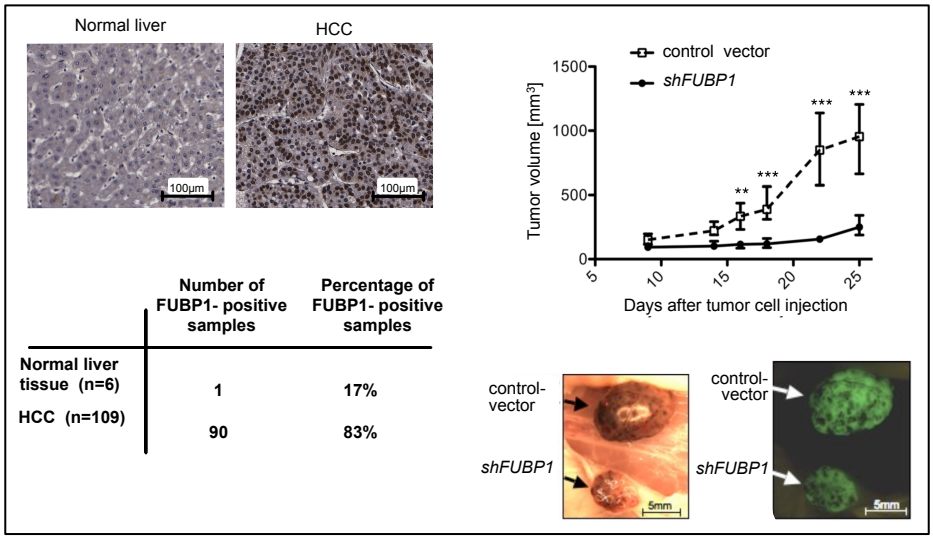

Figure 5: FUBP1 in hepatocellular carcinoma (Rabenhorst et al. 2009). Immunohistochemistry of liver carcinoma and normal liver samples with a specific anti-FUBP1 antibody (sc-11098) revealed that FUBP1 is highly overexpressed in HCC compared to normal liver tissue. Furthermore, a stable *FUBP1* knock-down led to impaired tumor growth in a murine xenograft transplantation experiment compared to the empty vector transduced Hep3B cells.

These findings led us to the assumption that FUBP1 might represent a potential novel therapeutic target for HCC treatment.

1.2 Hepatocellular Carcinoma

Hepatocellular Carcinoma (HCC) is the fifth most common cancer and the third most common cause of cancer-related death worldwide [29]. Conventionally, HCC was considered as a disease without curative options, with an overall survival of less than 6 month [30]. Improvements of the imaging techniques, in early detection and in novel therapies have led to a better patient selection and subsequent to improved treatment approaches [31]. Staging of the patients' disease is part of the routine clinical care, using the Barcelona Clinic Liver Cancer (BCLC) classification as a prognostic algorithm [30]. The classification uses three parameters, the tumor burden, the underlying liver dysfunction and the patients' symptoms, to stage the tumor disease and link this to an appropriate treatment approach [32] (see Figure 6, page 14). The treatment options of the very early stage (0) and early stage (A) tumors are curative, including resection, liver transplantation and local ablations. Unfortunately, the treatment options for intermediate stage (B) and advanced stage (C) are only palliative using transcatheter arterial chemoembolization (TACE) or the small molecule inhibitor sorafenib [33]. In the terminal stage (D) only symptomatic treatment is possible. One challenging problem in the treatment of those patients is the occurrence of two diseases, the HCC and the underlying cirrhosis (see paragraph 1.2.1). This problematic setting became visible in a phase III trial comparing sunitinib against sorafenib, which had to be stopped prematurely, because of excessive toxicity in the sunitinib arm [34]. The fact that the liver cirrhosis made the patients more accessible for toxic reactions and that conventional chemotherapy is ineffective in HCC [35], decreases the treatment options and makes the therapy more challenging.

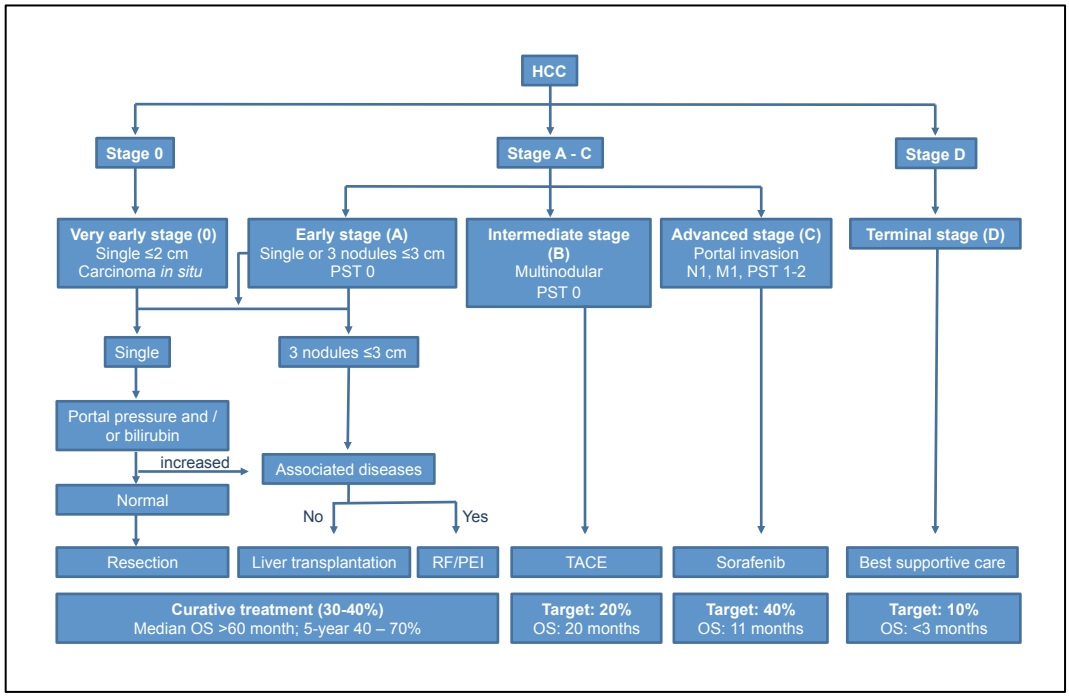

Figure 6: BCLC staging system and therapeutic strategy according to EALS-EORTC guidelines (adapted from Villanueva et al. 2013 [36]): Staging classification inherits 5 stages, selecting the best treatment options currently available for each patient. Abbreviations: BCLC: Barcelona Clinic Liver Cancer; EALS: European Association for the Study of Liver Disease; EORTC: European Organization for Research and Treatment of Cancer; RF: radiofrequency ablation; PEI: percutaneous ethanol injection; TACE: transcatheter aterial chemoembolization; OS: overall survival, PST: performance status.

Three well-known HCC risk factors, which lead to the underlying cirrhosis, are infections with hepatitis virus B and C (HBV and HCV), alcohol intake and toxins like aflatoxin [37].

1.2.1 Molecular Mechanisms of HCC Development

One downstream pathway of HBV- and HCV- infected cells promoting HCC is the activation of stem-cell activity through the upregulation of the epithelial cell adhesion molecule (EpCAM) and beta-catenin [38, 39].

Another HCC-promoting mechanism is explained as a secondary effect of liver cirrhosis. In the cirrhotic tissue, a decrease of vascular tissue is observed, leading to a hypoxic environment. These hypoxic conditions lead to the upregulation of the hypoxia inducible factor 1α (HIF1α), which in turn leads to the upregulation of the vascular endothelial growth factor (VEGF), cyclo-oxygenase 2, angiopotein 2, as well as several matrix metalloproteinases [40-42]. This massive activation of inflammatory and angiogenic signals results in a susceptibility of the parenchyma to damage, inhibition of regeneration and subsequent HCC formation [38].

Until today, no oncogenic addiction loop has been identified in hepatocellular carcinoma. An identification of such a loop is desirable to be able to define patient subgroups with targetable gene alterations [36].

1.2.2 Treatment Options in Hepatocellular Carcinoma

Treatment of HCC is strongly dependent on the progression of the disease, which is staged using the BCLC classification. As very early stage (0) and early stage (A) patients can be treated with curative options like resection, liver transplantation or local ablations, stage (B) and stage (C) patients can only be treated with palliative options like sorafenib or TACE.

1.2.3 Surgical Therapy

1.2.3.1 Resection

Surgical resections are first-line options for early stage HCC patients, providing five-year survivals of 68% in Child-Plugh class A patients (level of liver cirrhosis) with MILAN criteria (single tumor <5 cm, or three nodules <3 cm) and without major vascular invasion (MVI) [43]. Shi et al reported even a 100% 5-year survival of patients with an initial tumor size of <2 cm [44]. Local ablation has also been proposed as a therapy for tumors with a size of <2 cm [45]. Nevertheless, the perioperative mortality for HCC resections is 4 – 4.7% higher than for resections of benign tumors or colorectal liver metastasis [46].

1.2.3.2 Liver Transplantation

Transplantation is the only treatment that offers a cure for both, the HCC and the underlying cirrhosis [37]. After individual validation by different groups, it is accepted that patients, who fulfill the MILAN criteria and show a good MVI should be evaluated for liver transplantation [32, 47]. Despite the fact that transplantations seem to be the best treatment for this subset of patients, the lack of donor organs leads to a progression of the tumor in 20% of the cases while the patients are on the transplantation waiting list which eventually leads to the removal of these patients from the list [48, 49].

1.2.4 Locoregional Therapy

Local ablation is the standard care for early stage patients who are not suitable for surgery. It is based on the concept that the tumor cells will be directly destroyed through percutaneuos, laparoscopic, or open laparotomies using chemical toxicity, modifying neoplastic cell temperature, microwaves, radiofrequency or cryoablation [37]. Five-year survival rates for this treatment are in the range of 50-70% [32, 47].

Intermediate stage patients are treated with TACE with the palliative goal to delay the tumor progression and extension of the patients' survival [32, 47, 50].

1.2.4.1 Transcatheter Aterial Chemoembolization (TACE)

TACE was designed based on the observation that hepatic arteries directly supply the HCC. A catheter is inserted into the artery feeding the tumor, and a mixture of a chemotherapeutic agent in a lipid emulsion can be injected directly at the tumor site. Afterwards, the hepatic artery is embolized to help retaining the chemotherapy agent within the tumor, maximizing the exposure of the tumor to the drug and minimizing the toxicity for the parenchymal tissue [51, 52].

The method had been improved by the development of polymeric microsphere beads, which ionically bind the chemotherapeutic agents (DEB-TACE), providing medium survival rates beyond 30-40 month in referral centers [53].

1.2.5 Systemic (Targeted) Therapy

Until 2007, no systemic therapy had shown beneficial effects for HCC patients. In 2007, the SHARP (sorafenib HCC assessment randomized protocol) trial was performed in Europe, showing a survival benefit of 3 month in patients treated with sorafenib [33]. 600 patients with advanced HCC and good liver function (Child-Phugh A) were treated with either sorafenib or placebo. The study was stopped at the second interim analysis, because of the significant difference favouring the sorafenib arm (Medium survival 10.9 vs. 7.9 month). A second trial with 200 patients was performed in the Asia Pacific region with similar entry criteria and treatment plan. The survival benefit in the sorafenib treated arm was 2 month (6.5 month vs. 4.2 month) [54]. The FDA did approve sorafenib in 2007 for patients with late stage HCC and preserved liver function. Furthermore, several smaller trials could show that the tolerability and pharmacokinetic profile of patients with poorer liver function (Child-Phugh B) is not significantly different to those with good liver function [55].

Nevertheless, several subsequently performed smaller trials could show that most patients are not able to pursue the daily dose of 400 mg sorafenib twice, because of severe side effects [56].

Multiple targeted therapy studies are currently under evaluation. Unfortunately, regardless of the initial potential, none of them is showing additional benefit compared to the sorafenib treatment. The sunitinib (another multi-kinase inhibitor) trial had to be stopped prematurely due to excessive toxicity [34]. Brivanib (a potent VEGFR- and FGFR- (fibroblast growth factor receptor) kinase

inhibitor) showed an anti-tumor effect that did not significantly improve patient survival compared to the placebo group in second line therapies [57]. Furthermore, a combinational therapy using erlotinib (EGFR inhibitor) and sorafenib failed in comparison to sorafenib single treatment [58].

The need of new therapies in HCC treatment is urgent. The understanding of potential oncogenic addiction loops and the discovery of new molecular targets in HCC would lead to the desired development of new treatments and a subsequent better outcome for the patients.

1.3 Additional Cancer Therapeutics

1.3.1 Topoisomerase I Inhibitors

The topoisomerase is a molecule, which is highly conserved among species and ubiquitously expressed in eukaryotes, prokaryotes and archea [59]. Topoisomerase I regulates the topology of the DNA, facilitating three successive reactions in a so-called TopI cleavage complex (TOP1cc) (see Figure 7). First, it cleaves the backbone of the DNA, then it allows relaxations of the DNA supercoils, and third, it re-ligates the DNA. Under normal conditions, the cleavage is transient, whereas the re-ligation is favored over cleavage [60]. These processes are needed for the generation of DNA supercoiling due to DNA replication, transcription and chromatin remodeling.

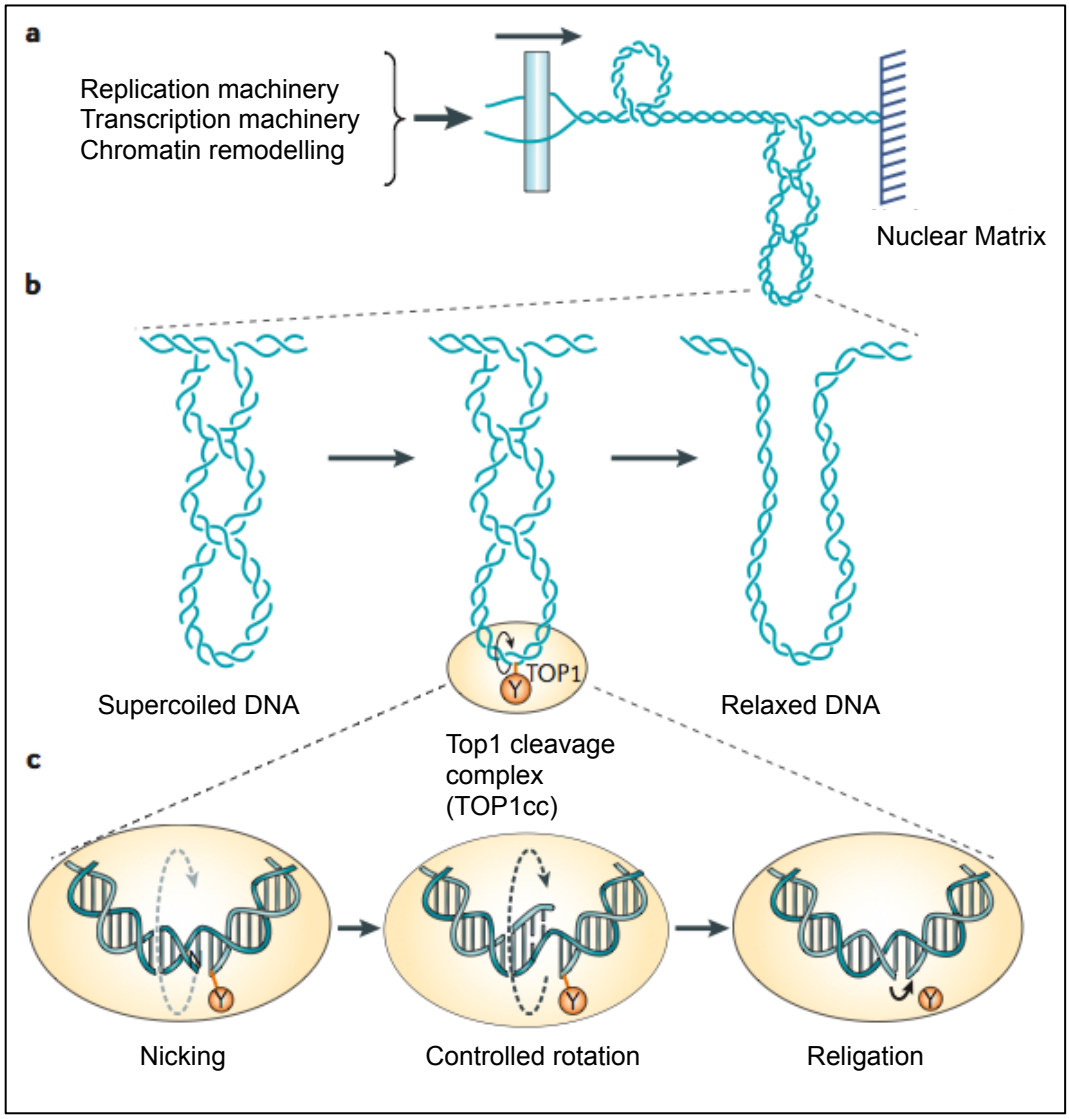

Figure 7: DNA supercoiling relaxation by TOP1-mediated DNA cleavage complexes. Adapted from Pommier et al. 2006 [60]. a) Generation of supercoiled DNA through replication, transcription or chromatin remodeling. b) TOP1 introduces single strand breaks to facilitate DNA relaxation. The cleavage intermediate is called “cleavage complex”, because TOP1 covalently binds to the 3’ end of the DNA. Tyrosine (Y723 for human), which is involved in the covalent binding, is depicted in yellow. c) Detailed look into the mechanism of the DNA knicking and relegation within the cleavage complex. First step: Transesterification reaction, during which the tyrosin becomes linked to the 3’ end of the DNA (Nicking). Second Step (Controlled rotation): The torsional stress caused by DNA supercoiling drives the 5’end of the nicked DNA around the intact strand. TOP1 encircles this nicked DNA and slows its rotation down. Third step (Religation): The 5’ end is relegated with the 3’ end, finally leading to relaxed DNA.

Drugs like camptothecin trap the topoisomerase I DNA complex by stabilizing it, which subsequently leads to apoptosis of the cell. Camptothecin is a topoisomerase I inhibitor and belongs to the group of interfacial inhibitors [59] (see Figure 8). Interfacial inhibitors selectively bind to interfaces as macromolecular machines assemble. In 2002, Staker et al. were able to crystallize a TOP1 tertiary complex with topotecan and solved the structure. The drug intercalated in the cleaved DNA and specifically bound to TOP1 [61]. In 2005 and 2006, two groups could show that not only camptothecin, but also the

indenoisoquinolines, the non-camptothecin TOP1 inhibitors, act as interfacial inhibitors [62, 63] (see Figure 8).

Until today, topoisomerase I is the only known target of camptothecin and the indenoisoquinolines, but the specific signaling pathways leading to apoptosis after topoisomerase I inhibition are not yet fully understood [64].

Nevertheless, due to high apoptosis-inducing potential, the camptothecin derivate topotecan is approved by the FDA for ovarian and lung cancer treatment and irinotecan for colorectal cancer therapy. The indenoisoquinolines NSC 725776 is currently tested in a phase II trial with relapsed solid tumors and lymphomas (http://clinicaltrials.gov).

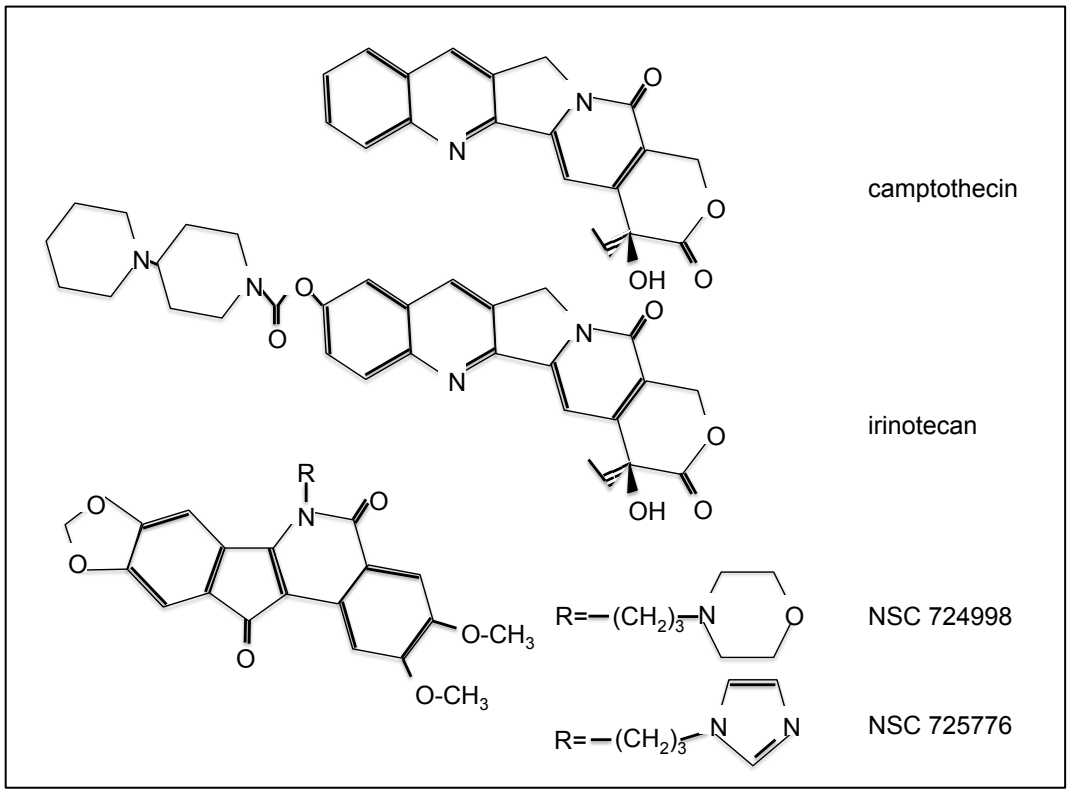

Figure 8: Topoisomerase inhibitors: Chemical structures of camptothecin and its derivate irinotecan, and of the non-camptothecin derived indenoisoquinoles NSC 724998 and NSC 725776.

1.3.2 Topoisomerase I Inhibitor Treatment in HCC

Until today, treatment of HCC with irinotecan failed in different studies as first line single therapy [65, 66] as well as in combinational approaches with flavopiridol [67] or capeticabine [68]. All of these studies had in common that the substance was administered intravenously.

Nevertheless, in 2009 Koushiro Ohtsubo et al. published a study describing hepatic aterial infusion (HAI) of irinotecan followed by proton beam therapy in HCC, leading to tumor suppression and long-term survival in a patient [69].

Furthermore, Brandi et al. showed in 2011 that intra-aterial infusion of irinotecan (HAI) is feasible in patients with hepatocellular carcinoma, with no major adverse drug-related events [70]. These studies led to the assumption, that irinotecan might be useful in HCC therapy, if administered directly at the tumor site.

1.4 Aim of this Project

The aim of this thesis was to evaluate the efficacy of targeting FUBP1 in hepatocellular carcinoma.

At the beginning of the study it was known that FUBP1 is highly deregulated in several cancerous tissues. In our group, we could show that FUBP1 is highly overexpressed in hepatocellular carcinoma compared to the normal liver tissue. Furthermore, a stable knockdown of *FUBP1* in the human HCC cell Hep3B led to impaired tumor growth in a xenograft transplantation model [1].

Based on these findings, FUBP1 might be a potential new target in HCC therapy. The goal of this project was to identify novel FUBP1 inhibitors and test their efficacy in *in vitro* and *in vivo* preclinical studies. For this purpose, the following issues were adressed:

I. The expression and purification of recombinant FUBP1 full length protein
II. The functional analysis of recombinant FUBP1
III. The establishment of an inhibitor screening system and the subsequent identification of potential inhibitory substances
IV. The validation of the screening “hits” in an independent binding assay
V. Studying the effects of the inhibitory substances *in vitro*
VI. Studying the anti-cancerous effects of the substances in an *in vivo* mouse model

2 Materials and Methods

2.1 Materials

2.1.1 Plasmids

Table 2: Original plasmids

Name	Description	Reference
pET28 b (+)	Bacterial Expression vector, kanamycin-resistance, optional N- or C-terminal Hexahistidine-tag, T7 promotor	*Novagen,* Darmstadt
coFUBP1/pUC57	Full length, human, codon optimized *FUBP1* sequence. Commonly used plasmid cloning vector in *E. coli*. The *pUC57* vector length is 2,710bp and is isolated from *E. coli* strain DH5α by standard procedures	*GenScript,* Hong Kong

Throughout the whole study, codon optimized *FUBP1* sequence (by *GenScript*), is referred to as co*FUBP1*.

Table 3: Modified plasmids

Name	**Description**
co*FUBP1*/pET28	Codon optimized FUBP1 sequence in *bacterial expression vector,* kanamycin-resistance, C-terminal Hexahistidine-tag, T7 promotor

2.1.2 Oligonucleotides

All oligonucleotides used in this study were synthesized by *BioSpring*, Frankfurt am Main, Germany.

2.1.2.1 Sequencing Oligonucleotides

Table 4: Sequencing Oligonucleotides

Name	**Gene**	**Sequence (5'-->3')**	**T_M [°C]**
coFBP1 rev 1	*FUBP1*	tacgactaatctgttcacgc	54
coFBP1 for 1	*FUBP1*	attcagatcgcaccggattc	52
coFBP1 rev 1	*FUBP1*	atcaccgtgatggaaacccg	62
coFBP1 for 2	*FUBP1*	tcaccgatctgctgcgtagc	56
coFBP1 rev 2	*FUBP1*	tacccgtcggcacaatgaag	62
coFBP1 for 3	*FUBP1*	aagctggtaccgacccgaac	56
coFBP1 rev 3	*FUBP1*	taatcgacctgaccagccg	61
coFBP1 for A1	*FUBP1*	actgaactcgaatgattatgg	61

2.1.2.2 Oligonucleotides used for Cloning

Table 5: Cloning oligonucleotides

Name	Gene	Sequence (5'→3')	T_M [°C]
coFBP1 NcoI for	*FUBP1*	aaaccatggcagactactcaacggtc	71
coFBP1 NheI for	*FUBP1*	aaaccatggcagactactcaacggtc	64
coFBP1 XhoI rev	*FUBP1*	aaactcgagttgaccctgcggagccg	71

2.1.2.3 qRT-PCR Oligonucleotides

Table 6: qRT-PCR oligonucleotides

Name	Gene	Sequence (5'→3')	T_M [°C]
qRT PCR huMYC for	*C-MYC*	cgtctccacacatcagcacaa	54
qRT PCR huMYC rev	C-MYC	cactgtccaacttgaccctcttg	57
118qRT-hGAPDH-for	GAPDH	aatggaaatcccatcaccatct	41
119qRT-hGAPDH-rev	*GAPDH*	cgccccacttgattttgg	50
63-qRT-p21-for	*CDKN1A*	tggagactctcagggtcgaaa	54
64-qRT-p21-rev	*CDKN1A*	ccggcgtttggagtggta	53
qRT PCR TRAIL for	*TNFSF10*	gagctgaagcagatgcaggac	56
qRT PCR TRAIL rev	*TNFSF10*	tgacggagttgccacttgact	54
qRT PCR BIK for	*BIK*	cttgatggagaccctcctgtatg	57
qRT PCR BIK rev	*BIK*	agggtccaggtcctcttcaga	56
Q21 Pmaip1 for 2	*Pmaip1*	cagttggaggctgaggttc	58
Q22 Pmaip1 rev 2	*Pmaip1*	gttgagtagcacactcgactt	52

2.1.2.4 Oligonucleotides for Binding Studies

Table 7: Oligonucleotides for binding studies

Name	Gene	Sequence (5'→3')	T_M [°C]
pGL3-p21-F1/-FUSE	*p21 FUSE*	ctggctttttgttttcattttgttttttgttttgttttgttttttgagacaa	62
p21/P3	*p21 FUSE*	ttttgttttcattttgttttttgttt	46
pGL3-p21-F1/-FUSE biotinyliert	*p21 FUSE*	ctggctttttgttttcattttgttttttgttttgttttgttttttgagacaa	62
p21/P3 biotinyliert	*p21 FUSE*	ttttgttttcattttgttttttgttt	46
p21/p31 FUSE	*p21 FUSE*	cagccctggctttttgttttcattt	54
p21/p31 FUSE biotinyliert	*p21 FUSE*	cagccctggctttttgttttcattt	54
p21/p39 FUSE	*p21 FUSE*	tttgttttgttttttgagacaaggt	48

2.1.3 Chemically Competent Bacteria

Table 8: Chemically competent bacteria

Host Strain	Genotype	Manufacturer
BL21(DE3)	F– *ompT gal dcm lon hsdSB(rB-* mB-) λ(DE3 [lacI *lacUV5-T7* gene 1 ind1 sam7 nin5])	*Agilent Technologies, Santa Clara USA*
One Shot® TOP10	F-mcrAΔ (mrr-hsdRMS-mcrBC) φ80 *lacZΔM15*ΔlacX74 *recA1 araD139Δ(ara-leu)7697 galU galK rpsL(StrR) endA1 nupG*	*Invitrogen GmbH*, Darmstadt

2.1.4 Enzymes

Table 9: Restriction endonucleases

Enzymes	Restriction site [5'-->3']	Concentration [U/ml^{-1}]	Manufacturer
NcoI	CCA TTG	20000	*NEBiolab*, Schwalbach
XhoI	CTC GAG	20000	*NEBiolab*, Schwalbach

Table 10: Additional Enzymes for molecular biology methods

Enzyme	Concentration [U/ml-1]	Manufacturer
Calf-intestinine Phosphatase (CIP)	10,000	*NEBiolab*, Schwalbach
DNAse I	5,000000*	*Sigma Aldrich Chemie*, Taufkirchen
Platinum® Pfx Polymerase	2,500	*Invitrogen GmbH*, Darmstadt
RNAse A	100 mg / ml^{-1}	*Roche*, Mannheim
Taq Polymerase	5,000	*Invitrogen GmbH*, Darmstadt
T4 DNA Ligase	200,000	*NEBiolab*, Schwalbach
Omniscript Reverse Transcriptase	4	*Qiagen GmbH*, Hilden

*Was used in lyophilized form, concentration in [U/mg^{-1}]

2.1.5 Bacteria Growth Media, Antibiotics and Supplement Stock Solutions

Table 11: Bacterial growth media

Media	Ingredients for 1 L	Preparation
LB-Medium	5 g yeast extract 10 g peptone 10 g NaCl	MQ-water (ddH_2O) ad 1L, adjust to pH 7.2, autoclave for 30 minutes
LB-Agar	5 g yeast extract 10 g peptone 10 g NaCl 15 g agar-agar	MQ-water (ddH_2O) ad 1L, adjust to pH 7.2, for selective LB-agar plates allow media to cool down to 50°C before adding selective antibiotic(s)
Auto-induction Medium	925 ml LB-media 20 ml 5052 50 ml NPS 1 ml $MgSO_4$ 4 ml Kanamycin	Prepare LB- medium as descripted above allow media to cool down to room temperature before adding remaining reagents immediately before inoculation

Table 12: Supplements

Media	Ingredients for 1 L / Concentration	Preparation
5052	37.5 g glucose 150 g α-lactose 375 g glycerol	MQ-water (ddH_2O) ad 1L,stirr at 50°C, filter sterilize (0.2 µm)
NPS	66 g $(NH_4)SO_4$ 136 g KH_2PO_4	MQ-water (ddH_2O) ad 1L, autoclave for 30 minutes
$MgSO_4$	1 M	Dissolve in ddH_2O, filter sterilize (0.2 µm)
Glucose 20% (w/v)	20% (w/v)	Dissolve in ddH_2O, filter sterilize (0.2 µm)
IPTG	1 M	Dissolve in ddH_2O, filter sterilize (0.2 µm), store at -20°C (1 ml Aliquots)
Kanamycin	25 mg/ml^{-1}	Dissolve in ddH_2O, filter sterilize (0.2 µm), store at -20°C (1 ml Aliquots)
Ampicillin	100 mg/ml^{-1}	Dissolve in ddH_2O, filter sterilize (0.2 µm), store at -20°C (1 ml Aliquots)

2.1.6 Kits

Table 13: Kits

Name	Manufacturer
Plasmid Maxi Kit	*Qiagen GmbH*, Hilden
Qiaquick® Gel Extraktion Kit	*Qiagen GmbH*, Hilden
Omniscript® Reverse Transcription	*Qiagen GmbH*, Hilden
Amersham ECL Western Blotting Detection	*GE Healthcare*, Munich

2.1.7 Buffers and Solutions

2.1.7.1 Buffer for Molecular Biological Methods

Table 14: Buffer for plasmid DNA preparations

Buffer	Ingredients / Concentration	Preparation
GTE buffer	50 mM Glucose 25 ml Tris-HCl pH 8.0 10 mM EDTA	filter sterilize (0.2 µm)
Lysis buffer	200 mM NaOH 1% SDS	freshly prepared
Neutralization buffer	3 M KoAc, pH 5,2	filter sterilize (0.2 µm)

Table 15: Buffer for agarose gel electrophoresis

Buffer	Ingredients / Concentration
Running buffer (0.5x TBE)	44.5 mM Tris 44.5 mM boric acid 1 mM EDTA, pH 8.0
DNA loading buffer	100 mM EDTA 1% SDS 0.25% (w/v) bromphenol blue 0.25% (w/v) xylenecylanol 20% (w/v) glycerol

2.1.7.2 Buffer for Protein Biochemical Methods

Table 16: SDS-PAGE gel electrophoresis

Buffer	Ingredients / Concentration
SDS sample buffer	62.5 mM Tris-HCl, pH 6.8 2% (w/v) SDS 20% (w/v) glycerol 0.1% (w/v) bromphenol blue 50 mM DTT
SDS-PAGE runnning buffer	50 mM Tris 200 mM glycine 0.15% (w/v) SDS

Table 17: Coomassie staining buffer

Buffer	Ingredients / Concentration
Quick Coomassie staining solution	MQ-water (ddH_2O) ad 1L 0.3% HCl conc. Coomassie blue R-250, 80 mg / 1L solution
Coomassie gel stain	MQ-water (ddH_2O) ad 1L 45% (v/v) methanol 1% glacial acetic acid Coomassie blue R-250, 1 g / 1L solution
Coomassie gel destain	MQ-water (ddH_2O) ad 1L 10% methanol 10% glacial acetic acid

Table 18: Lysis buffer

Buffer	Ingredients / Concentration
Bacterial lysis buffer	50 mM MES, pH 6.5 50 mM NaCl 1 tablet *Complete* EDTA-free Protease Inhibitor Cocktail ad 50 ml solution
RIPA buffer	10 mM Tris-HCl, pH 7.4 20 mM KCl 1.5 mM MgCl2 0.5% SDS 1.3 mM PMSF 1 tablet Complete EDTA free Protease Inhibitor Cocktail ad 50 ml solution

Table 19: Western blot analysis buffer

Buffer	Ingredients / Concentration
Blotting buffer	48 mM Tris, pH 7.5 39 mM glycine 20% (v/v) methanol
TBS-T	25 mM Tris, pH 8.1 150 mM NaCl 0.1% Tween20
Blocking buffer	3% non-fat milk powder in TBS-T

2.1.7.3 Buffer for Chromatographic Methods

Table 20: Immobilized metal ion affinity chromatography (IMAC); HisTrap

Buffer	Ingredients / Concentration
Bacterial lysis buffer	50 mM MES, pH 6.5 50 mM NaCl 1 tablet *Complete* EDTA free Protease Inhibitor Cocktail ad 50 ml solution
Wash buffer	50 mM MES, pH 6.5 50 mM NaCl 4 mM Imidazole
Elution buffer	50 mM MES, pH 6.5 50 mM NaCl 404 mM Imidazole

Table 21: Affinity chromatography; HeparinTrap

Buffer	Ingredients / Concentration
Wash buffer (low salt)	50 mM MES, pH 6.5 50 mM NaCl 3 mM DTT
Elution buffer (high salt)	50 mM MES, pH 6.5 2 M NaCl 3 mM DTT

Table 22: Size exclusion chromatography; Gelfiltration

Buffer	Ingredients / Concentration
Running buffer	50 mM MES, pH 6.5
	50 mM NaCl
	3 mM DTT

2.1.7.4 Buffer for Interaction Studies

Table 23: Alpha screen buffer

Buffer	Ingredients / Concentration	Preparation
Screening buffer	50 mM Tris, pH 7.4	
	100 mM NaCl	
	0.01% Tween20	
	0.1% BSA	filter sterilized (0.2 µm), stored at 4°C

Table 24: SPR and MST binding study buffer

Buffer	Ingredients / Concentration	Preparation
SPR buffer	50 mM Tris, pH 7.4	filter sterilized (0.2 µm)
	100 mM NaCl	
	0.1% BSA	
	1% DMSO	freshly added prior to use
MST buffer	50 mM Tris, pH 7.4	filter sterilized (0.2 µm)
	100 mM NaCl	
	0.1% BSA	

2.1.8 Antibodies

Table 25: Primary Antibodies

Name	Species	Dilution	Manufacturer
Anti-human FUBP1 (N-15)	goat	1: 1,000	*Santa Cruz Biotechnology*, Heidelberg
Anti-human β-Actin	goat	1: 2,000	*Santa Cruz Biotechnology*, Heidelberg

Table 26: Secondary Antibody

Name	Species	Dilution	Manufacturer
Anti-goat-HRP	rabbit	1: 10,000	*Invitrogen GmbH*, Darmstadt

2.1.9 Size Markers for Gelelectrophoresis

Table 27: BenchmarkTM Prestainend Protein ladder

Band No.	Apparent molecular weight [kDa]
1	181.8
2	115.5
3	82.2
4	64.2
5	48.8
6	37.1
7	25.9
8	19.4
9	14.8
10	6.0

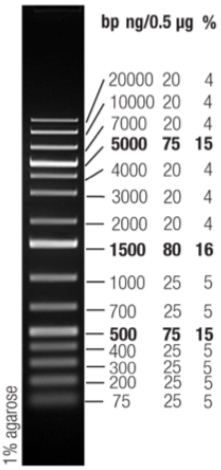

Figure 9: Gene Ruler™ 1kB Plus DNA ladder, *Invitrogen, Darmstadt*

2.1.10 Cell Culture Materials

Table 28: Cell lines

Name	Description	Source
HEK 293T	Human embryonic kidney cells, cell line generated by adenovirus transformation with SV40 "large T"-antigen, S1	AG Grez, GSH, Frankfurt
Hep3B	Human hepatocellular carcinoma cells, positive for HepB viral DNA sequences, S1	ATCC (HB-8064™)
HepG2	Human hepatocellular carcinoma cells, S1	ATCC (HB-8065™)
HuH7	Human hepatocellular carcinoma cell line, S1	AG Piiper, University Hospital Frankfurt

Table 29: Cell culture media

Name	Description	Manufacturer
DMEM	Dulbecco's Modified Eagle Media 4.5 g / L^{-1} glucose	*GIBCO*, Eggenstein
Advanced DMEM	Dulbecco's Modified Eagle Media 4.5 g / L^{-1} glucose	*GIBCO*, Eggenstein
DMSO	Dimethylsulfoxide, highly purified	*Merck*, Darmstadt
FCS	Fetal calf serum	*PAA Laboratories*, Pasching
L-Glutamine	200 mM solution	*PAA Laboratories*, Pasching
Pen / Strep	10,000 U / ml^{-1} Penicillin 10,000 µg / ml^{-1} Streptomycin	*PAA Laboratories*, Pasching
Trypsin-EDTA	0.05% Trypsin EDTA	*GIBCO*, Eggenstein
PEI	Polyethylenemine	*Sigma-Aldrich Chemie GmbH*, Steinheim

2.1.11 Chemotherapeutics and Small Molecule Compounds

Table 30: Chemotherapeutics and small molecules

Name	Concentration	Preparation	Manufacturer
mitomycin C	0.4 mg/ml	Dissolved in ddH2Osteril / methanol (4:1)	*Roche*, Mannheim
cisplatin	1 mg/ml	Dissolved in ddH_2Osteril	*Teva*, Israel
doxorubicin	10 mg/ml	Dissolved in ddH_2Osteril	*Sigma-Aldrich, Chemie GmbH, Steinheim*
sorafenib	10 mM	Dissolved in DMSO, stored at -20°C (1 ml Aliquots)	*Selleckchem*, Boston
camptothecin	10 mM	Dissolved in DMSO, stored at -20°C (1 ml Aliquots)	*Santa Cruz Biotechnology, Heidelberg*
7-ethyl-10-hydroxy-camptothecin	1000 µM	Dissolved in DMSO, stored at -20°C, (1 ml Aliquots)	Selleckchem, Boston
pregnenolone	10 mM	Dissolved in DMSO, stored at -20°C, (1 ml Aliquots)	*Santa Cruz Biotechnology, Heidelberg*
tosufloxacin	10 mM	Dissolved in DMSO, stored at -20°C, (1 ml Aliquots)	*Santa Cruz Biotechnology, Heidelberg*
NSC724998	10 mM	Dissolved in DMSO, stored at -20°C, (20 µl Aliquots)	kindly provided by Prof. Yves Pommier, NIH
NSC725776	10 mM	Dissolved in DMSO, stored at -20°C, (20 µl Aliquots)	kindly provided by Prof. Yves Pommier, NIH

Table 31: Screening libraries

Name	Manufacturer	Source
Prestwick Chemical library®	*Prestwick Chemical*, Illkirch, France	kindly provided by Ricardo Biondi, Med. Klinik1, Uniklinikum Frankfurt
Maybridge HitFinder™ library	*Thermo Fisher Scientific, Waltham, USA*	kindly provided by Ricardo Biondi, Med. Klinik1, Uniklinikum Frankfurt

2.1.12 Laboratory Equipment

Table 32: Centrifuges

Name	Manufacturer
Beckman J2-HS	*Beckman*, Munich
Biocentrifuge, J2-21M/E with JA-10 and JA-20 rotors	*Beckman*, Munich
Cold-Centrifuge Megafuge 1.0R	*Heraeus*, Hanau
Cold-Centrifuge Minifuge GL	*Heraeus*, Hanau
Desk-Centrifuge Biofuge pico	*Heraeus*, Hanau

Table 33: Incubators

Name	**Manufacturer**
Bacterial Incubator Function Line	*Heraus,* Hanau
Bacterial-Shaker-Incubator Multitron model	*Infors AG*, Bottmingen (Switzerland)
Cell Culture Incubator MCO 17 AI	*Sanyo Component Europe GmbH,* Ingolstadt

Table 34: Heat Blocks and Waterbath

Name	Manufacturer
Cooling-Thermomixer MKR 13	*HLC Biotech*, Bovenden
Dri.Block DB-2D	*Techne Dexford*, Cambridge (England)
Thermomixer Compact for 1.5ml Tubes	*Eppendorf AG*, Hamburg
Water-Bath	*GFL*, Burgwedel

Table 35: Electrophoresis

Name	Manufacturer
BioRad Power Pac 300	*BioRad Laboratories*, Munich
DNA Mini-Subcell for Agarose Gels	*BioRad Laboratories*, Munich
Electrophoresis Power Supply EPS 301	*Amersham Pharmacia Biotech*
Gel-Chamber Model Hoefer HE 33 for Mini Gels	*Amersham Pharmacia Biotech*
Mini-Protean® 3 Cell Gel Chamber	*BioRad Laboratories*, Munich
Semidry Blotting Unit Semiphor Transphor Unit	*Hoefer Pharmacia Biotech*

Table 36: Chromatography material, devices and filters

Name	Manufacturer
Äkta Purifier	*GE Healthcare Europe GmbH*, Munich
Amicon Ultrafiltration Membrane MWCO 10 kDa	*Millipore GmbH*, Schwalbach/Ts.
Amicon Ultrafiltration Membrane MWCO 30 kDa	*Millipore GmbH*, Schwalbach/Ts.
Hi-Load Superdex 16/60 200	*GE Healthcare Europe GmbH*, Munich
HiTrap heparin HP 5 ml	*GE Healthcare Europe GmbH*, Munich
Ni-Sepharose High Performance, 25 ml	*GE Healthcare Europe GmbH*, Munich
Omnifit® Chromatography Columns	*Diba Industries Ltd*, Cambridge
Sample loop 5 ml	*GE Healthcare Europe GmbH*, Munich
Superloop 50 ml	*GE Healthcare Europe GmbH*, Munich

Table 37: Material and devices for MST and SPR binding studies

Name	Manufacturer
BioRad ProteOn™ XPR 36	*BioRad Laboratories*, Munich
Capillary sealing wax	*NanoTemper Technologies,* Munich
Monolith NT.115	*NanoTemper Technologies,* Munich
ProteOn™ NLC sensor chip	*BioRad Laboratories*, Munich
Standard capillaries	*NanoTemper Technologies,* Munich

Table 38: Material and devices for Alpha Screen® experiments

Name	Manufacturer
1000 µl pipette tips	Steinbrenner Laborsysteme GmbH
200 µl pipette tips	Steinbrenner Laborsysteme GmbH
384-well liquidator adapter	Steinbrenner Laborsysteme GmbH
384-well plate	Greiner Bio one
96-well plate	Greiner Bio one
AlphaScreen® General IgG (Protein A) Detection Kit	Perkin Elmer, Waltham MA
Envision® multilable plate reader	Perkin Elmer, Waltham MA
Liqudator 96	Steinbrenner Laborsysteme GmbH

Table 39: Others

Name	Manufacturer
Autoclave Tuttnauer Systec 2540 EL	*Systec*, Wettenberg
Bunsen Burner Model 1230/1	*Carl Friedrich Usbeck KG*, Radevormwald
CryoPure tubes 1.8 ml	*Sarstedt,* Nümbrecht
Fluorescence Microscope Nikon Eclipse Te300	*Nikon*, Düsseldorf
Freezer (-20°C)	*Liebherr*, Ochsenhausen
Freezer CFC Free (-80°C)	*Sanyo*, Wiesbaden
Freezing container	*Qualilab*, France

Gene Amp® PCR System 9700	*PE Applied Biosystems*
Hypercassette	*Amersham*, Buckinghamshire (England)
Integra Pipetboy	*Integra Biosciences*, Fernwald
Laminar Air Flow (NSF 49 BS 5726 DIN (1-4))	*Clean Air*, Woerden (Netherlands)
Magnetic-Stirrer Model IKA-Combimag RCH	*IKA Labortechnik*, Staufen
Microscope for Cell Culture	*Helmut Hund GmbH*, Wetzlar
Mircowave Sharp R-3V10	*Sharp Corp*.
NanoDropTM 1000 Spectrophotometer	*Thermo Fischer Scientific*, Bonn
Neubauer Improved Hemocytometer	*Marienfeld Superior*, Darmstadt
pH-Meter Model PHM 83 autocal	*Radiometer*, Copenhagen (Denmark)
Refrigerator (4°C)	*Bosch*
Roller RM5 Assistant 348	*Karl Hechst GmbH&Co.KG*, Sondheim
Rotate roller	*Gerlinde Kister*, Mühlhausen
UV-Transluminator with video camera and -printer	*UVP Inc.*, San Gabriel (USA)
vacuum pump	*KNF Neuberger LABOPORT*, Freiburg
Vortex Genie 2	*Scientific Industries*, New York (USA)
Water-Bath	*GFL*, Burgwedel

2.1.13 Chemicals and Reagents

Table 40: Reagents

Name	Manufacturer
Acrylamide Solution (Rotiphorese Gel 30)	*Carl Roth GmbH&Co.KG*, Karlsruhe
Agarose UltraPure (TM) Agarose	*Invitrogen GmbH*, Darmstadt
Ampicillin	*AppliChem GmbH*, Darmstadt
APS (10% in H2O)	*Sigma-Aldrich Chemie GmbH*, Steinheim
Boric Acid	*Carl Roth GmbH&Co.KG*, Karlsruhe
Bradford Reagent (Roti®-Quant)	*Carl Roth GmbH&Co.KG*, Karlsruhe
Bromphenol Blue	*Carl Roth GmbH&Co.KG*, Karlsruhe
Complete Mini Protease Inihibitor Cocktail	*Roche*, Mannheim
DTT	*Sigma-Aldrich Chemie GmbH*, Steinheim
EDTA	*Sigma-Aldrich Chemie GmbH*, Steinheim
EGTA	*Sigma-Aldrich Chemie GmbH*, Steinheim
EtBr	*Carl Roth GmbH&Co.KG*, Karlsruhe
EtOH	*Carl Roth GmbH&Co.KG*, Karlsruhe
Glucose	*Carl Roth GmbH&Co.KG*, Karlsruhe
Glycerol	*Carl Roth GmbH&Co.KG*, Karlsruhe
Glycine	*Carl Roth GmbH&Co.KG*, Karlsruhe
HEPES	*Carl Roth GmbH&Co.KG*, Karlsruhe
Illustra™ dNTP Set	*GE Healthcare Europe GmbH*, Munich
Isopropanol (2-Propanol)	*Carl Roth GmbH&Co.KG*, Karlsruhe
KCl	*Carl Roth GmbH&Co.KG*, Karlsruhe
KH_2PO_4	*Carl Roth GmbH&Co.KG*, Karlsruhe
KoAc	*Carl Roth GmbH&Co.KG*, Karlsruhe
Kolliphore® EL	*Sigma-Aldrich Chemie GmbH*, Steinheim

MeOH	*Carl Roth GmbH&Co.KG*, Karlsruhe
MES-buffer	*AppliChem GmbH*, Darmstadt
$MgCl_2$	*Sigma-Aldrich Chemie GmbH*, Steinheim
Na-β-glycerophosphate	*Sigma-Aldrich Chemie GmbH*, Steinheim
Na-pyrophosphate	*Sigma-Aldrich Chemie GmbH*, Steinheim
Na_2HPO_4	*Carl Roth GmbH&Co.KG*, Karlsruhe
NaAc	*Carl Roth GmbH&Co.KG*, Karlsruhe
NaCl	*Carl Roth GmbH&Co.KG*, Karlsruhe
NaF (Natriumfluorid)	*Sigma-Aldrich Chemie GmbH*, Steinheim
NaOH	*AppliChem GmbH*, Darmstadt
Nonfat dried milk powder	*AppliChem GmbH*, Darmstadt
PMSF	*Carl Roth GmbH&Co.KG*, Karlsruhe
Ponceau S Solution	*Sigma-Aldrich Chemie GmbH*, Steinheim
Roti®-Quant	*Carl Roth GmbH&Co.KG*, Karlsruhe
SDS	*Carl Roth GmbH&Co.KG*, Karlsruhe
Sodium Chlorid	*Roth*, Karlsruhe
Sucrose	*Carl Roth GmbH&Co.KG*, Karlsruhe
TEMED	*Carl Roth GmbH&Co.KG*, Karlsruhe
Tris	*Carl Roth GmbH&Co.KG*, Karlsruhe
TrisBase	*Roth*, Karlsruhe
Triton-X-100	*Fluka*, Buchs (Switzerland)
Tween-20	*Carl Roth GmbH&Co.KG*, Karlsruhe

Table 41: Software and databases

Table 42

Name	Manufacturer
NTControl (MST data analysis)	*NanoTemper Technologies*, Munich
NTAnalysis (MST data acquisition)	*NanoTemper Technologies*, Munich
ProteOn Manager Software	*BioRad Laboratories*, Munich
Microsoft Excel	*Microsoft* (USA)
Microsoft Office	*Microsoft* (USA)
GraphPad® Prism	*GraphPad Software Inc*, La Jolla (USA)
Lasergen software package	DNAstar, *Madison* (USA)
UniProt	www.uniprot.org
Expasy	www.expasy.org
ModFit LT	*Verity Software House*

2.2 Methods

2.2.1 Molecular Biology Methods

2.2.1.1 Polymerase Chain Reaction (PCR)

The polymerase Chain reaction is a commonly used method to amplify single and double stranded oligonucleotides from template DNA. During this thesis, this

method was used to amplify coFUBP1, while deleting the intrinsic stop codon and adding the restriction sites for the enzymes NcoI and XhoI.

Table 43: PCR- Mixture

Components
Template DNA (20 ng/µl)
Pfx buffer solution (10 x)
Forward and reverse primer (10 µM)
MgSO4 (50 mM)
dNTP Mix (2.5 mM)
Platinum® Pfx DNA Polymerase (2.5 U / ml)
Add H_2O to a final volume of 50 µl

The typical PCR-program consists of three parts: Denaturation, annealing and elongation. Denaturation is performed at 94°C, when the double stranded DNA is melted into two single strands. Subsequently, the temperature is lowered to 55°C - 63°C (depending on the melting temperatures of the specific primers). Reduction of the temperature leads to hybridization of the oligonucleotides (primers), which are present in an excessive amount. Afterwards, the temperature is increased to 68°C, resembling the temperature optimum of the Platinum® Pfx polymerase, to elongate the primers until double stranded DNA strand is produced, which resembles the original DNA template. Since the elongation takes place on both strands, the amount of DNA is doubled after every cycle. The assembly of the new strands is dependent on the presence of desoxynucleotides triphosphates (dATP, dGPT, dTPT, dCTP), serving as building elements and $MgSO_4$ as a polymerase cofactor [71].

The initialization is performed at 94°C for 5 minutes. Afterwards, 25 cycles consistent of 94°C for 1 minute, 63°C for 45 seconds and finally 68°C for 2.5 minute are run. Lastly, a final elongation at 68°C for 10 minutes is followed by cooling to 4°C (see Table 44).

Table 44: PCR program for *coFUBP1* amplification

PCR step	Time	Temperature	No. of Cycles
Initialization	5 minutes	94°C	1
Denaturation	1 minute	94°C	
Annealing	45 seconds	63°C	25
Elongation	2.5 minutes	68°C	
Final elongation	5 minutes	68°C	1
	∞	4°C	

Subsequently, all PCR products were purified using the Qiaquick® PCR Purification kit, according to the manufactures manual.

2.2.1.2 Digestion of DNA by Restriction Endonucleases

Restriction enzymes are classified according to their recognition and cleavage sites. Three types of endonucleases are known (class I, II and III). Class I enzymes consist of three subunits; the S- subunit recognizes the DNA sequence, the M- subunit methylates and the R- subunits cleaves the DNA. The recognition site is specific, whereas the cleavage site is accidental. Class III endonucleases consist of several subunits, recognizing specific DNA sequences and cleave 20 - 25 bp up- or downstream of those. Only class II endonucleases are widely used in every day laboratory practice. They cleave the DNA at a highly defined site. These endonucleases consist of two different proteins, the restriction endonuclease and the methylation enzyme. Recognizing the same sequence, the endonuclease cleaves the DNA, while the other methylates the hemi-methylated DNA, to protect it [71].

In this study, the *coFUBP1* fragment was ligated into *pET28b* plasmid, using the restriction endonucleases NcoI and XhoI. The digestion of both, the *coFUBP1* fragment and the plasmid, was performed as a “double digestion”, using both enzymes at the same time.

Table 45: Double digestion of *coFUBP1* and *pET28b*

Component	Plasmid-DNA	DNA-fragment
DNA	20 µl (4 µg) *pET28b*	30 µl PCR-product
Endonucleases:		
NcoI	1.5 µl	1.5 µl
XhoI	1.5 µl	1.5 µl
10x buffer 4	4 µl	5 µl
10x BSA	4 µl	5 µl
H2O	9 µl	7 µl
final volume	40 µl	50 µl

The digestion reactions were incubated for 3 hours at 37°C and subsequently loaded on an agarose gel. Desired fragments were extracted using the Qiaquick® gel extraction kit, according to the manufactures manual.

2.2.1.3 Ligation Reaction

To enzymatically link the linearized plasmid and the digested PCR-product, a ligation reaction was performed using T4 ligase. The enzyme covalently links the DNA fragments via the formation of stable phosphodiester bounds [71].

The ligation reaction was performed in a total volume of 10 µl and incubated for 3 hours at room temperature.

Table 46: Ligation reaction of *coFUBP1* and *pET28b*

Component	Plasmid-DNA
pET28b	2 µl
coFUBP1	4 µl
10x buffer	1 µl
T4 ligase	1 µl
H2O	2 µl
final volume	10 µl

Afterwards, the whole ligation reaction was transformed into chemically competent bacteria (see page 23, paragraph 2.1.3).

2.2.1.4 Transformation of Chemically Competent Bacteria

The process of non-viral free plasmid DNA transfer into competent bacteria is called transformation. In this study, the *coFUBP1*/*pET28b* plasmid was transformed into two different competent bacteria cell types: One Shot® TOP10 and BL21(DE3). One Shot® TOP10 bacteria were used for the amplification of the plasmids, BL21(DE3) cells for the recombinant expression of the protein (see page 23, paragraph 2.1.3).

Chemically competent cells were thawed on ice for 30 minutes. Afterwards, either the whole ligation reaction, or 3 µl of a Mini DNA preparation, was given to the bacteria and mixed gently. The mixture was heated at 42°C for 1.5 minutes and afterwards, cooled on ice for 1 minute. 1 ml LB-medium was given to the reaction, before incubating at 37°C and 200 rpm for 1.5 hours.

200 µl of the bacterial solution was plated on a LB-Agar plate supplemented with kanamycin. The rest of the transformation reaction was centrifuged at 830 x g for 3 minutes and the supernatant was discarded, leaving 200 µl for re-suspension of the bacterial cells. Bacteria plated on a LB-Agar plate supplemented with kanamycin and the plates were incubated over night at 37°C.

The newly formed colonies were analyzed for the presence of the transformed plasmid DNA by plasmid Mini DNA preparation with subsequent restriction endonuclease digestion (see page 36, paragraph 2.2.1.2).

2.2.1.5 Plasmid Mini DNA Preparation

Plasmid Mini preparation was used for a small-scale *coFUBP1/pET28b* preparation from previously transformed One Shot® TOP10 bacteria. After successful inoculation, several clones were picked and used to inoculate 5 ml LB medium, while shaking at 130 rpm and 37°C on a vertical shaker over night.

Afterwards, 3 ml of the inoculated culture were centrifuged at 16,000 x g for 2 minutes. The supernatant was discarded, the bacterial cells were re-suspended in 100 µl pre-chilled GTE buffer and subsequently lysed by the addition of 200 µl lysis buffer. 150 µl of ice-cold neutralization buffer was used to precipitate undesired bacterial DNA, proteins and detergents. The cell suspension was incubated on ice for 5 minutes, followed by a centrifugation at 16,000 x g for 5 minutes. The supernatant containing the desired plasmid DNA was transferred to a new reaction tube, and the DNA was precipitated by the addition of 1 ml 100% ethanol and thorough vortexing. The suspension was centrifuged at 16,000 x g for 10 minutes, afterwards the supernatant was discarded and the

DNA pellet was re-suspended in 500 µl 70% ethanol and washed via centrifugation at 16,000 x g for 10 minutes. Subsequently, the DNA pellet was air-dried for 10 minutes and later on dissolved in 30 µl HPLC purified water containing 200 µg/ml RNAse A.

To analyze the plasmid DNA, an analytical digestion with the same enzymes used for the previous cloning was performed. The generated fragments were analyzed by agarose gel electrophoresis (see page 40, paragraph 2.2.1.10). Furthermore, all clones used for protein expression were sequenced and stored as glycerol stocks at -80°C.

2.2.1.6 Glycerol Stock Preparation

To keep competent bacteria containing the desired plasmid alive, the culture is mixed with 100% sterile glycerol for long term storage at -80°C. Accordingly, 1 ml of sterile glycerol were added to 1 ml bacteria culture and mixed thoroughly by vortexing.

2.2.1.7 Plasmid Maxi DNA Preparation

Large scale preparations of plasmid DNA were performed according to the manufacturers manual of the Maxi Kit® by Qiagen. The precipitated DNA was diluted in 100 µl ddH_2O_{steril}, and to verify the successful preparation, an analytical restriction enzyme digestion and sequencing was performed (see page 40, paragraph 2.2.1.9). The concentration of the plasmid DNA was determined by the use of a NanoDrop100 device from Thermo Fisher.

2.2.1.8 Quantification of DNA Concentration and Purity

Spectrophotometric analysis was used to determine the quantity and purity of plasmid DNA and RNA samples. As nucleotides absorb ultraviolet light at 260 nm, the concentration can be calculated using the following equation.

Equation 1:

$$c\left(\frac{\mu g}{\mu l}\right) = \frac{OD_{260nm} * D * F}{M * L}$$

c= Concentration

D= Dilution factor

F= Multiplication factor (e.g. 50 for dsDNA)

M= Molecular weight of each base pair (660 g /mol)

L= Length in bp

2.2.1.9 Sequencing

The sequencing reactions were performed either by an in-house sequencing service (AG Dietrich; Georg-Speyer-Haus), or by *GATC Biotech AG* (Cologne). According to the companies guidelines, 1 µmol sequencing primer was added to 100 ng DNA for each sequencing reaction. The sequences were analyzed using Lasergene® software.

2.2.1.10 Agarose Gel Electrophoresis

To separate different DNA fragments according to their length, agarose gel electrophoresis was performed. All samples were diluted in 6x DNA sample buffer and loaded on a 0.8% - 2% agarose gel, containing 10 µg ethidium bromide (EtBr) ad 100 ml gel for visualization of the DNA.

Due to the negative charge of the DNA, the fragments migrate to the positive charge, when a direct current of 120 V to 150 V is applied. As the migration of the fragments is negatively correlated to their length, larger oligonucleotides migrate slower than the shorter ones. To define the length of the fragments, a so-called DNA-marker, with defined fragment sizes, was also applied to the gel to serve as a size standard.

The Gel Doc XR System from *BioRad* (Munich) was used to document the agarose gels. For subsequent analysis of the DNA fragments, the Qiagen Gel Extraction® Kit was used according to the manufacturer's manual.

2.2.1.11 RNA Isolation and Analysis

2.2.1.11.1 RNA Isolation

To isolate RNA from mammalian cells, 1 x 10^6 cells were first washed with PBS and afterwards collected by the use of a cell scraper in 1 ml PBS and transferred to a reaction tube. After centrifugation at 1,000 x g (3,000 rpm) for 3 minutes, cells were immediately used for RNA isolation. RNA was isolated using the RNeasy® Mini Kit by Qiagen according to the manufacturers manual. The lysis of the cells was performed using QIAshredder® columns by Qiagen. The RNA was immobilized on silica-membrane columns, where an on-column DNAse I digestion was performed to remove contaminating DNA.

2.2.1.11.2 Reverse Transcription

To convert RNA into cDNA,'s manual. 1.5 µg RNA was transcribed in a 20 µl reaction mix containing RT reaction buffer, oligonucleotide (poly dT) and random hexamer primer (*Fermentas*), dNTPs, RNAse inhibitor (*RiboLock*®, *Fermentas*) and reverse transcriptase.

2.2.1.11.3 Quantitative Real Time PCR

To determine the copy number of a given RNA molecule in a sample (e.g. cultivated cells), quantitative real time PCR (qPCR) was performed. The RNA has to be transcribed into cDNA before the analysis (see page 40 paragraph 2.2.1.11.2).

The principle of qPCRs is based on the same principle as normal qualitative PCRs (see page 34 paragraph 2.2.1.1). The difference to a conventional PCR is the use of a fluorescent dye as a quantitative indicator for the amplified target sequence, whose emitted light signal is measured during the process. Throughout all PCR cycles, quantification of the fluorescent signal allows to monitor the target amplification.

The fluorescent dye SYBR Green is a DNA intercalator and acts as a non-specific dye. To ensure the specificity of a reaction performed with SYBR Green, a combinational analysis of melting peaks, agarose gel analysis and sequencing of the PCR product has been used.

The acquired fluorescence signal is plotted against the number of cycles to quantify the target sequence. Defining of a fluorescence background threshold is used to determine the cycle at which the measured signal crosses this threshold (cycle threshold (C_T) value) for each sample.

The target copy number differences are calculated by the following equation:

Equation 2:

$$\boldsymbol{N = N_0 * E^n}$$

$$\mathrm{N = Number\ of\ amplified\ copies}$$

$$\mathrm{N_0 = Number\ of\ targeted\ copies\ at\ the\ beginning\ of\ the\ reaction}$$

$$\mathrm{E = PCR\ efficacy}$$

$$\mathrm{n = Number\ of\ cycles}$$

Measurement of the C_t value occurs at the exponential phase of the reaction, and therefore the PCR efficacy can be assumed as equal 2 (see Equation 3).

Equation 3:

$$\boldsymbol{N = N_0 * 2^n}$$

$$\mathrm{N = Number\ of\ amplified\ copies}$$

$$\mathrm{N_0 = Number\ of\ targeted\ copies\ at\ the\ beginning\ of\ the\ reaction}$$

$$n = \text{Number of cycles}$$

A relative quantification was performed using a housekeeping gene for normalization. Housekeeping genes should be stably expressed in all samples and are used to normalize possible variations in the amount and quality of the RNA samples used in every reaction. C_t values are determined from both the target and the housekeeping gene, to calculate the ΔC_t value (see Equation 4).

Equation 4:

$$\boldsymbol{\Delta C_t = C_t\,(target\ sequence) - C_t\,(housekeeping\ gene)}$$

To further compare the relative amount of a target sequence in different samples, the ΔC_t value can be used to calculate the $\Delta\Delta C_t$ value (see Equation 5).

Equation 5:

$$\boldsymbol{\Delta\Delta C_t = \Delta C_t\,(sample\ 1) - \Delta C_t(sample\ 2)}$$

Assuming a PCR efficacy of 2, the relative target sequence abundance can then be calculated by the following equation:

Equation 6:

$$\boldsymbol{relative\ target\ sequence\ abundance = 2^{-\Delta\Delta Ct}}$$

2.2.1.11.3.1 qPCR using SYBR Green –based Assays

The mRNA expression levels of all mammalian cells used in this study were analyzed by SYBR Green qPCRs. RNA was isolated and transcripted to cDNA as described before (see page 40, paragraph 2.2.1.11.1 and page 40, paragraph 2.2.1.11.2). For each sample, qPCR reactions were performed in technical duplicates and biological triplicates in a reaction volume of 24 µl. To ensure the absence of DNA contaminations, reactions were performed using nuclease-free water. Furthermore, a reaction where the cDNA was replaced by nuclease-free water was set up as a negative control. Assays were performed on a LightCycler®480 (Roche) with 4-titude 96-well plates.

The PCR-protocol was performed as followes:

Table 47: qPCR protocol

PCR step	Time	Temperature	No. of Cycles
Denaturation	15 minutes	95°C	1
Amplification	20 seconds	95°C	
	30 seconds	58°C	40
	30 seconds	72°C	
Melting Curve	10 seconds	50°C	1
	10 seconds	+2.2°C	
	…	95°C	

2.2.2 Mammalian Cell Culture

2.2.2.1 Freezing and Thawing of Mammalian Cells

To be able to store cells for long-term, cells were frozen in FCS containing 10% dimethyl sulfoxide (DMSO). The solvent prevents excessive formation of ice crystals during the freezing process, thereby protecting the cell membrane.

To freeze mammalian cells, 80%-90% confluent cells were washed with PBS, trypsinized at 37°C for 5 minutes and finally re-suspended in fresh media before passaging into a 15 ml reaction tube. Cells were centrifuged (5 minutes, 4°C, 400 x g) before decantation of the supernatant. The cell pellet was diluted in FCS containing 10% DMSO and transferred to a cryo tube (*Nunc*, Wiesbaden). Tubes were stored in a freezing container (*Cryo1°C, Nalgene*, Roskilde, Denmark) and kept at -80°C in a refrigerator over night. Afterwards, cryo tubes were removed from the freezing container and kept at -80°C for long-term storage.

Thawing of the cells was performed in a 37°C water bath. The cells were immediately diluted in 10 ml cell culture media and harvested by centrifugation (5 minutes, 4°C, 400 x g). The supernatant was decanted, and the cells were seeded in fresh medium into a new cell culture dish.

2.2.2.2 Culture of Mammalian Cells

All cells were cultured in a MCO 17 AI incubator at 37°C with 5% CO_2 in a humidified atmosphere. Hep3B and HuH7 cells were cultured in AdvancedMEM and HepG2 in RPMI medium, both containing 10% FCS, 1% P/S (10 µg/ml) and 1% L-Glutamin (100 mM). FCS was inactivated by incubation at 56°C for 30 minutes prior to use.

Cells were usually passaged twice a week (Hep3B 1:5, HuH7 1:7, HepG2 1:5). The medium was removed via aspiration, before washing the cells carefully with

PBS. 0.05% Trypsin-EDTA was given to the cells and incubated for 3 to 5 minutes in an incubator. Afterwards, detached cells were diluted in fresh media and transferred to new cell culture plates.

2.2.2.3 Determination of Cell Numbers using a Neubauer Improved Hemocytometer

To quantify cell numbers in a given solution, a Neubauer improved Hemocytometer was used. 10 µl cell suspension was applied to the counting chamber. The number of cells was counted in four large squares (each containing 16 small squares) under a microscope at 100 x magnification. The cell number was calculated according to the following equation:

Equation 7:

$$\boldsymbol{number\ of\ cells/ml = \frac{counted\ cells}{4} * 10^4}$$

2.2.2.4 Cell Lysis of Mammalian Cells With RIPA Lysis Buffer

1 x 10^6 cells were washed with PBS and then, by use of a cell scraper, collected in 1 ml PBS and transferred to a reaction tube. After centrifugation at 1,000 x g (3,000 rpm) for 3 minutes, cells were immediately used for cell lysis. Depending on the size of the cell pellet, the cells were diluted in 100 µl – 200 µl RIPA buffer (including protease inhibitor cocktail) and subsequently incubated on ice for 40 minutes. Afterwards, the lysis suspension was centrifuged at 4°C and 20,800 x g for 10 minutes. The supernatant was transferred into a new reaction tube, and the protein concentration was measured by a Bradford assay (see page 51, paragraph 2.2.4.1.1) before storage at -20°C.

2.2.2.5 Treatments of Cells

2.2.2.5.1 Treatment of Cells with Chemotherapeutic Substances and subsequent Analysis of Target Gene Expression (qRT-PCR) and Protein Expression (Western Blot)

1 x 10^6 cells were seeded in 10 cm plates. Compounds were pre-diluted in 100% DMSO to a concentration of 1,000 µM. Medium was removed via aspiration and replaced by fresh medium ad 10 ml. Cells were treated for 6 hours according to the following table. qPCR experiments were performed in biological triplicates and technical duplicates, WT and a DMSO-treated control cells were included for each experiment.

Table 48: Treatment schedule for target gene expression studies (qPCR)

Compound	Initial Concentration [µM]	Final Concentration [µM]	Quantity of Compound [µl]	Final Volume [ml]
untreated				10
DMSO (ctrl.)			100	10
camptothecin	1,000	1	10	10
		5	50	10
		10	100	10
7-ethyl-10 hydroxy camptothecin	1,000	1	10	10
		5	50	10
		10	100	10
NSC 724998	1,000	1	10	10
		5	50	10
		10	100	10
NSC 725776	1,000	1	10	10
		5	50	10
		10	100	10

After 6 hours of treatment, cells were harvested, and either RNA preparation (see page 40, paragraph 2.2.1.11), or cell lysis (see page 44, paragraph 2.2.2.4) was performed as described before.

2.2.2.5.2 Cell Treatment

To determine the effect of different compounds on cell death and cell cycle alterations in HCC cell lines, 5 x 10^5 cells were seeded in 6 cm plates. Medium was removed via aspiration and replaced by fresh media ad 4 ml. Compounds were pre-diluted in 100% DMSO to a concentration of 1,000 µM. Cells were treated for 24 hours and 72 hours in single treatments, or for 24 hours in double treatments combined with doxorubicin, mitomycin C, cisplatin or sorafenib (Treatment schedule see below).

Table 49: Nicoletti assay single treatment schedule

Compound	Initial Concentration	Final Concentration	Quantity of Compound [µl]	Final Volume [ml]
untreated				4
DMSO ctrl.			200	4
MeOH ctrl.			400	
DMSO/MeOH ctrl.			200 + 400	
camptothecin	1,000µM	1 µM	4	4
		5 µM	20	4
		10 µM	40	4
tosufloxacin	1,000µM	1 µM	4	4
		10 µM	20	4
		50 µM	200	4
pregnenolone	1,000µM	1 µM	4	4
		10 µM	20	4
		50 µM	200	4
mitomycin C	400µg/ml	5 µg/ml	50	4
		10 µg/ml	100	4
		20 µg/ml	200	4
		40 µg/ml	400	4
sorafenib	1,000µM	2.5 µM	10	4
		5 µM	20	4
		10 µM	40	4

Single treatment was performed in technical duplicates, as was the double treatment with pregnenonlone, tosufloxacin or 7-ethyl-10-hydroxycamptothecin (see page 30). Double treatments with camptothecin were performed in biological triplicates and technical duplicates.

Table 50: Camptothecin double treatment

	WT	1.25 µM CPT	2.5 µM CPT	5 µM CPT
WT	x	x	x	x
DMSO	x			
MeOH	x			
DMSO/MeOH	x			
4 µg/ml mitomycin C	x	x	x	x
1.25 µg/ml doxorubicin	x	x	x	x
2.5 µg/ml cisplatin	x	x	x	x
2.5 µM sorafenib	x	x	x	x

Table 51: Tosufloxacin double treatment

	WT	1 µM tosu	10 µM tosu	30 µM tosu
WT	x	x	x	x
DMSO	x			
MeOH	x			
DMSO/MeOH	x			
4 µg/ml mitomycin C	x	x	x	x
1.25 µg/ml doxorubicin	x	x	x	x
2.5 µg/ml cisplatin	x	x	x	x
2.5 µM sorafenib	x	x	x	x

Table 52: Pregnenolone double treatment

	WT	1 µM pregno	10 µM pregno	50 µM pregno
WT	x	x	x	x
DMSO	x			
MeOH	x			
DMSO/MeOH	x			
4 µg/ml mitomycin C	x	x	x	x
1.25 µg/ml doxorubicin	x	x	x	x
2.5 µg/ml cisplatin	x	x	x	x
2.5 µM sorafenib	x	x	x	x

Table 53: 7-ethyl-10-hydroxycamptothecin double treatment

	WT	1.25 µM HC	2.5 µM HC	5 µM HC
WT	x	x	x	x
DMSO	x			
MeOH	x			
DMSO/MeOH	x			
4 µg/ml mitomycin C	x	x	x	x
1.25 µg/ml doxorubicin	x	x	x	x
2.5 µg/ml cisplatin	x	x	x	x
2.5 µM sorafenib	x	x	x	x

2.2.2.6 Nicoletti Assay

During apoptotic cell death, genomic DNA is hydrolyzed by specific nucleases, a process which can be measured by different techniques, to discriminate between apoptotic and normal cells. Propidium Iodid (PI), a dye that specifically intercalates into nucleic acids, is used in to determine the quantity of dead cells via flow cytometry. For this purpose, cells were fixed in 70% ethanol and

subsequently stained with PI, in the presence of RNAse. After RNA digestion, the intensity of the PI signal is directly proportional to the DNA amount. Not only the amount of apoptotic cells, but also the cell cycle distribution of living cells can be determined using this assay. Fixation with ethanol leads to permeabilisation of the nuclear membrane, and DNA fragments leak out of the dead cells, which then appear in a subG_1 peak during the flow cytometry analysis [72]

Cells were harvested with trypsin and transferred to FACS tubes. After centrifugation (5 minutes, 4°C, 400 x g), the supernatant was discarded, cells were washed with 1 ml PBS and again pelleted by centrifugation. Afterwards, cells were fixated by adding 1 ml ice-cold 70% ethanol with thorough mixing, and subsequently stored at 4°C for at least 24 hours up to 14 days.

Cells were then washed with 38 mM Na-Citrate (pH 7.4), centrifuged and stained with 200 – 500 µl PI staining solution, depending on the amount of cells. For the staining reaction, cells were kept 20 minutes at room temperature in the dark. Flow cytometry measurement was performed on a *Becton Dickinson Biosciences FACS Calibur*. The PI fluorescence was measured in FL2 at 585 nm, separated into FL-A/FL-W channel (DDM module) and analyzed using Cell Quest-*Pro* software (*Becton Dickinson Biosciences*). For each sample, at least 20,000 events were collected to ensure significance of the statistics. Cell cycle profile analysis was performed using ModFit LT (*Verity Software House*).

Staining solution: 38 mM Na-Citrate (pH7.4), 50 µg/ml propidium iodide, 5 µg/ml RNAseA.

2.2.2.7 WST Assay

WST assays are used to quantify living cells by determination of the metabolic activity of the cells. The underlying principle is the enzymatic conversion of a dye into a cleavage product, whose absorption spectrum is different from the one of the uncleaved dye. If cells expand, it results in an increase in the overall mitochondrial dehydrogenases, leading to increased enzyme activity and subsequently to an increased amount of cleavage product. The amount of cleavage product directly correlates with the amount of active enzymes. Its quantification can be achieved by spectrophotometric measurements.

WST assays were performed according to the user manual of the Cell Proliferation Reagent WST-1® by *Roche Diagnostics, Mannheim*. Hep3B cells were seeded with a density of 3,000 cells per well in a 96-well plate. Cells were

treated for 48 hours with compound or vehicle in the presence of 10% FCS. Afterwards, the WST-1 reagent was incubated for 4 hours, before cell viability was assessed using a microplate reader (*infinite M200, Tecan Group Ltd, Crailsheim, Germany*). Values were calculated as a ratio of the absorbance between treated samples and solvent control.

Experiments were performed in the laboratory of Prof. Dr. Eugen Proschak, University of Frankfurt.

2.2.3 Recombinant Protein Expression Methods

2.2.3.1 Protein Expression in an E. coli Auto-Induction System

2.2.3.1.1 Principles of protein expression using lac promoter-driven genes

Originally in bacterial cells, lac gene products were required for the metabolization of lactose to glucose and galactose in the absence of glucose in the surrounding media, to provide a secure carbon source. The lac operon is composed of four genes: lac I, lac Z, lac Y and lac A. Whereas the last three genes are under the control of the lac promotor, lac I is under the control of its own weak promotor, transcribing the lac repressor. In a tetraedic conformation, the lac repressor can bind to the lac promotor and thus prevent the transcription of downstream targets. In the presence of glucose in the bacterial medium, cAMP (cyclic adenoside-monophosphate) levels are reduced, leading to diminished amounts of CRP (cAMP response protein), which results in less activation of lac gene transcription. Furthermore, glucose inhibits the function of lactose permease, which is needed for the transport of lactose into the bacteria cell, leading to low intracellular lactose amounts. Depletion of glucose in the media leads to diminished amounts of lac repressor, followed by an increase of lactose import into the cell via lactose permease activity. β-Galactosidase, the product of the lacZ gene transforms lactose into allolactose. Allolactose in turn, is able to bind to the lac repressor, inhibits its binding to the lac promotor and thus leads to the transcription of lac Z, lac Y and lac A.

Elevation of cAMP, serving as a starvation signal in bacteria, leads to the binding of CRP and enhanced transcription levels of *lac* [73].

BL21(DE3) bacterial cells contain a T7 RNA polymerase, which is provided via the chromosomal DNA of the D3 prophage. This polymerase is under the control of a lac promotor, therefore its transcription can be induced via allolactose.

Consequently, target gene expression, which is under the control of T7 promotor, can occur.

2.2.3.1.2 Auto–Induction of coFUBP1 protein expression

Auto-induction was performed according to the protocol established by Studier et al. (2005) [74] in a 10 L fermenter. A freshly prepared 100 ml overnight culture was used to inoculate the 10 L main culture. Cells were grown to an optical density of OD_{600}= 1.4 at 37°C. Afterwards, the temperature was reduced to 22°C, and cells were grown for 35 hours before harvesting. To prevent excessive amounts of foam formation, 2 ml anti-foam was added daily. The ventilation of the system was ensured by a constant airflow between 4 and 12 l/min. The bacterial pellet was distributed into 6 parts and stored at -20°C.

2.2.3.2 Cell Lysis of Bacterial Cells using a Constant Cell Disruption System

Different types of pressures and stresses are applied to the cells via a cell disruption system by *Constant System Limited* (Northhants, United Kingdom) to disrupt bacterial cells.

2.2.3.2.1 Large Scale Cell Lysis of BL21(DE3) bacteria

To purify the expressed co*FUBP1* from BL21(DE3) bacteria, 3 out of 6 cell pellets obtained from 10 L auto-inducted cell suspension were used. The pellets were thawed on ice and re-suspended in bacterial lysis buffer, containing DNAse and complete EDTA-free pills®. Subsequently, the cell suspension was processed in a constant cell disruption system using a three-step protocol. Beforehand, the system was washed with 100 ml lysis buffer, while applying a pressure of 0.5 kbar. Afterwards, the cell suspension was applied with a pressure of 1 kbar, followed by two runs at 2 kbar pressure. All steps were performed at 4°C. After cell disruption, the system was cleaned with 200 ml ddH_2O and 2 N 200 ml NaOH.

2.2.4 Protein Biochemistry Methods

2.2.4.1 Protein Concentration Quantifications

2.2.4.1.1 Bradford Assay

During the binding of Coomassie brilliant blue G-250 to proteins, the absorption maxima of the dye shifts from 465 nm (without protein) to 595 nm (with protein). The absorption increase at 595 nm provides the signal for the quantification of the protein concentration in the tested solution [75].

5 µl protein solution were diluted in 800 µl ddH_2O and mixed thoroughly. Afterwards, 200 µl RotiQuant Bradford (5 x) from *Carl Roth GmbH&CoKG*

(Karlsruhe) were given to the dilution, mixed and incubated at room temperature for 5 minutes. Subsequently, absorbance at 595 nm was measured in a spectrometer, and the protein concentration was determined via a standard calibration curve.

2.2.4.1.2 NanoDrop 1000

To determine protein concentrations between 0.1 and 100 mg/ml of purified protein solutions, the absorption spectra at 280 nm were measured. At 280 nm, the aromatic ring systems of tryptophan and tyrosin, as well as cysteine disulfide bonds absorb UV radiation. The quantification with the NanoDrop 1000 is only reliable, if the mass extinction coefficient and the molar mass of the tested protein sample are included. In this study, these parameters were generated using the ExPASy ProtParam tool (*Bioinformatics Resource Portal*).

Table 54: Mass extinction coefficient of FUBP1

Protein	Molar mass (kDA)	Molar extinction coefficient ($M^{-1}cm^{-1}$)	Mass extinction coefficient ($L\ gm^{-1}\ cm^{-1}$)
co*FUBP1*	68.6	67,270	0.996

2.2.4.2 Sodium Dodecyl Sulfate Polyacrylamide Gel Electrophoresis (SDS-PAGE)

Gel electrophoresis serves as an analytic tool to determine the apparent molecular weights of proteins in a solution. The proteins bind to the detergent SDS, which leads to a negatively charged SDS-protein complex with a constant charge-mass ratio (1.4 g SDS / g protein in 1% SDS-solutions). Furthermore, SDS denatures disulfide bridges, and thereby prevents protein-protein interactions, leading to protein-SDS complexes of various proteins, which only differ in mass. Upon loading on a polyacrylamide gel in a continuous electric field, these complexes migrate to the positive pole [75].

In this study, 10% and 12% SDS-gels with a thickness of 100 or 150 mm were used.

Table 55: SDS-PAGE composition

Ingredient	2.5% stacking gel	10% running gel	12% running gel
ddH_2O	5.52 ml	6.25 ml	5.25 ml
Acrylamid/Bisacrylamid (37.5 : 1)	1.25 ml	5 ml	6 ml
SDS 20% (w/v)	37.5 µl	75 µl	75 µl
1.5M Tris-HCl pH 6.8	-	3.75 ml	3.75 ml
1M Tris-HCl pH 8.8	925 µl	-	-
APS 10% (w/v)	100 µl	100 µl	100 µl
TEMED	5 µl	10 µl	10 µl

Protein samples were diluted in 5 x SDS-loading buffer and heated to 95°C for 5 minutes, before loading on a SDS-PAGE gel. The electrophoresis was performed using a *Mini-Protean II System* from *BioRAD* (Munich), filled with 1 x SDS-running buffer, and with a current voltage of 80 V for the stacking gel and 150 V for the running gel. Additionally, 18 µl *BenchMark® Prestained Protein Ladder* (*Invitrogen*, Karlsruhe) were applied to the gel as a size standard.

2.2.4.3 Coomassie Staining of SDS-Gels

To fixate and visualize proteins in a SDS-PAGE gel, Coomassie staining was performed. Gels with a thickness of 150 mm were stained in Coomassie staining Solution for one hour on a vertical shaker. De-staining was performed in water over night.

Gels with a thickness of 100 mm were stained with Quick Coomassie. For this purpose, gels were first boiled in water (30 seconds, microwave), afterwards in Quick Coomassie (30 seconds, microwave), in which they were finally incubated on a vertical shaker for 10 minutes. De-staining was performed with MiliQ-H_2O for 1 hour on a vertical shaker.

2.2.4.4 Protein Transfer onto Nitrocellulose Membranes

Semi-dry blotting was used to transfer proteins from SDS-PAGE gels onto a nitrocellulose membrane. First, the nitrocellulose membrane has to be activated by a short incubation in blotting buffer with 20% methanol. The activated membranes are able to bind protein migrating along an applied voltage due to their hydrophobic surface property [75].

Blotting was performed according to the following set up: 3 pieces of pre-wetted whatman paper, nitrocellulose membrane, SDS-gel and 3 pieces of pre-wetted whatman paper. Proteins were transferred for 2 hours with 45 mA current per membrane, in a blotting chamber (*Keutz*, Reiskirchen).

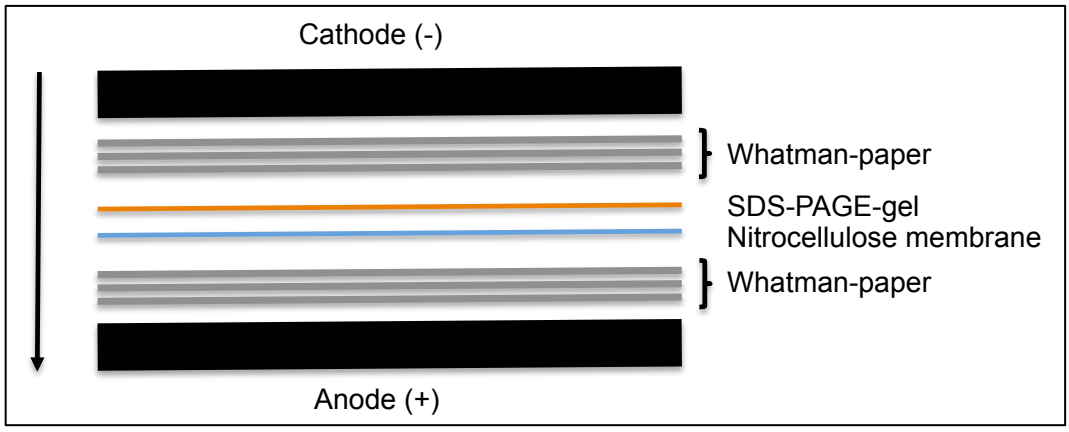

Figure 10: Semi-dry-blot construction

To verify successful blotting of the proteins, the membrane was incubated with *Ponceau S* (*Fluka*, Buchs, Switzerland) for 10 minutes on a vertical shaker, to stain proteins. Removal of background staining was achieved by pouring ddH_2O onto the membrane.

2.2.4.5 Immunodetection of Blotted Proteins

Prior to immune blotting, membranes were incubated with 3% skimmed-milk powder in TBS-T for 1 hour at room temperature on a vertical shaker. This procedure is required to saturate unspecific protein binding sites on the nitrocellulose membrane, leading to decreased background signals. After blocking, membranes were incubated with primary antibodies diluted in blocking buffer and incubated at 4°C and mild shaking over night. Afterwards, membranes were washed 3 times with TBS-T for 10 minutes, each time at room temperature. Incubation with the secondary antibody diluted in blocking buffer was performed at room temperature for 1 hour with mild shaking. Subsequently, membranes were again washed 3 times, before the proteins were visualized using Amersham ECL Prime Western Blotting Detection Reagent from *GE Healthcare* (Munich). Horseradish peroxidase (HRP), which is coupled to the secondary antibody, catalyzes the oxidation of luminol, which results in a to a chemiluminescent signal [75].

3 ml freshly prepared ECL-reagent was poured onto the membrane for 1 minute, and residual liquid was removed carefully, before the signals were detected with a photosensitive film.

2.2.4.6 Immobilized Metal Ion Affinity Chromatography (IMAC)

To purify recombinant proteins containing hexa-histidin tags, 25 ml Ni Sepharose High Performance affinity media for high-resolution (GE Healthcare, Munich) was packed onto an Omnifit® Chromatography Column (*Diba Industries*, USA). Ni Sepharose High Performance consists of highly cross-linked agarose beads to which a chelating group has been coupled. This chelating group is pre-charged with Ni^{2+} that selectively retains proteins with exposed histidine groups. The purification was performed at 4°C using an Äkta purifier® system.

Cell lysate, prepared from the Constant Cell Disruption System, was centrifuged at 20,000 x g for 1 hour at 4°C. The supernatant was applied to the Ni-Sepharose column via a peristaltic pump system with flow rate of 2.5 ml / minute at 4°C.

After absorption of the his-tagged proteins to the column, it was equilibrated with 4 column volumes of washing buffer with a flow rate of 4 ml / minute. Afterwards, the loaded column was washed with a gradient of up to 55% elution buffer (final imidazole concentration 222 mM) for 6.25 column volumes, wile fractionating 13 ml volume samples using a flow rate of 2 ml / minute. Elution of protein was achieved using a flow of 1 ml / minutes of a continually increasing IMAC elution buffer gradient up to 95% for 18.75 column volumes, while fractionating 12 ml volume samples. The final elution step was performed with 100% elution buffer and a flow rate of 2 ml / minute for 2 column volumes, while fractionating 13 ml volume samples. Upon analysis of the chromatogram, fractions showing an elution peak at A_{280} absorption were analyzed by SDS-PAGE electrophoresis. Fractions containing co*FUBP1* were pooled and applied to a heparin affinity column.

2.2.4.7 Heparin Affinity Chromatography

Heparin is a negatively charged, polydispersed linear polysaccharide, which selectively interacts with many enzymes and, among others, with DNA-binding proteins [76].

Following the IMAC purification protocol, this absorption chromatography was used as a second purification step for recombinantly expressed co*FUBP1*. The purification was performed at 4°C using an Äkta Purifier® system. Pooled fractions of the IMAC purification were applied to 5 x 5ml HiTrap heparin HP columns (*GE Healthcare*, Munich) via a peristaltic pump system with a flow rate of 2.5 ml / minute at 4°C.

After absorption of the protein to the column, it was washed with 10 column volumes 10% (0.2 M NaCl) heparin elution buffer with a flow rate of 2 ml / minute and fractionation of 13 ml volume samples. The elution of proteins was achieved in 3 steps with a flow rate of 2 ml / minute each. First, a continually increasing elution buffer gradient from 0% to 17% for 51 column volumes and a fractionation in 13 ml volume samples were performed. Secondly, a gradient from 17% to 21% elution buffer was performed for 15 column volumes, fractionating 5 ml volume samples. In the third step, a gradient from 21% to 28% elution buffer was used, fractionated in 13 ml volume samples for 18 column volumes. The final elution was performed with 100% elution buffer for 1 column volume with a flow rate of 2 ml / minute without fractionation. Upon analysis of the chromatogram, fractions showing an elution peak at A_{280} absorption were analyzed by SDS-PAGE electrophoresis. Fractions containing co*FUBP1* were pooled, concentrated and applied to a HiLoad 16/60 Superdex 200 column (*GE Healthcare*, Munich) for size exclusion chromatography.

2.2.4.8 Size Exclusion Chromatography (SEC)

Size exclusion chromatography was performed using a HiLoad 16/60 Superdex 200 column (*GE Healthcare*, Munich). Pooled fractions from the heparin column purification were concentrated to an end volume of 4 ml. The initial volume of 36 ml was first concentrated in an Amicon stirr cell system to a volume of 20 ml, using a 10 kDa membrane. The remaining volume of 16 ml was reduced to an end volume of 4 ml using a 30 kDa membrane with an input concentration of 0,378 µg/µl.

The protein solution was applied via an Äkta Purifier® system in a volume of 4 ml with an initial flow rate of 0.5 ml / minute. Afterwards, the flow rate was increased to 1 ml / minute and fractionation was performed in 2 ml volume samples.

2.2.5 Binding Studies

2.2.5.1 Surface Plasmone Resonance

Surface plasmone resonance (SPR) is a method used to determine binding events on a surface, enabling the determination of kinetic and thermodynamic binding constants.

To calculate binding constants, one partner, the ligand, is bound to a metal surface (mostly gold), whereas the other partner, the analyte, is applied in a fluid phase.

At the interface between the metal and the di-electrium (air, water, etc.) an electronic cloud is formed, which can be set into oscillation via a light wave with a matching frequency. Based on the conservation law of energy, the light energy will be included in the electronic cloud, which leads to the stimulation of the surface plasmone. A plasmone is described as a light wave, which travels along the metal surface, containing an electromagnetic pulse, which is decreasing exponentially to the distance from the surface. A helium-neon-laser is used as the light source and the gold surface as well as an adjacent glass prism are located at a rotatable platform, leading to a modifiable incidence of light. The light, reflected by the gold surface, is measured with a photocell. For incidence angles higher than the critical angle of total reflection, the light intensity decreases with higher angles reaching a minimum, which describes the maximal excitation of the plasmone, before rising again to its original intensity. If molecules bind to the surface, its refractive index changes, leading to a change in the critical light angle for total reflection, which can be detected by the photocell.

In SPR studies, the modification of the optical layer thickness, described as the modification of the refractive index, is measured [77]. The results are displayed in a SPR sensogram where movement of the measured signal (shown as Response Units [RU]) are measured over time.

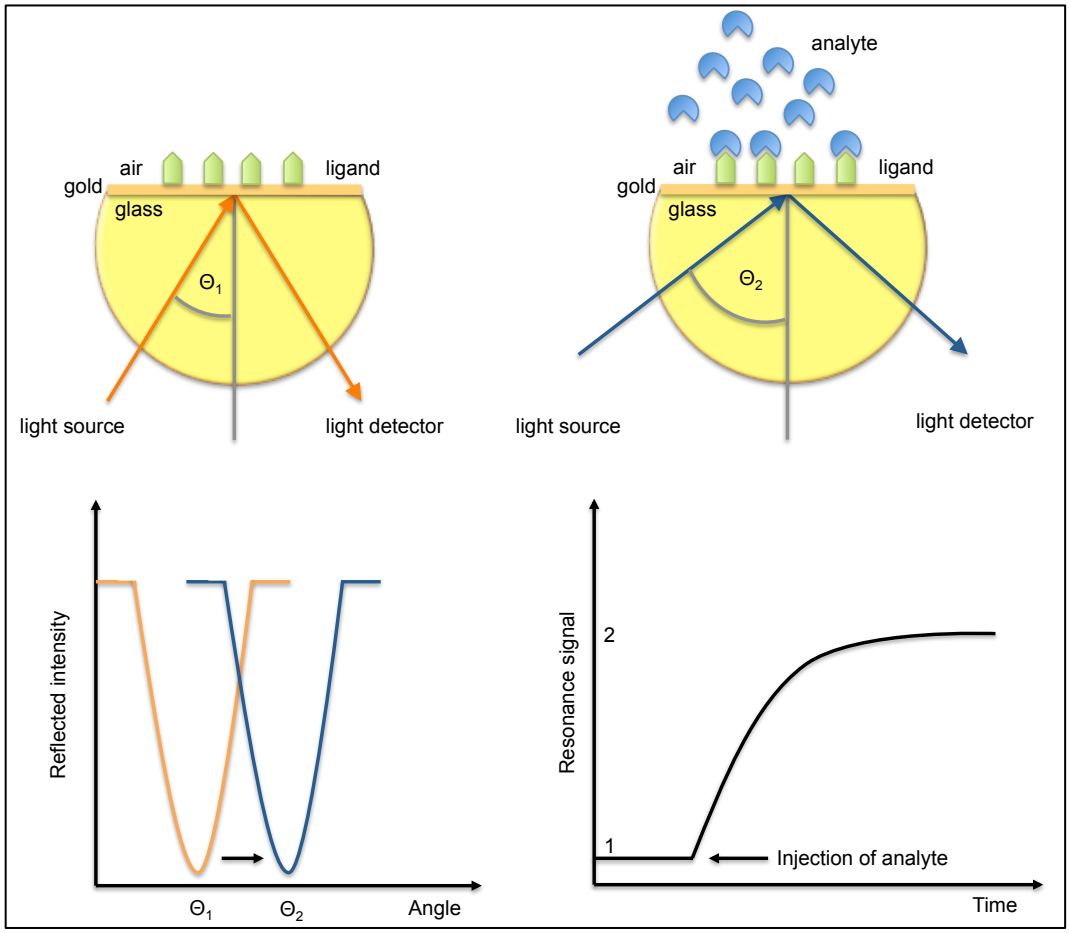

Figure 11: Schematic illustration of the SPR mechanism: On the gold sensor surface, a ligand is bound. Monochromatic, polarized light is used to determine the angle needed for the excitation of the surface plasmone. At this time point, a dip in the reflected light intensity is measureable. If an analyte is binding to the ligand, the refractive index of the surface changes, leading to a shift of the reflected light intensity dip to higher angles. The change of the SPR-dip is the measured signal and its movement over time generates the SPR sensorgram.

2.2.5.1.1 The Equilibrium Mode Analysis

The analysis of the equilibrium is used to determine the strength of the binding. The analyte is given to the ligand until the signals level out, meaning that the net association is equal to the net dissociation. This process is repeated with several analyte concentrations. The response rates are afterwards plotted versus the analyte concentration, and a fit is used to determine the binding affinity constant (K_D).

2.2.5.1.2 Determination of the Binding Constant for coFUBP1 and FUSEp21

To determine the binding constant for the interaction between coFUBP1 and *FUSEp21*, two different approaches were chosen with the ProteOn^{TM} XPR36 system.

In one approach, a ProteOn™ GLM Sensor Chip to covalently bind the recombinant protein, and in a second approach, a ProteOn™ NLC Sensor Chip to bind the biotinylated *FUSEp21* oligonucleotide were used. With both chips, 6 parallel channels could be used simultaneously to immobilize one of the binding partners. Both approaches were tested to ensure that the immobilization of either partner does not interfere with the binding of coFUBP1 and *FUSEp21*.

The GLM Chip is used to covalently bind proteins via general amine coupling. The surface of the chip was activated with 0.1 x and 0.5 x NHS/EDC, before loading of the protein. coFUBP1 was loaded with 3,800 response units (RU). Furthermore, MBP (maltose-binding-protein, approximately 45 kDa), used as a negative control protein, was loaded with 1,800 response units. Two negative control oligonucleotides *31* and *39* of the *FUSEp21* locus were used in addition to *FUSEp21*, to prove the specificity of the binding. Oligonucleotides were chosen from the EMSA assays performed by Rabenhorst et al. 2009 [1].

To determine the thermodynamic binding capacity of coFUBP1 and *FUSEp21*, the oligonucleotide was used in a dilution series of 0 nm, 10 nM, 50 nM and 100 nM. Analysis was performed in the equilibrium mode using a Langmuir fit.

The NLC Chip was used to immobilize the 5'-end biotinylated *FUSEp21* oligonucleotide via the streptavidin-coated chip surface. 50 nM *FUSEp21* was immobilized with a final RU of 120.

2.2.5.1.3 Hit-Confirmation by SPR Measurements

To ensure that all inhibitors can be tested in the SPR system (independently of their potential, individually used FUBP1 binding motif), the oligonucleotide was used as ligand leading to a high degree of freedom for the unbound, recombinant protein, used as the analyte.

FUSEp21 was used as a ligand immobilized with 120 RU, bound to a ProteOn™ NLC Sensor Chip via its biotinylated 5'-end. coFUBP1 was used as the analyte (50 nM). Differences in the response units after 300 seconds dissociation time were used to determine inhibitory effects of the tested hit compounds. A dilution series of each compound (0 µM (DMSO control), 1 µM, 10 µM and 50 µM) was used to determine the inhibitory effect. The analyte and the compounds were mixed immediately prior to measurement.

2.2.5.2 Microscale Thermophoresis

Microscale thermophoresis (MST) is used to determine molecular interactions via the measurement of changes in the hydration shell, charge or size of the molecules due to their interaction. It can be performed under close-to-nature conditions, as molecules can be measured label-free and/or immobilization-free in any buffer or complex bioliquid. Any change of the hydration shell of the analyzed biomolecules due to changes in their structure affects the movement along a temperature gradient and can be used to determine binding affinities via an altered thermal movement (*Nano Temper Technologies*).

To generate a precise temperature gradient within thin glass capillaries filled with the examined samples, an infrared laser is used. To monitor the movement of the molecules along the temperature gradient, the fluorescence of the molecules is detected at the heated spot of the capillary. This fluorescence can either be intrinsic (e.g. tryptophane) or extrinsic through the use of a dye or a coupled fluorescence protein (e.g. GFP) (*Nano Temper Technologies*).

The thermophoretic movement takes place in different steps. First, the laser is switched on, resulting in a fast heating of the capillary and a temperature jump, which leads to a decrease of the fluorescence signal. Afterwards, the thermophoresis occurs until the molecular movement reaches steady state. Finally, the laser is turned off again, and the back diffusion is measured.

If one molecule is used in different dilutions, the normalized fluorescence (F_{hot} / F_{cold}) of each measurement can be plotted against the concentration of the diluted binding partner, allowing the determination of a K_D value.

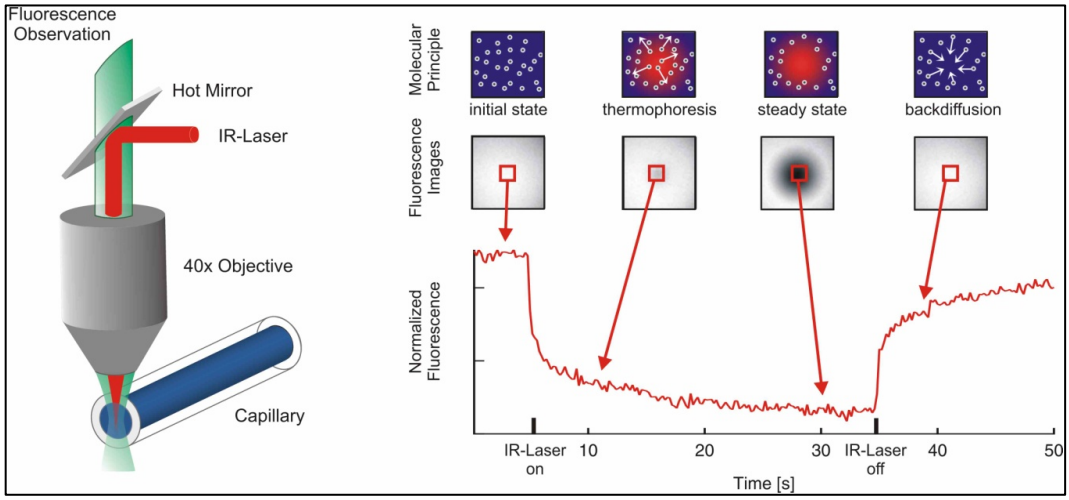

Figure 12: Schematic Illustration of MST measurements (http://www.nanotemper-technologies.com): In the initial state, the molecules are equally distributed in the capillary. If the laser is switched on, thermophoresis of the molecules take place, which leads to a rapid drop of the normalized fluorescence signal. After 30 seconds, a steady state of the molecule movement is reached, before the laser is turned off, followed by the backdiffusion of the molecules.

2.2.5.2.1 Binding Constant Determination for coFUBP1 and FUSEp21 by MST

The recombinant coFUBP1 protein was labeled through the help of a NT.115 Protein labeling kit RED-NHS, performed according to the manufacturer's manual. The single stranded oligonucleotide remained unlabeled. The *FUSEp21* oligonucleotide was titrated to a stable concentration of 1 µM recombinant coFUBP1.

The measurement was performed in a Monolith NT.115^{TM} device from Nano Temper Technologies (Munich). Monolith^{TM} Standard Treated Capillaries were used. Fluorescence was excited using red LED light (100%) with an intensity of 15%.

2.2.5.3 AlphaScreen® Technology

The Amplified luminescent proximity homogenous assay (Alpha) screen is used to determine inter-molecular interactions of various molecules including DNA, RNA and proteins. It represents a bead-based assay system, which is performed in a 96-, 384- or 1536- well plate format. If the molecules, captured on the surface of different beads, are binding to each other, illumination of the donor bead leads to a signal transfer to the acceptor bead, resulting in the production of luminescence, which can be detected. The donor beads contain a photosensitizer, phtalocyanine, which converts ambient oxygen to singlet oxygen, when excited with a light signal at 680 nm. The singlet oxygen can travel up to 200 nm in solution within its 4 µsec half-life. If an acceptor bead is located within this proximity, the singlet oxygen transfers its energy to thioxene derivatives on

the bead, resulting in a light production at 520-620 nm. In absence of the acceptor bead, the singlet oxygen falls back into its ground state, and no signal is produced (*Perkin Elmer*).

2.2.5.3.1 Inhibitor Screening to Interfere with the Binding of FUBP1 and FUSEp21

Recombinant coFUBP1 was bound to a protein-A acceptor bead via the specific anti-FUBP1 antibody N-15 (*Santa Cruz biotechnology*, Heidelberg), whereas *FUSEp21* was biotinylated at its 5'-end and bound to a streptavidin donor bead. To perform the screening, a two-step protocol was established. First, potential inhibitors were diluted to a final concentration of 50 µM. 10 µl of each potential inhibitor was given into one well of a 384-well plate. Afterwards, two mixtures were prepared, according to the schedule below (Table 56). Mixture I (10 µl) was given into each well, centrifuged for 12 seconds in a quick run mode and afterwards incubated for 1 hour at room temperature in a dark room. Mixture II (5 µl) was added, the plate was centrifuged again and afterwards incubated for 20 hours at room temperature in a dark room, before evaluating the results with the Envision® multilable plate reader SN 1040002, *Perkin Elmer*. Hits were defined as molecules that diminished the signal intensity down to 30% or less.

Table 56: AlphaScreen® experimental setup

	final concentration	Mix1	Mix 2
coFUBP1	3 nM	x	
FUSEp21	1.6 nM	x	
poly dIdC	3 µM	x	
N-15 antibody	10 pM	x	
Acceptor beads	1: 100	x	
Donor beads	1: 50		x

2.2.6 Xenograft Experiments

Hep3B cells (passage 16 after thawing) were harvested by trypsinization and collected in a sterile reaction tube. Cells were separated by carefully pipetting them through a 100 µm cell strainer. This procedure was repeated a second time, before using a 40 µm cell strainer for the last separation step. For each mouse, 5×10^6 Hep3B cells were diluted in a total volume of 75 µl PBS and distributed in

individual reaction tubes. Shortly before injection of the cells into the flank of immune compromised NOD/SCID mice, 25 µl matrigel was mixed to each vial. Tumors were allowed to grow to an average size of 100 mm^3. Mice were grouped (6 – 8 mice per group) and treated according to the schedule below (Table 57). During the treatment period, mice were weighed daily for 21 days, and tumor volumes were measured every third day. After the treatment period, tumor size and mouse weights were measured twice a week. Mice were sacrificed, when tumors reached a volume of 1000 mm^3. The effects of six different treatments on tumor growth were evaluated: irinotecan, mitomycin C, irinotecan + mitomycin C, sorafenib, i.p. control, and oral control.

Table 57: First xenograft experimental grouping and experimental setup

Groups	Concentration	Solvent	Application	Application schedule
i.p. control		0.9% NaCl	i.p	5 days / week, 3 weeks
oral control		Kolliphore® EL / Ethanol (50/50)	oral	7 days / week, 3 weeks
sorafenib	30 mg/kg	Kolliphore® EL / Ethanol (50/50)	oral	7 days / week, 3 weeks
irinotecan	20 mg/kg	0.9% NaCl	i.p.	5 days / week, 3 weeks
mitomycin C	3.25 mg/kg	0.9% NaCl	i.p.	1 day / week, 3 weeks
irinotecan + mitomycin C	10 mg/kg 0.8125 mg/kg	0.9% NaCl	i.p.	5 days / week, 3 weeks

i.p.: intra peritoneal

For the second treatment experiment, concentrations were reduced according to Table 58.

Table 58: Second xenograft experimental grouping and experimental setup

Groups	Concentration	Solvent	Application	Application schedule
i.p. control		0.9% NaCl	i.p	5 days / week, 3 weeks
irinotecan	10 mg/kg	0.9% NaCl	i.p.	5 days / week, 3 weeks
mitomycin C	0.8125 mg/kg	0.9% NaCl	i.p.	1 day / week, 3 weeks
irinotecan + mitomycin C	see single treatment concentrations	0.9% NaCl	i.p.	5 days / week, 3 weeks

i.p.: intra peritoneal

3 Results

3.1 Recombinant Protein Expression and Purification of Codon-Optimized Human FUBP1 in *E. coli*

*3.1.1 Cloning Strategy for C-terminally His_6-tagged Codon-Optimized FUBP1 (co*FUBP1*) in pET28b*

Bacterial codon-optimized human *FUBP1*, synthesized by GenScipt®, was delivered in a *pUC57* plasmid. For subsequent cloning of *FUBP1* into the *pET28b* vector, the restriction sites NcoI and XhoI were introduced by PCR amplification at the 5'- and 3'- ends. Furthermore, this amplification led to the desired deletion of the intrinsic STOP codon TGA.

Subsequently, the construct was purified and ligated into a *pET28b* expression vector, harboring a c-terminal His_6-tag (Figure 13).

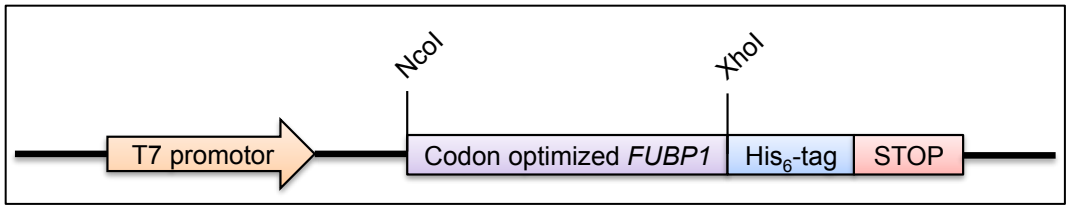

Figure 13: Cloning strategy for c-terminal His_6-tagged codon-optimized FUBP1 in *pET28b*. *coFUBP1* was cloned into the multiple cloning site (MCS) of the *pET28b* plasmid using the unique cloning sites NcoI and XhoI. The *FUBP1* coding sequence is under the control of a *T7* promotor, suitable for protein expression in bacterial cells via IPTG or lactose induction. The TGA Stop codon of the coding sequence was deleted, leading to a c-terminal His_6-tag delivered by the *pET28b* vector.

After ligation into the MCS of *pET28b*, using the unique restriction sites NcoI and XhoI, the plasmid was transformed into BL21-DE3 expression bacteria. Four of the resulting clones were used to inoculate twelve different liquid cultures, 3 each. Plasmid preparations were used to verify the presence of *coFUBP1* by test cleavage and sequencing of different constructs.

The analysis of the test cleavage with a 0.8% agarose gel revealed that all clones showed the expected fragment sizes for co*FUBP1* (1944bp) and the *pET28b* backbone (5326bp) (see Figure 14). Furthermore, sequencing analysis of the clones 1A, 2A, 3A and 4A demonstrated that all of them inherited the correct sequence of co*FUBP1*.

For the subsequent protein expression, clone 2A was used.

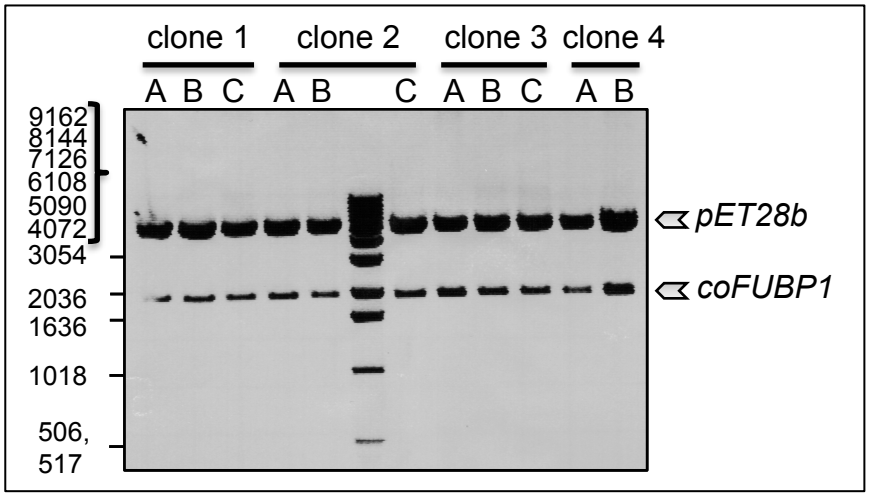

Figure 14: Test cleavage of coFUBP1/pET28b plasmid preparations. DNA Plasmid preparations were performed. Beforehand, each clone was subdivided into two to three liquid cultures (A, B, C). The DNA was cleaved by NcoI and XhoI and subsequently analyzed using a 0.8% agarose gel. All clones show the expected cleavage products, resembling the size of *coFUBP1* and the *pET28b* vector backbone.

3.1.2 Expression of coFUBP1 using an Auto-Induction System

3.1.2.1 Cell Growth and Harvesting

The frozen glycerol stock of clone 2A was used to inoculate a 200 ml overnight culture of LB-medium containing 1% glucose and 10 mg kanamycin. 100 ml of the aforesaid overnight culture were used to inoculate a 10 l fermenter. Cells were grown to an optical density of OD_{600}= 1.4 at 37°C. Afterwards, the temperature was reduced to 22°C, and cells were grown for 35 hours before harvesting. The growth of cells was monitored every few hours by optical density measurements (see Figure 15). After harvesting of the cells, the cell sediment was stored at -20°C.

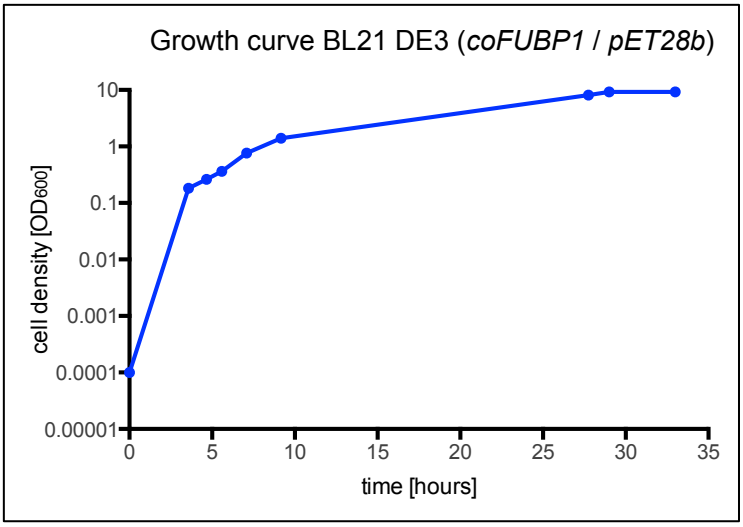

Figure 15: Growth curve of BL21DE3 [*coFUBP1/pET28b*]. *E. coli* were grown in a 10 l fermenter using an auto-induction medium. After inoculation at 37°C, the optical density was measured every few hours. When the culture reached a density of OD_{600}= 1.4, the temperature was reduced to 22°C. After 35 hours, cells were harvested, the cell sediment was stored at -20°C.

3.1.3 Recombinant coFUBP1 Protein Purification using a 3-step Protocol

Purification of recombinant human coFUBP1 was performed using a three - step protocol. All purification steps were performed with the Äkta Purifier. Fractions obtained during each purification step were analyzed by SDS-PAGE and Coomassie staining in order to evaluate the expression level and purity of the recombinant protein. Eventually, the purified protein was aliquotated and shock-frozen with liquid nitrogen before storing at -80°C.

The first step of the purification procedure was an immobilized metal-ion affinity chromatography (IMAC) using a Ni-NTA resin (25 ml volume, *GE Healthcare*, Munich), followed by a heparin column (5 x 5 ml, *GE Healthcare*, Munich) and finally a size exclusion chromatography using gelfiltration (*GE Healthcare*, Munich)

3.1.3.1 Purification of His_6-tagged coFUBP1 *via a His-Trap Column*

The cell sediment, harvested from a total amount of 5 l bacterial culture, was thawed on ice and diluted in 200 ml lysis buffer. The lysate was processed in a Constant Cell Disruption System (*Constant Systems Ltd.*, England) and subsequently centrifuged. Afterwards, the supernatant was loaded on a Ni-NTA column and purified using a "Äkta Purifier".

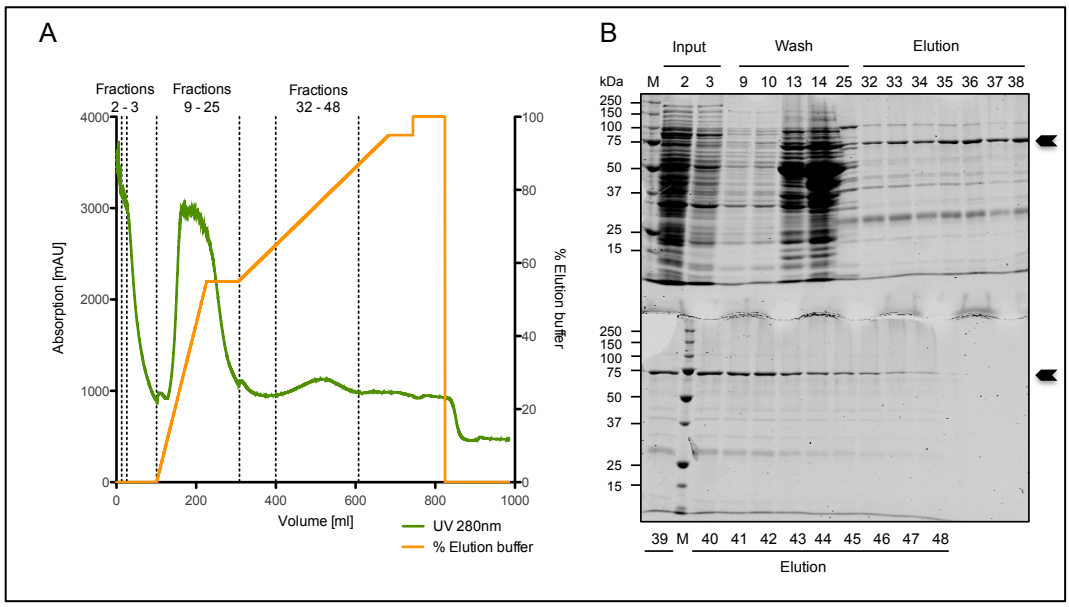

Figure 16: First purification step of recombinant co*FUBP1* using a Ni-NTA column. (A) Chromatogram of the Ni-NTA purification. (B) Fraction analysis of the Ni-NTA purification. Fraction 2 and 3 resemble the input, fractions 9-25 the wash fractions. The elution of a protein resembling the expected size of *coFUBP1* (68 kDa) is shown in fraction 32-48, indicated by the black arrow.

The chromatogram showed a high UV-absorbance in the input fractions 1-6, as well as in the washing fractions 9-25. Elution of a protein with the expected size of approximately 68 kDa was predominantly seen in fractions 32-48. The amount of other, undesired proteins in these fractions was reduced compared to those seen in the input and wash fractions (see Figure 16). Aforesaid fractions were immediately pooled and loaded on a HeparinTrap.

3.1.3.2 Further Purification of His_6-tagged coFUBP1 via a Heparin Column

The pooled fractions 32-48 were loaded on a 25 ml HeparinTrap (5 serially connected 5 ml heparin columns) through an electric peristaltic pump with a flow rate of approximately 2.5 ml / min, resulting in a loading time of 1 ½ hours at 4°C. Afterwards, the HeparinTrap was connected to an Äkta Purifier system.

The chromatogram of the heparin purification showed two different UV absorbtion peaks at 14,6% - 17% NaCl and 23,9% - 25,9% NaCl (Figure 17 A). SDS-PAGE analysis showed that both resemble the elution of an approximately 68 kDa

protein with no detectable amount of undesired impurities. Fractions 28 to 30 were pooled for further purification using gel filtration (Figure 17 B).

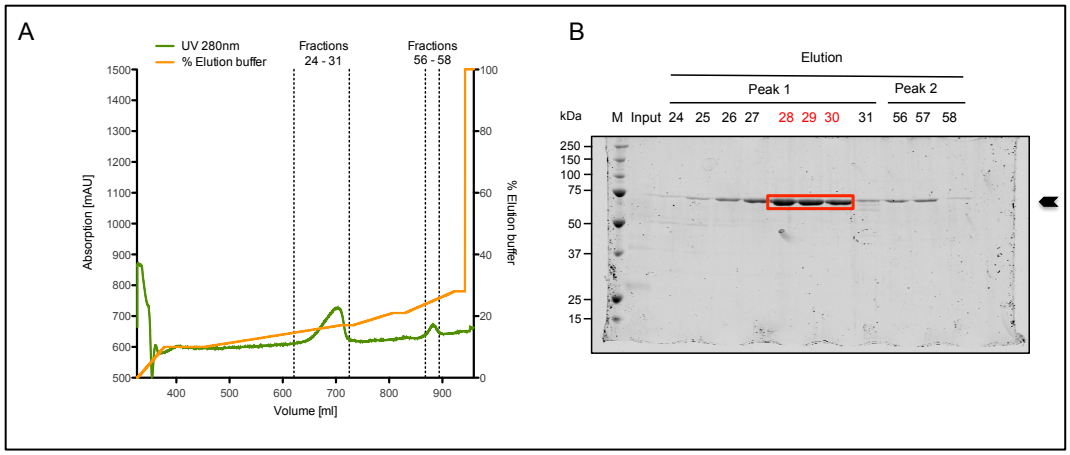

Figure 17: Second purification step for recombinant coFUBP1 using a heparin column. (A) Chromatogram of the heparin purification. (B) Fraction analysis of coFUBP1 after heparin purification. Elution of protein was seen in two different elution steps. Both peaks resemble the elution of an approximately 68 kDA protein (indicated with black arrow) without any undesired impurities visible.

3.1.3.3 Final purification of His_6-tagged coFUBP1 via preparative size exclusion chromatography

The pooled fractions 28-30 of the heparin column were concentrated to an end volume of 4 ml: The initial volume of 36 ml was first concentrated in an Amicon stirr cell system to a volume of 20 ml, using a 10 kDa membrane. The remaining volume of 16 ml was reduced to an end volume of 4 ml using a 30 kDa membrane with an input concentration of 0,378 µg/µl. After size exclusion chromatography, one sharp UV absorption peak was visible in the chromatogram (Figure 18 A). Fractions B5-B8 (Figure 18 B) were pooled and concentrated using a 30 kDa membrane to a final concentration of 0,388 µg/µl, leading to the overall yield of 0.27 mg recombinant protein (obtained from 5 l bacterial culture).

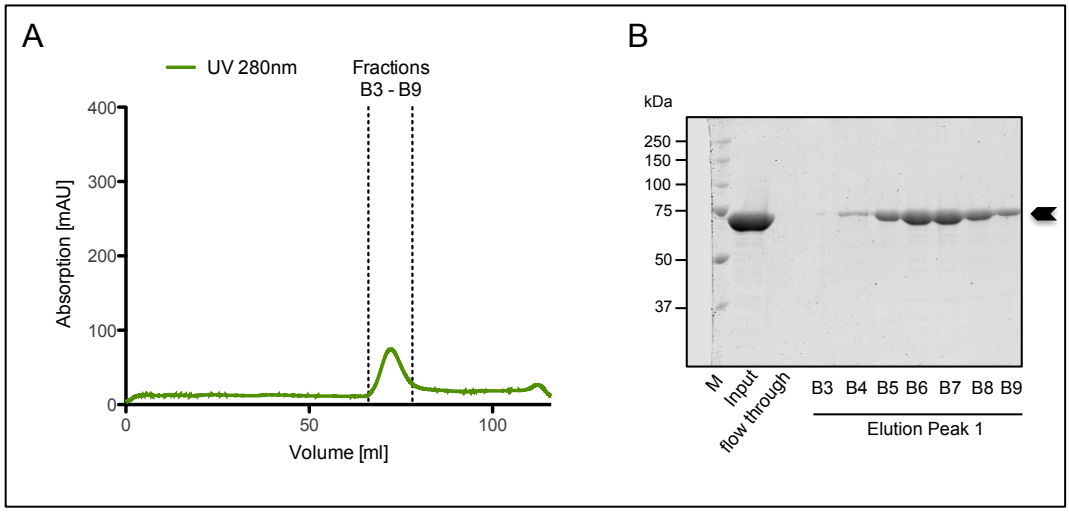

Figure 18: Third purification step of recombinant coFUBP1 using size exclusion. (A) Chromatogram of the gel filtration. (B) Fraction analysis of coFUBP1 after size exclusion chromatography. Elution of an approximately 68 kDa protein was seen in one elution peak (indicated with black arrow) without any undesired impurities visible. Fractions B5 to B8 were pooled and aliquotated with a final concentration of 0.388 µg/µl before shock freezing in liquid nitrogen and storage at -80°C.

3.1.4 Verification of the Identity of the Purified Recombinant Protein coFUBP1 using Western Blot and MS-Analysis

To confirm the identity of the purified, recombinant protein, two different analyses were performed. Following SDS-PAGE, purified protein samples were stained with Coomassie followed by a subsequent analysis of those bands via MS-analysis. Alternatively, the protein samples were hybridized with a specific anti-FUBP1 antibody and detected via Western blot technique. Both analyses could verify that the purified recombinant protein was indeed human FUBP1 (Figure 19). The analysis of different fractions via Coomassie staining and Western blot analysis after size exclusion chromatography showed a protein with a size of approximately 68 kDA, without any undesired impurities, which is specifically recognized by the anti-FUBP1 antibody (Figure 19 A).

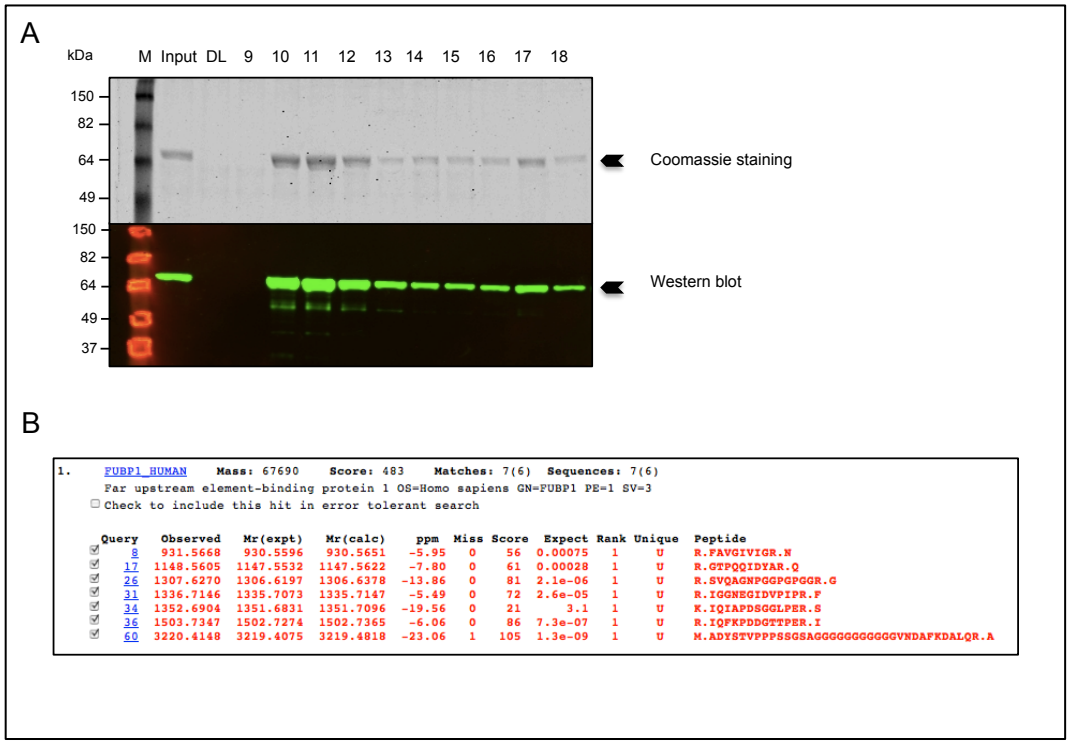

Figure 19: Verification of human FUBP1 using Western blot- and MS-analysis. (A) Fraction analysis of coFUBP1 after size exclusion purification using Coomassie staining and Western blot analysis. A protein of approximately 68 kDa without any undesired impurities could be seen upon Coomassie staining and Western blot analysis using an anti-FUBP1 antibody (N-15, SantaCruz). (B) Mass spectrometry analysis of the protein samples also proved that the purified recombinant protein was human FUBP1.

3.2 Functional Analyses of Recombinant coFUBP1

Recombinant coFUBP1 was tested for its ability to specifically bind to its single stranded target DNA FUSE sequence. The *FUSE* oligonucleotide *FUSEp21*, used in the following assays, is part of the *FUSE* upstream of the *p21* promoter. The oligonucleotide, a 53- mer, was earlier used in EMSA assays by Rabenhorst et al. 2009 and is a confirmed binding partner of FUBP1 [1]. During this study, it was used in surface plasmone resonance (SPR), as well as in microscale thermophoresis (MST) measurements.

3.2.1 Surface Plasmone Resonance Measurements Revealed Specific Binding of coFUBP1 to its Single Stranded Target DNA FUSEp21

To determine the binding constant of coFUBP1 and *FUSEp21*, surface plasmone resonance studies were performed. Negative controls, the FUBP1 non-binding oligos *p31* and *p39* [1], were included to evaluate the specificity of the binding. Recombinant protein was used as ligand, covalently bound to the surface of a ProteOn™ GLM sensor chip. *FUSEp21* oligonucleotide served as the analyte in the liquid phase.

3.2.1.1 Negative Controls using Non-Binding FUSE Oligonucleotides and Dummy Proteins Confirmed Specificity of coFUBP1 Binding to FUSEp21

The FUBP1 non-binding oligonucleotides *p31* and *p39* as well as an unrelated protein, “maltose-binding-protein (MBP)”, were used to confirm the binding specificity between recombinant coFUBP1 and *FUSEp21*. Increasing concentrations of the analyte *FUSEp21* resulted in increasing response units when titrated to covalently bound coFUBP1 ligand. Covalently bound MBP on the other hand showed no response to any concentration of the *FUSEp21* analyte (Figure 20).

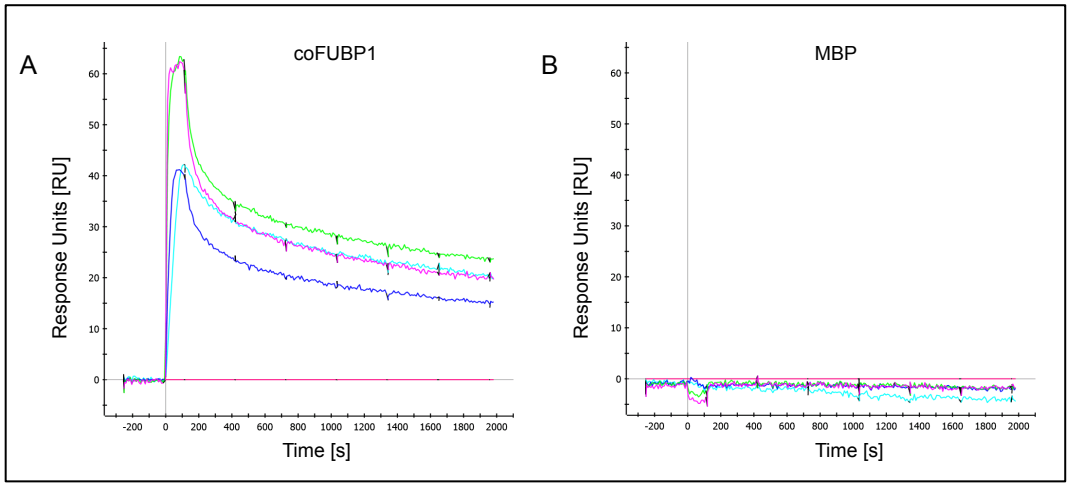

Figure 20: Specificity control of coFUBP1 binding to *FUSEp21* using MBP as unrelated protein. *FUSE p21* was titrated (light pink: 0 nM, dark blue: 10 nM, light blue: 25 nM, green: 50 nM, dark pink: 100 nM) to either coFUBP1 (A) or MBP (B). Increasing concentrations of *FUSEp21* led to increasing response units in the coFUBP1 channel (A) whereas no response was visible in the MBP channel (B). The response unit (RU) is defined as 1 RU= 1 pg/mm^2, it is an arbitrary value displaying the actual measured value (wavelight and angle).

Titration of the non-binding oligonucleotides *p31* and *p39* showed almost no response in the coFUBP1 channel (maximum 20 RU) compared to the response units when using *FUSEp21* as an analyte. In this case, a dose-dependent increase in response units (RU) with a maximum of 60 RU was seen (Figure 21).

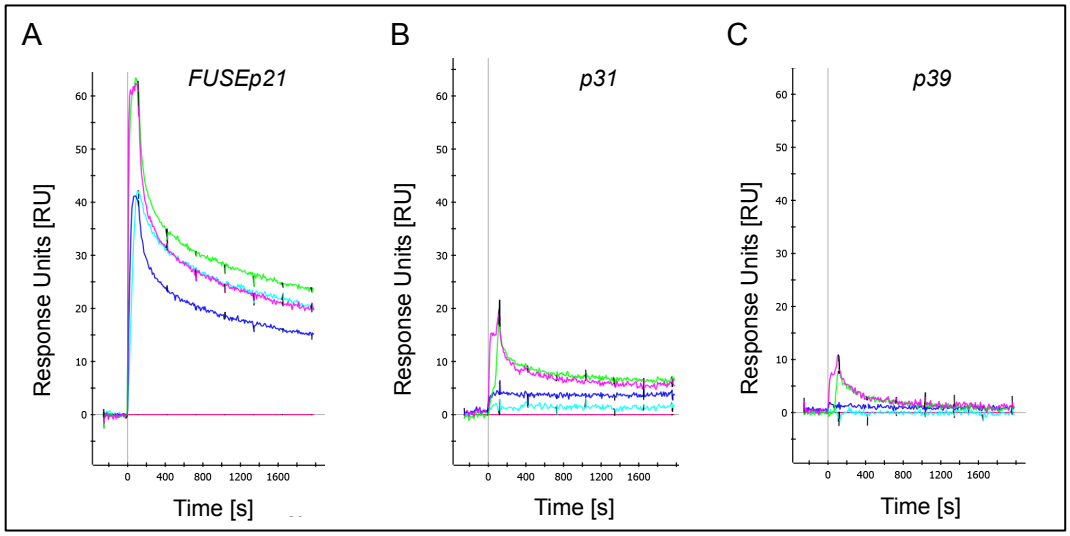

Figure 21: Specificity control of coFUBP1 binding to *FUSEp21* using the non-binding oligonucleotides *p31* and *p39*. *FUSE p21* (A), *p31* (B) or *p39* (C) were titrated to coFUBP1 (light pink: 0 nM, dark blue: 10 nM, light blue: 25 nM, green: 50 nM, dark pink: 100 nM). Increasing concentrations of *FUSEp21* led to a dose-dependent increase in response units in the coFUBP1 channel (A). Increasing concentrations of *p31* and *p39* showed only minor or no response ((B) and (C)).

3.2.1.2 Quantification of the Dissociation Constant of FUBP1 and FUSEp21 using SPR Measurements Revealed a Tight Binding between both Molecules

To determine the thermodynamic binding capacity of coFUBP1 and *FUSEp21*, the oligonucleotide was used as the analyte in a dilution series of 0 nM, 10 nM, 50 nM and 100 nM. The increasing amounts of *FUSEp21* led to a subsequent increase of the measured response units [RU]. Plotting of the response units [RU] measured in the saturation phase (equilibrium mode, see page 58, paragraph 2.2.5.1.1) against the *FUSEp21* concentration, revealed a dissociation constant (K_D) of 12.9 nM between recombinant FUBP1 and *FUSEp21* (Figure 22).

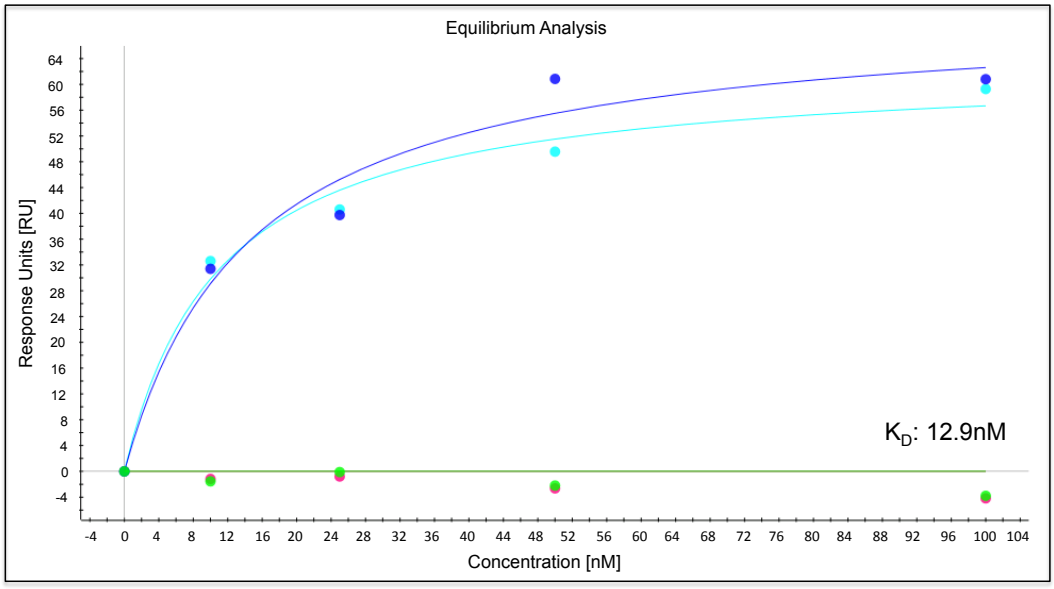

Figure 22: Surface Plasmone Resonance measurement of the interaction between coFUBP1 and the *FUSEp21* oligonucleotide. coFUBP1 served as the ligand, covalently bound to the surface of a GLM sensor chip. The *FUSEp21* oligonucleotide was used in a dilution series (0 nM, 10 nM, 25 nM, 50 nM and 100 nM) as the analyte in the liquid phase. A dissociation constant of approximately 12.9 nM between recombinant FUBP1 and *FUSEp21* could be determined under steady state conditions.

3.2.2 Microscale Thermophoresis Measurements of Recombinant coFUBP1 and the FUSEp21 Oligonucleotide Confirmed the Tight Binding between both Molecules

The recombinant protein was labeled using a NT.115 Protein labeling kit RED-NHS according to the manufacturers manual. The single stranded *FUSEp21* oligonucleotide remained unlabeled. The fluorescence of FUBP1 is used to monitor the motion of the molecules along a temperature gradient. LED power was set to 100%, infra-red laser (IR) power to 15%. The on-off cycle of the laser was set to the following schedule: Initial laser off: 5 seconds, laser on: 30 seconds, final laser off: 5 seconds. Standard capillaries were used during the measurements. Lower temperature limit was set to 20°C, upper temperature limit to 40°C. When titrating the *FUSEp21* oligonucleotide to a stable concentration of 1 µM recombinant coFUBP1, a dissociation constant of 12.31 nM could be determined by the change of the fluorescence signal in the hot and cold areas through thermophoretic movement of the molecules (Figure 23).

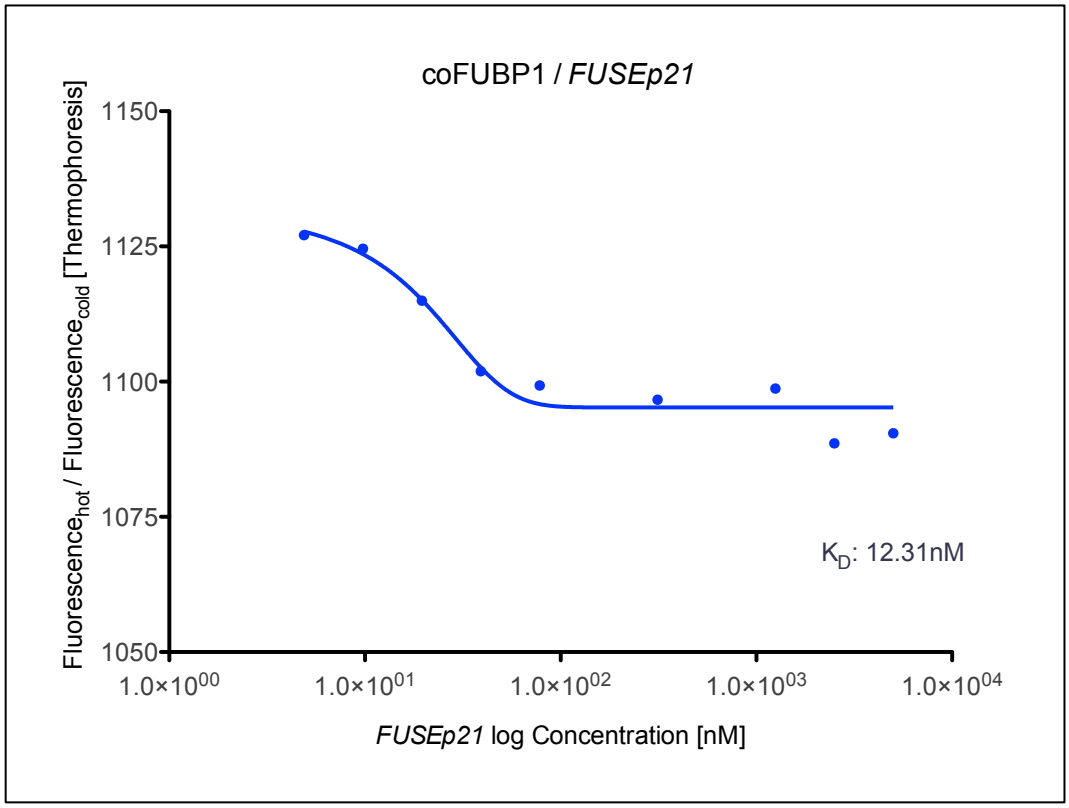

Figure 23: Quantification of the binding constant between recombinant FUBP1 and *FUSEp21* by microscale thermophoresis. *FUSEp21* oligonucleotide (5,000 nM, 2,500 nM, 1,250 nM, 625 nM, 312.5 nM, 78.125 nM, 39.06 nM, 19.5 nM, 9.7 nM, 4.88 nM) was titrated to a stable concentration of 1 µM recombinant coFUBP1. The thermophoresis is defined as the change of the fluorescence signal in the hot and cold capillary areas at steady state conditions. Plotting of those values against the *FUSEp21* oligonucleotide concentration led to the determination of a dissociation constant of 12.31 nM between recombinant FUBP1 and *FUSEp21*.

3.3 AlphaScreen® Interaction Studies for the Identification of FUBP1 Inhibitors

The AlphaScreen® technology was used to identify potential inhibitors of FUBP1. This bead dependent assay system is used to determine inter-molecular interactions of various molecules including DNA, RNA and proteins (see page 61, paragraph 2.2.5.3). The inhibition of binding between coFUBP1 and *FUSEp21* by different compounds was determined by the reduction of light emission at 520 - 620 nm. Recombinant coFUBP1 was bound to a protein-A acceptor bead via its specific antibody N-15 (santa cruz biotechnology), whereas *FUSEp21* was biotinylated at its 5'-end and bound to a streptavidin donor bead.

3.3.1 Determination of Optimal Binding Conditions via Cross Titrations

Increasing concentrations of recombinant coFUBP1 and *FUSEp21* were used to determine optimal binding conditions for the subsequent screening of *FUBP1* inhibitors. Light emission at 520 – 620 nm (referred to as counts) was depicted against the concentrations used for coFUBP1 and *FUSEp21*. Increasing concentrations led to increasing counts with a maximum of 230,000 counts

(Figure 24). After evaluation, concentrations of 3 nM coFUBP1 and 1.6 nM *FUSEp21* (resulting in approximately 100,000 counts) were chosen for further experiments, as those values displayed the highest possible signals in the exponential phase.

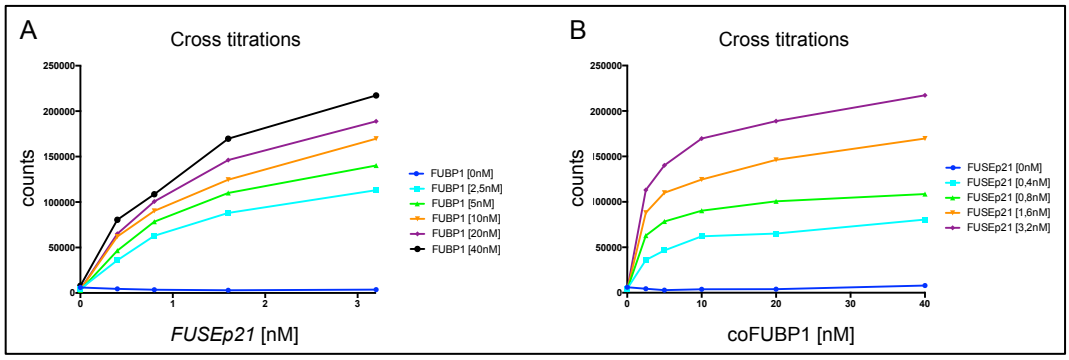

Figure 24: Cross titrations of coFUBP1 and *FUSEp21* to determine optimal binding conditions. To define optimal concentrations for the subsequent FUBP1 inhibitor screen, increasing concentrations of recombinant coFUBP1 and *FUSEp21* were tested in the Alpha Screen setup. Dilution series of both, FUBP1 and *FUSEp21,* were prepared and subsequently mixed in every possible variation. Concentrations of 3 nM coFUBP1 and 1.6 nM *FUSEp21* resulted in a signal of approximately 100,000 counts and were chosen for further experiments.

3.3.2 Competitive Assay using Unbound FUSEp21 Confirmed Functionality of the AlphaScreen® Experimental Setup as an Inhibitor Screening System

To test whether it is possible to interfere with the interaction between FUBP1 and *FUSEp21*, a proof-of-principle experiment was performed. Increasing concentrations of free *FUSEp21* were titrated to the AlphaScreen setup described before to compete with coFUBP1 binding to the bead-coupled *FUSEp21* and to mimic a potential inhibitor. Administration of free *FUSEp21* led to a dose-dependent decrease of the signal counts down to 7,500 counts at a concentration of 100 nM unbound *FUSEp21*, compared to 100,000 counts, when no competitor was given to the reaction (Figure 25).

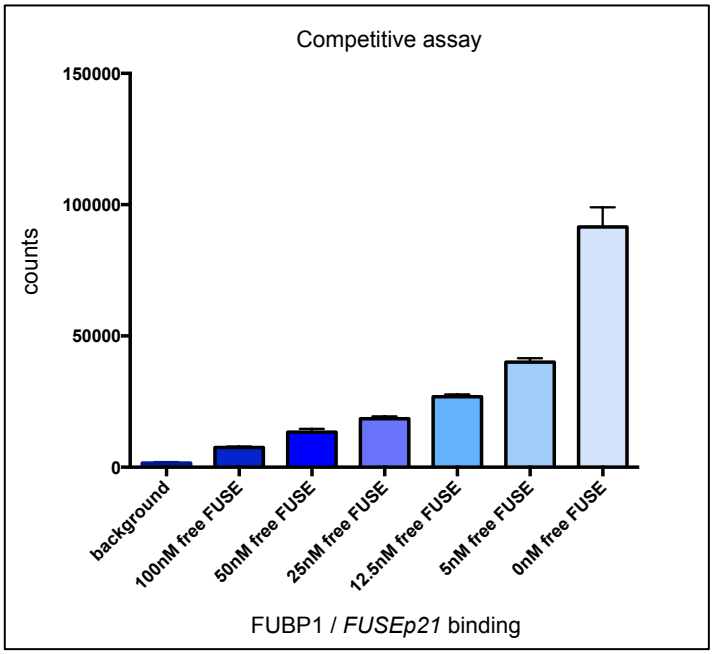

Figure 25: Increasing concentrations of free *FUSEp21* led to a dose-depended decrease of signals in a competitive assay setup. Free *FUSEp21* oligonucleotides mimicking potential FUBP1 inhibitors demonstrated that interference with the binding of coFUBP1 and *FUSEp21* is possible in the established Alpha Screen setup.

3.3.3 Minimizing the Effects of DNA-Intercalators by the Use of Poly dIdC

Poly (2′-deoxyinosinic-2′-deoxycytidylic acid) sodium salt (poly dIdC) is used as a DNA mimic, to intercept DNA intercalators and thereby minimize the false positive hits in the experimental setup. To ensure that poly dIdC does not influence the binding of coFUBP1 to *FUSEp21* itself, increasing concentrations were added to the mixture and the resulting light signals were compared to the signal occurring without addition of poly dIdC. To furthermore evaluate the effect of a real DNA intercalator, 50 µM ethidiumbromide were added to each mixture. The addition of poly dIdC did not show an influence on the binding of coFUBP1 to *FUSEp21*, even at high doses of 100 µM. The addition of ethidiumbromide, on the other hand, led to a huge signal decrease of almost 3/4 of the original value, independently of the amount of poly dIdC used (Figure 26). After evaluation, a concentration of 3 µM poly dIdC was chosen for further experiments.

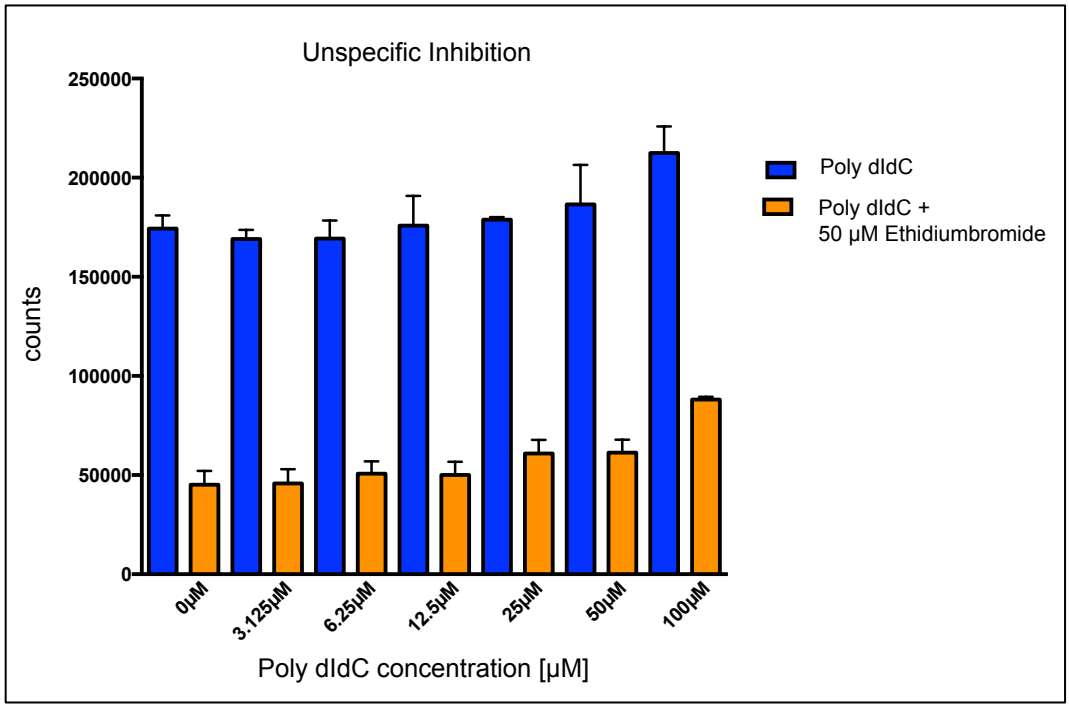

Figure 26: Unspecific inhibition of coFUBP1/*FUSEp21* binding facilitated by the DNA intercalator ethidiumbromide. The addition of poly dIdC did not influence the binding of coFUBP1 to *FUSEp21* at concentrations up to 25 µM. The addition of 50 µM ethidiumbromide reduced the signal to 1/4 of the original value, independently of the poly dIdC concentration.

3.3.4 FUBP1 Inhibitor Screening Resulted in a Total of 158 Hit Compounds

To find potential small molecule FUBP1 inhibitors, two different libraries were screened, the Prestwick Chemical library and the Maybridge Hit Finder™ library, both together containing approximately 16,000 compounds. Molecules, whose addition to the coFUBP1/*FUSEp21*-coupled beads led to a signal decrease of 70% or more in the Alpha Screen®, were defined as positive hits. All hits were re-screened in the AlphaScreen® system and subsequently bioinformatically evaluated, using a self-organizing map (SOM), designed by Janosch Achenbach, AG Proschak, University of Frankfurt. 103 hit compounds were found in the Maybridge Hit Finder™ library (displaying ≤1% of the total compound amount in this library), whereas the Prestwick Chemical library yielded a total of 55 hits (displaying ~3.43% total compound amount in this library) (Figure 27).

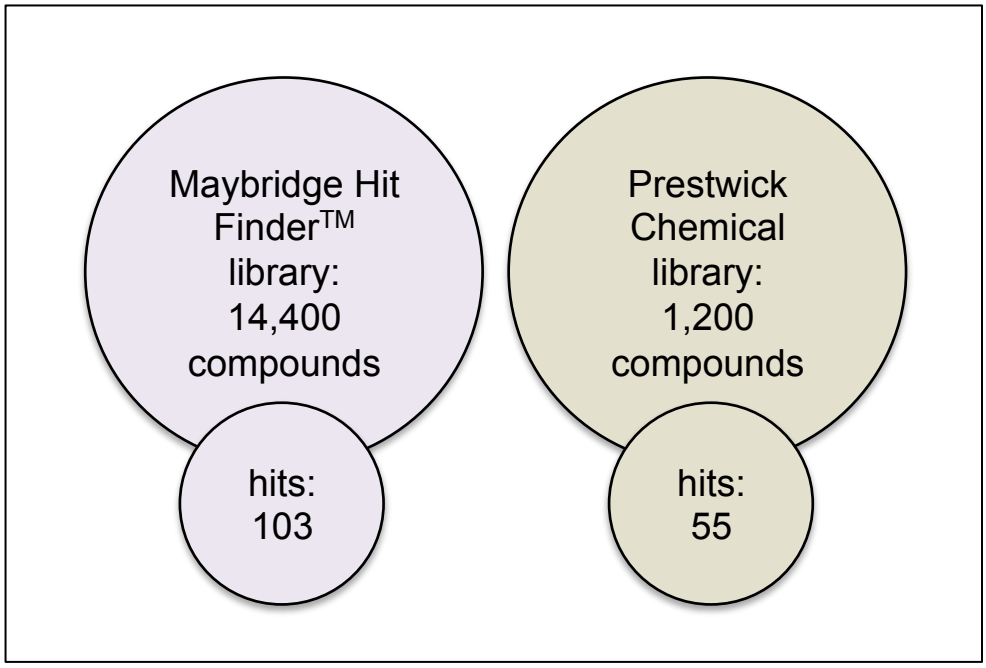

Figure 27: Screening results after bioinformatical evaluation. Two libraries, the Prestwick Chemical and the Maybridge Hit Finder™ library with a total of approximately 16,000 compounds, were screened to find potential new FUBP1 small molecule inhibitors. Molecules were defined as hits, whose addition led to a signal decrease of ≥ 70% in the AlphaScreen®. All hits were re-screened in the same setting and subsequently bioinformatically evaluated, using a self-organizing map (SOM) (Janosch Achenbach, AG Proschak, University of Frankfurt). The hit evaluation resulted in 103 hit compounds in the maybridge Hit Finder™ library, and 55 hits in the Prestwick Chemical library.

3.4 SPR Measurements Confirmed Potential FUBP1 Inhibitor Hit Compounds

To confirm that the molecules identified in the AlphaScreen® indeed interfered with FUBP1 binding to *FUSEp21*, they were re-tested in a SPR setup (see page 59, paragraph 2.2.5.1.3). *FUSEp21* was used as the ligand, immobilized with 120 RU, bound to a neutravidin chip via its biotinylated 5'-end. coFUBP1 was used as the analyte in increasing concentrations (2.5 nM, 5 nM, 10 nM 15 nM and 20 nM). All compounds were diluted with DMSO and used in a concentration of 100 µM each. If a compound showed the expected FUBP1/*FUSEp21* binding inhibition, it was tested with a stable coFUBP1 concentration of 50 nM in a dilution series (0,1 µM, 1 µM, 10 µM, 50 µM and 100 µM). Analyte and compound were added immediately prior to SPR measurements.

Molecules of the Prestwick library, positively tested for their ability to prevent or inhibit the binding between FUBP1 and *FUSEp21* in AlphaScreen® and SPR setups, were subsequently tested in cell culture experiments.

3.4.1 SPR-Measurements Confirmed Four Compounds of the Maybridge Hit Finder™ Library as Potential FUBP1 Inhibitors

17 hit substances were re-tested in SPR measurements to confirm the Alpha Screen® results. Only four substances showed the expected dose-dependent decrease in response units (RU). The molecule HTS 06795 showed the strongest dose-dependent inhibitions with a signal decrease of 75% at a compound concentration of 10 µM (Figure 28).

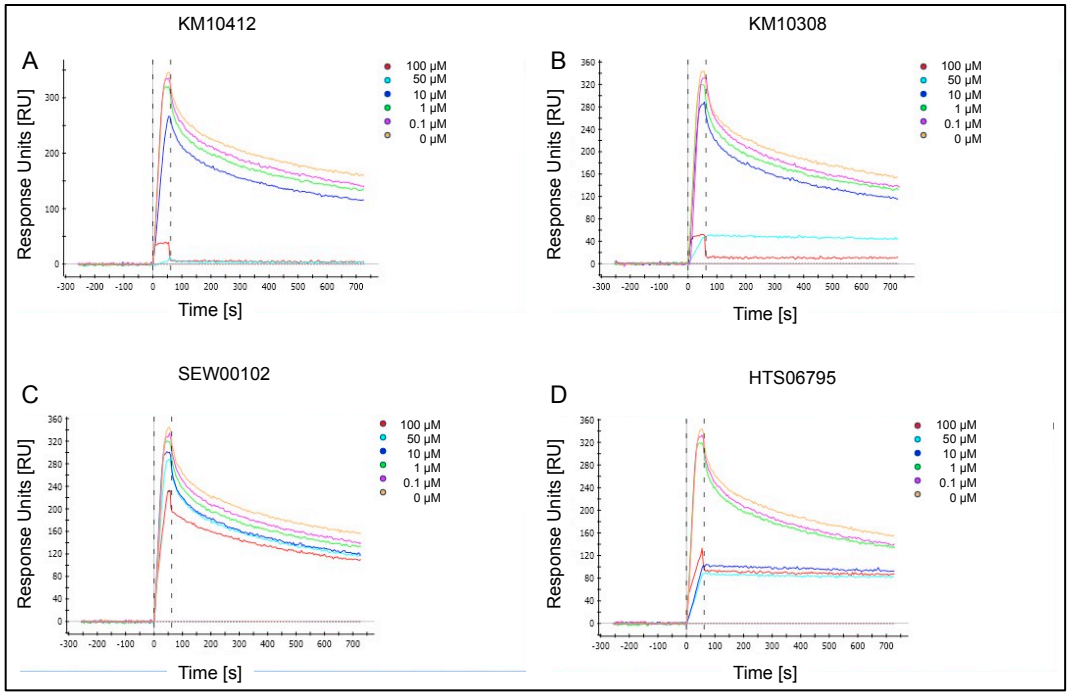

Figure 28: Alpha Screen hit confirmation by SPR measurements. *FUSEp21* was immobilized with 120 RU, coFUBP1 was used as the analyte (20 nM). Dilution series of four different compounds showed a dose-dependent inhibitory effect on FUBP1 / *FUSEp21* binding (yellow: DMSO control 0 µM, pink: 0.1 µM, green: 1 µM, dark blue: 10 µM, light blue: 50 µM, red: 100 µM). (D) The best inhibitory effect was achieved using compound HTS 06795. A concentration of 10 µM decreased FUBP1 / *FUSEp21* association to 25% residual binding, compared to the DMSO control.

3.4.2 SPR-Measurements Confirmed Three Compounds of the Prestwick Chemical Library as Potential FUBP1 Inhibitor: Camptothecin, Pregnenolone and Tosufloxacin

13 hit substances were re-tested in SPR measurements to confirm the Alpha Screen results. Three substances showed the expected dose-dependent decrease in FUBP1 / *FUSEp21* binding measured in response units [RU]. The best inhibitory effects were seen when camptothecin and pregnenolone were given to FUBP1 / *FUSEp21*. At 10 µM, both compounds decreased the response units to 30% of the original signal. The addition of tosufloxacin to FUBP1 / *FUSEp21* led to 50% signal reduction, when used at 10 µM concentration. Furthermore, all three substances were able to diminish the signal to almost zero,

when used at concentrations of 50 µM to 100 µM (Figure 29). This experiment was done in collaboration with Stefanie Hauck, AG Zörnig [78].

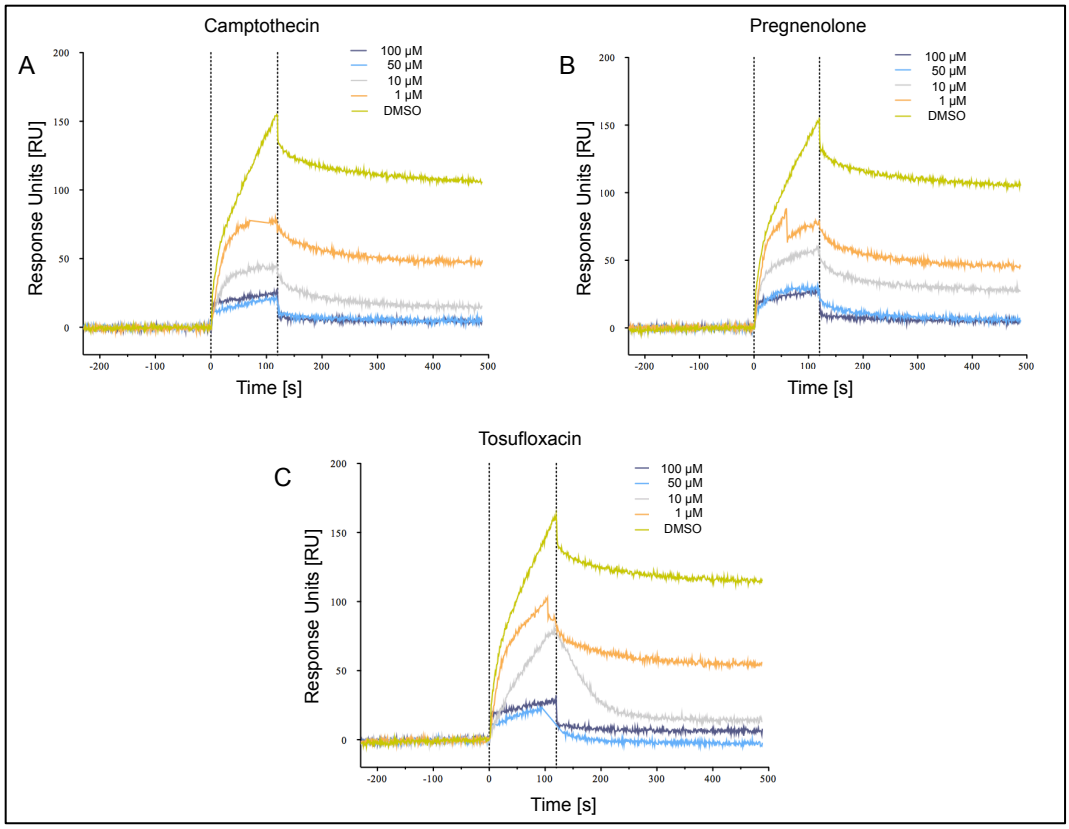

Figure 29: Dose-dependent decrease of the SPR signal upon addition of three identified FUBP1 inhibitors. *FUSEp21* was used as ligand immobilized with 120 RU, bound to a neutravidin chip via its biotinylated 5'-end. coFUBP1 was used as the analyte (50 nM). The analyte was mixed immediately prior to measurement to the dilution series of camptothecin, pregnenolone and tosufloxacin, respectively. camptothecin (A), pregnenolone (B) and tosufloxacin (C) were used at four different concentrations (dark blue: 100 µM, ligth blue: 50 µM, grey: 10 µM, orange: 1 µM and yellow: DMSO control with 50 nM FUBP1). All three compounds showed the capacity to diminish the binding of FUBP1 / *FUSEp21*, depicted as response units [RU], to almost zero, when treated with concentrations of 50 µM and 100 µM.

3.4.2.1 SPR Measurements of Camptothecin Structurally Related Compounds Revealed a Potent FUBP1/FUSEp21 Binding Interference by Different Topoisomerase I Inhibitors

Since camptothecin behaved in both experimental setups (Alpha Screen® and SPR measurements) as a potential FUBP1 inhibitor, further topoisomerase I inhibitors were tested. NSC 724998 and NSC 725776 were kindly provided by Professor Yves Pommier (NIH, USA) and were tested as additional, potential FUBP1 inhibitors. Furthermore, the active group of irinotecan, 7-ethyl-10-hydroxycamptothecin, was also tested in a dilution series (0 µM: DMSO control, 1 µM, 10 µM and 50 µM). Comparison of the response units after 300 seconds dissociation time revealed that all topoisomerase I inhibitor were able to interfere with the binding between coFUBP1 and *FUSEp21*. Camptothecin and NSC 725776 decreased the response signal at 10 µM down to 30% of the

original response. At 50 µM, the response signal diminishes to almost zero when treated with NSC 725776 (Figure 30). These measurements were done in collaboration with Stefanie Hauck, AG Zörnig [78].

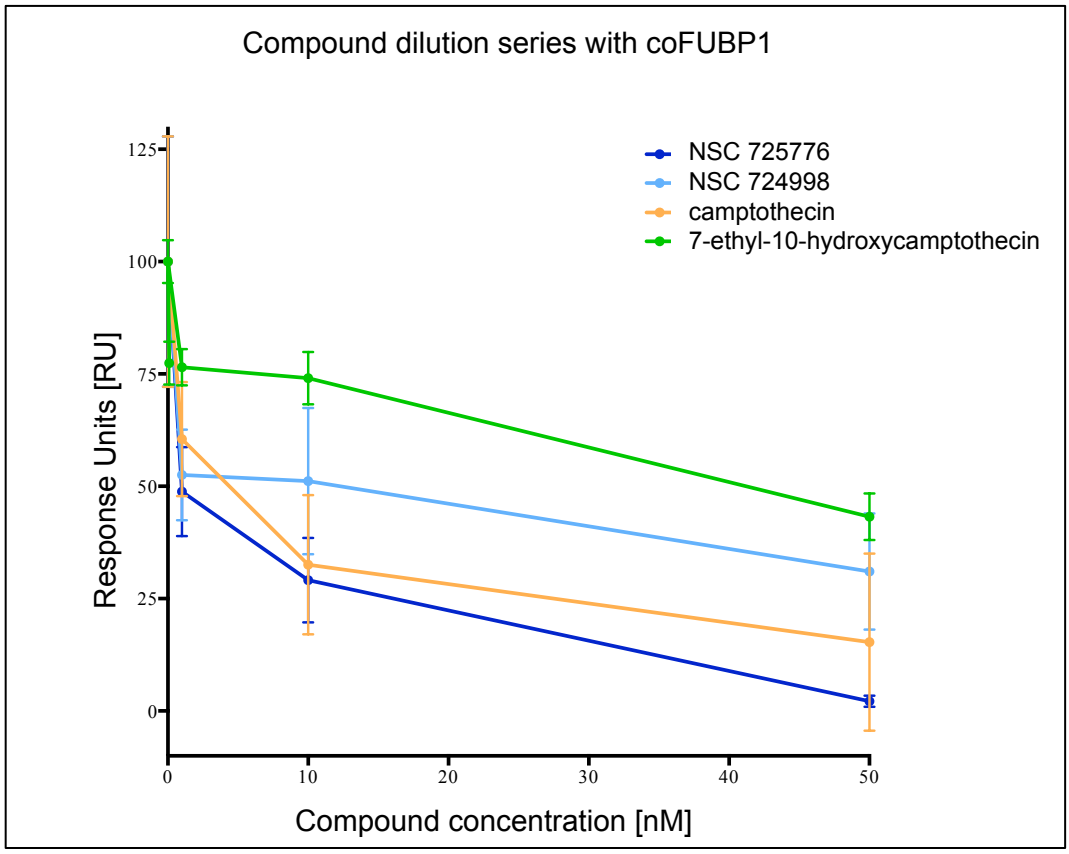

Figure 30: All tested Topoisomerase I inhibitors were able to interfere with the binding of FUBP1 and *FUSEp21*. This experiment was performed in the same manner as the one depicted in **Figure 29**. Comparison of the response units after 300 seconds dissociation time revealed that all tested topoisomerase I inhibitors were able to interfere with the binding between FUBP1 and *FUSEp21*. The response units after 300 seconds dissociation time were normalized to values representing the interaction between coFUBP1 and *FUSEp21* diluted with DMSO. Three independent binding tests were used to calculate the error bars (10 RUs, 12.5 RUs and 50 RUs of immobilized *FUSEp21*).

3.5 Evaluation of the FUBP1 Inhibition Effect on Human HCC Cell Lines

Tosufloxacin, pregnenolone, camptothecin and all topoisomerase I inhibitors positively tested for their interference of the binding between FUBP1/*FUSEp21* were subsequently tested in different cell culture experiments to evaluate their effects on cancers cell lines with regard to proliferation, apoptosis and expression of the FUBP1 target gene *p21*. All compounds were diluted in DMSO and stored at -20°C.

3.5.1 *Camptothecin-Treated HCC Cells Showed Reduced Cell Expansion Similar to Those Treated with Sorafenib, the Current HCC "Gold Standard Therapy"*

1 x 10^5 Hep3B cells were seeded into 6-well plates and treated with camptothecin, tosufloxacin or pregnenolone in increasing concentrations for 72 hours. Control cells were either untreated or treated with DMSO. The medium was changed every 24 hours. For each time point, an individual plate was collected, cells were stained with crystal blue and counted in a "Neubauer improved counting chamber". Treatment of HCC cells with sorafenib cells currently serves as a "gold standard" for HCC therapy. Cells treated with pregnenolone and tosufloxacin showed only minor changes in their cell expansion. Only high concentrations of 10 µM to 100 µM showed an effect on the number of expanding cells. On the other hand, cells treated with camptothecin or sorafenib showed an inhibition of cell expansion after 24 hours even at low drug concentrations (1 µM). After 72 hours, all cells, apart from those treated with 1 µM sorafenib, were killed by the treatment (Figure 31).

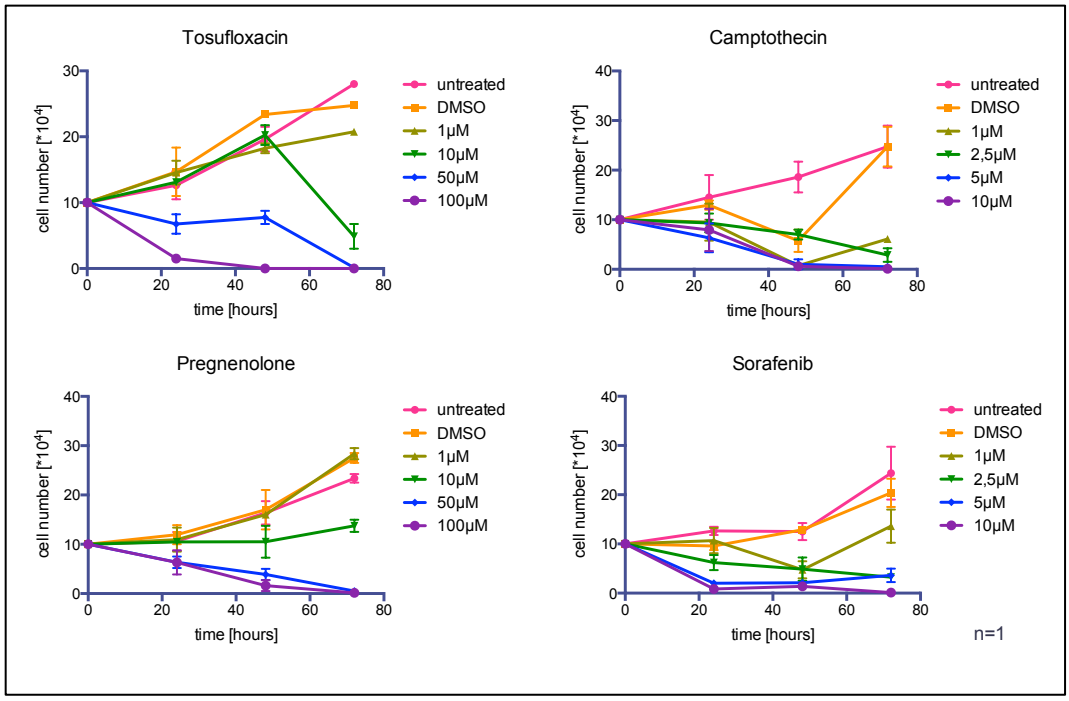

Figure 31: Cell expansion assays showed almost no cellular response to tosufloxacin and pregnenolone treatment, whereas camptothecin efficiently interfered with cell growth. 1 x 10^5 Hep3B cells were seeded into 6-well plates and treated with DMSO (as a control), camptothecin, tosufloxacin or pregnenolone in increasing concentrations up to 72 hours. After 24 hours, 48 hours and 72 hours, cells were collected, stained with crystal blue and counted in a "Neubauer improved counting chamber". Only cells treated with camptothecin showed a dramatic cell number decrease in cell numbers, comparable to the one seen sorafenib-treated cells.

3.5.2 *Monitoring the Effect of Potential FUBP1 Inhibitors on Cell Viability using WST Assays*

To identify the percentage of viable cells after treatment with camptothecin, tosufloxacin and pregnenolone, WST assays were performed. Hep3B cells were treated for 24 hours, before the cell viability was measured.

3.5.2.1 *Camptothecin Single-Treated Hep3B Cells showed a Dose-Dependent Cell Viability Decrease*

Pregnenolone and tosufloxacin showed no specific effect on cell viability measured in the WST assay. The pregnenonlone- and tosufloxacin-treated cells lost their metabolic activity only at high concentrations of 100 µM. Cells treated with camptothecin showed a loss of 50% cell activity even with the lowest camptothecin concentrations of 100 nM. The IC_{50} value of sorafenib-treated cells was 1 µM (Figure 32). The WST assays were performed in the laboratory of Eugen Proschak, University of Frankfurt.

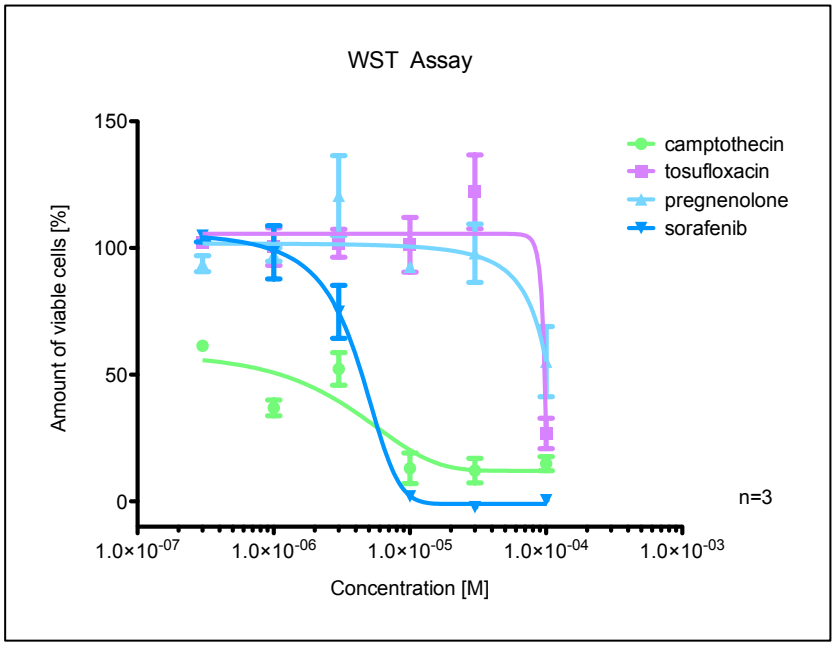

Figure 32: Hep3B WST Assay after 24 hours of single treatment with different hit compounds from the inhibitor screen. Cells were treated for 24 hours, with single treatments of camptothecin tosufloxacin, pregnenolone or sorafenib in increasing concentrations. Afterwards, the cell proliferation reagent WST-1 (*La Roche*) was administered to the cells for 4 hours, before evaluating the cell activity via a spectrophotometric quantification. Results were normalized to DMSO-treated cells. Experiments were performed in biological triplicates, the mean ± SD was calculated. Camptothecin- and sorafenib-treated cells show a sigmoidal, dose-dependent cell activity decrease, wheras pregenolone- and tosufloxacin-treated cells only responded to the highest concentration of 100 µM compound with a loss of cell activity.

3.5.2.2 *Double Treatment of Hep3B Cells with a Combination of 7-Ethyl-10-Hydroxycamptothecin and Mitomycin C Showed a High Synergistic Effect*

To identify possible synergistic effects, WST assays were performed with cells receiving double treatment of chemotherapeutics and inhibitors. To Hep3B cells,

both 7-ethyl-10-hydroxycamptothecin and mitomycin C (Figure 33 A), or 7-ethyl-10-hydroxycamptothecin and sorafenib (Figure 33 B) were given. The amount of viable cells was measured in % of DMSO-treated cells. The combination of 0.3 µM 7-ethyl-10-hydroxycamptothecin and 3 µM mitomycin C showed a high synergy and led to an amount of 15.6% viable cells compared to the amount of the single-treated cells of 88% and 115%, respectively.

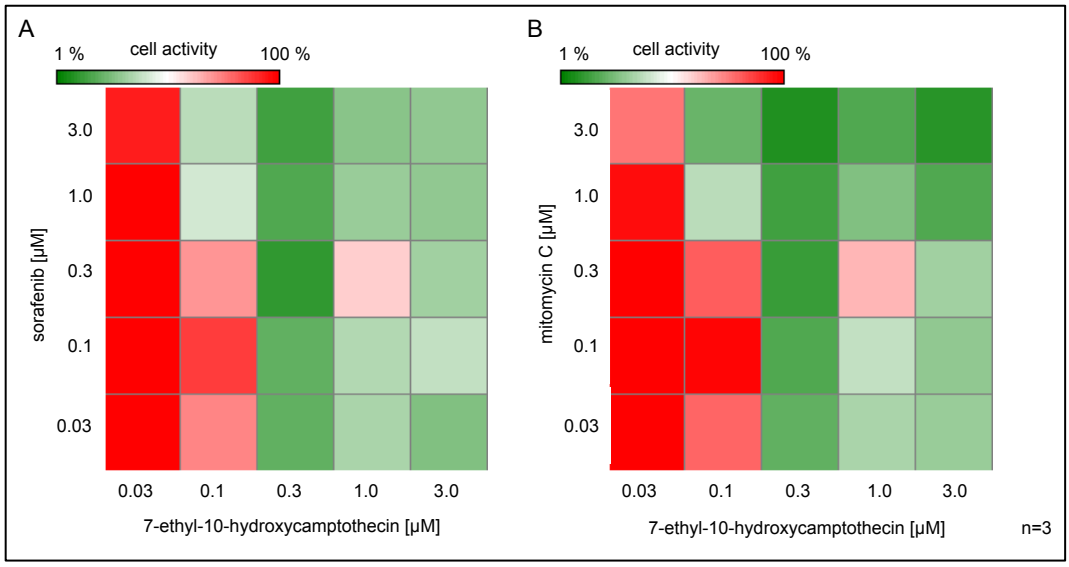

Figure 33: Hep3B WST Assays after 24 hours double treatment with 7-ethyl-10-hydroxycamptothecin and mitomycin C or 7-ethyl-10-hydroxycamptothecin and sorafenib showed synergistic effects. Cells were treated for 48 hours, with single- and double-treatments of 7-ethyl-10-hydroxycamptothecin and mitomycin C, or 7-ethyl-10-hydroxycamptothecin and sorafenib in increasing concentrations. Afterwards, the cell proliferation reagent WST-1 was administered to the cells for 4 hours, before evaluating the cell activity via a spectrophotometric quantification. Results were normalized to DMSO-treated cells. Experiments were performed in biological triplicates, the mean ± SD was calculated and depicted in a red (100% cell activity) and green (0% cell activity) color code.

3.5.3 Determination of Apoptosis Induction via Potential FUBP1 Inhibitors in Human HCC Cell Lines

3.5.3.1 Single Treatment of Hep3B Cells With Camptothecin led to a Dose-Dependent Killing of Cells after 72 Hours of Treatment

To identify the amount of apoptotic cells after treatment with camptothecin, tosufloxacin or pregnenolone, Nicoletti assays were performed. 2 x 10^5 Hep3B cells were seeded in 6-well plates to measure the amount of apoptotic cells after 24 hours of treatment. To evaluate the effect after 72 hours, 1 x 10^5 Hep3B cells were seeded in 6-well plates. Media substituted with the potential inhibitors were changed every 24 hours, to maintain stable concentrations of the given substances. Cells were fixed, stained with propidium iodide (PI) and analyzed via flow cytometry.

Regardless of the kind of treatment, after 24 hours, the cell cycle profile of all living cells was not altered compared to those of the DMSO-treated control cells. mitomycin C- and sorafenib-treated cells showed a dose-dependent increase in the number of dead cells. Cells treated with either tosufloxacin or pregnenolone did not exhibit increased amounts of cell death, as the rate of dead cells was equivalent to those treated with the DMSO solvent. Treatment with 5 µM camptothecin led to 17% dead cells. All three tested compounds showed a lower amount of induced cell death compared to those treated with mitomycin C or sorafenib (Figure 34).

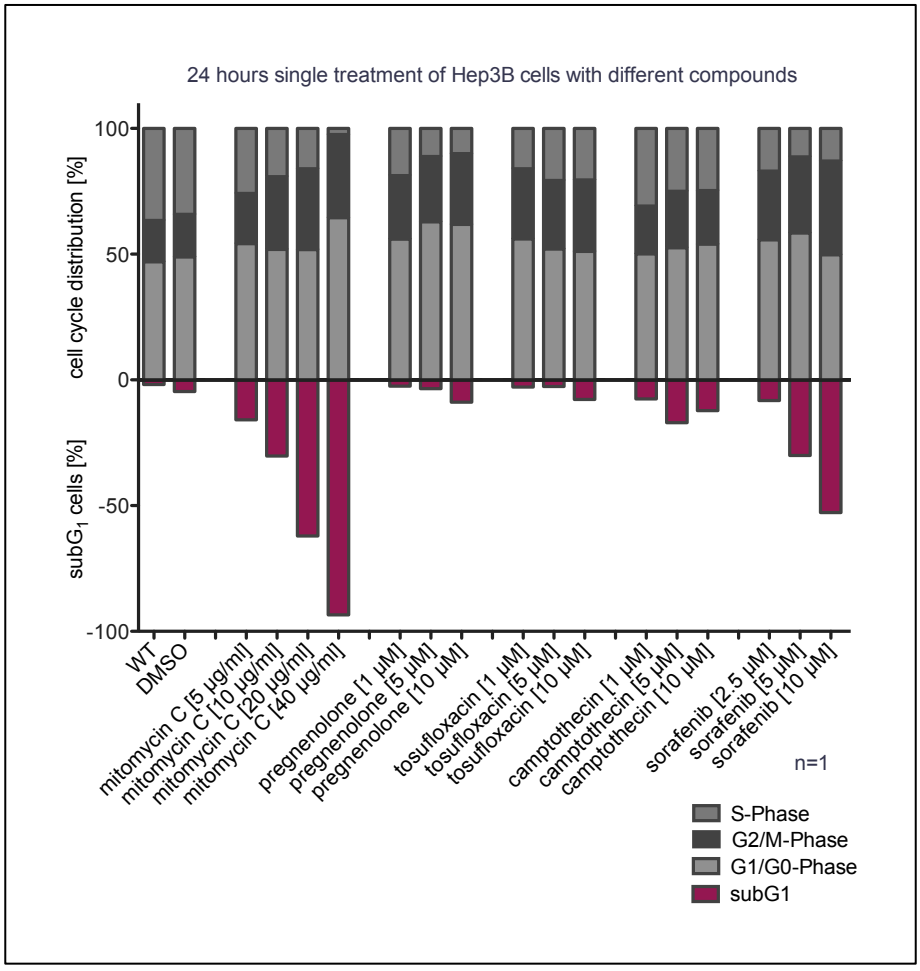

Figure 34: Cell cycle distribution and cell death rates of pregnenolone, tosufloxacin and camptothecin single-treated Hep3B cells after 24 hours. Cell cycle profiles and cell death rates were obtained by cell fixation and subsequent staining via propidium iodide using the Nicoletti protocol. Mitomycin C- and sorafenib-treated cells served as controls. None of the tested potential FUBP1 inhibitors was able to increase cell death rates as potent as the controls mitomycin C and sorafenib, when administered as single agents. Experiments were performed once in technical duplicates. Mean values were calculated.

The absolute number of cells in the subG1 peak increased significantly after 72 hours treatment (Figure 35). With all concentrations used (5, 10, 20 and 40 µg/ml) treatment with mitomycin C led to 58% to 85% dead cells after

72 hours. Furthermore, the cell cycle profile of the living cells was altered compared to the DMSO-treated and -untreated WT cells. Furthermore, incubation with 5 µg/ml and 10 µg/ml mitomycin C led to an increased cell population in the G_0/G_1- and S-phases, however, this effect reversed upon treatment with higher concentrations of this chemotherapeutic. The cell cycle profile of the living sorafenib-treated cells was comparable to those of the DMSO-treated and -untreated WT cells. Interestingly, the amount of cells in $SubG_1$ was decreased compared to the 24 hours treatment. A maximum cell death rate was seen at a concentration of 10 µM, where approximately 50% of the fixed cells were visible in the apoptotic $subG_1$ peak. Cells treated with pregneneolone or tosufloxacin alone showed no specific killing, as the rate of dead cells was almost equivalent to those treated with the DMSO solvent. Treatment with camptothecin led to two different consequences. First, the cell cycle of the living cells was significantly altered to those of the DMSO-treated cells. The G_0/G_1 phase was almost completely abolished, while the G_2/M cell cycle phases were increased. Second, cell death rates were dose-dependently increased with a final proportion of approximately 60% at the 10 µM camptothecin concentration.

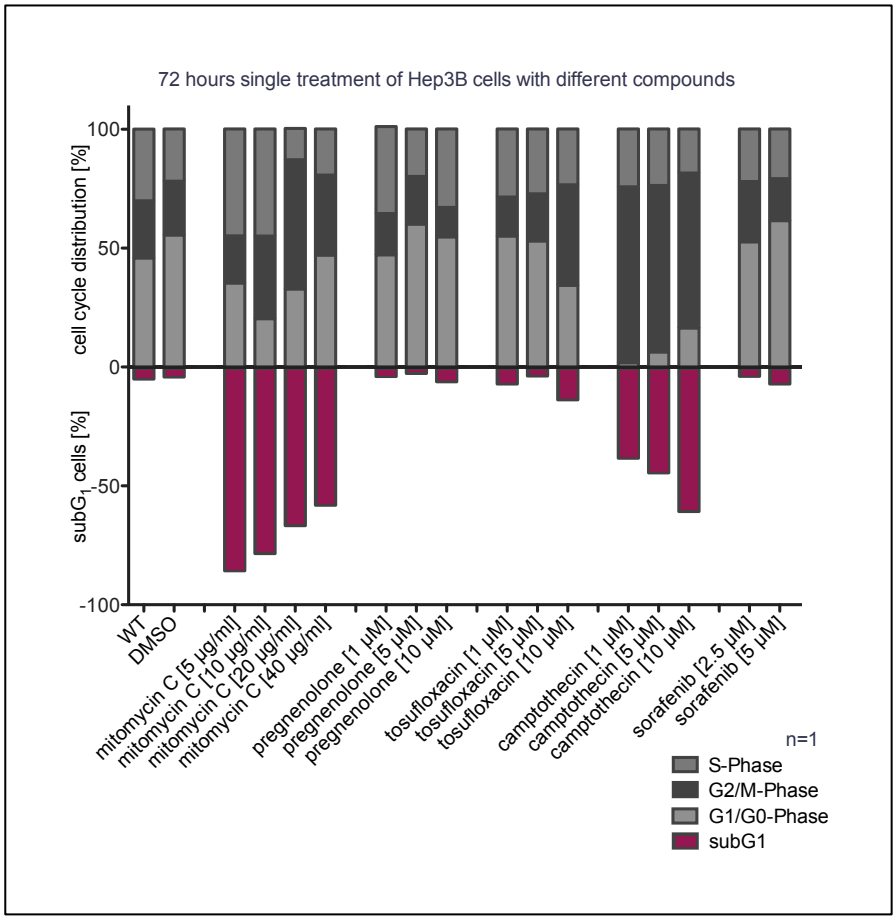

Figure 35: Cell death distribution and cell death rates of pregnenolone, tosufloxacin and camptothecin single-treated Hep3B cells after 72 hours. Cells were treated with different compounds for 72 hours before fixation and staining with propidium iodide (Nicoletti protocol). Mitomycin C- and sorafenib-treated cells served as chemotherapeutic control-treated cells. Camptothecin-treated cells did not only show a dose-dependent increase in cell death rates, but also an alteration of the cell cycle distribution, with an increased G_2/M Phase and a decreased G_1/G_0 Phase in all given concentrations. Experiments were performed once in technical duplicates. Mean values were calculated.

3.5.3.2 Double Treatment of Hep3B Cells with Different Hit Compounds from the Inhibitor Screen and Known Chemotherapeutics Exposed Synergistic Effects on Cell Death Rates

To increase the impact of the compounds camptothecin, pregnenonlone and tosufloxacin on cell death, their application was combined with known chemotherapeutics like mitomycin C, cisplatin and doxorubicin. Hep3B cells were treated for 24 hours. Afterwards, the percentage of cells in the $subG_1$ peak was measured using PI-staining of fixed cells via flow cytometry.

3.5.3.2.1 Double Treatment with Pregnenolone and other Chemotherapeutics Showed No Synergy in Cell Killing Efficacy

Cells were treated with all substances in single and combined applications. None of the single pregnenolone concentrations (1, 10, 50 µM) was sufficient to induce cell death in Hep3B cells. Furthermore, no additional or synergistic effect was

seen when pregnenolone was combined with doxorubicin, cisplatin or mitomycin C (Figure 36).

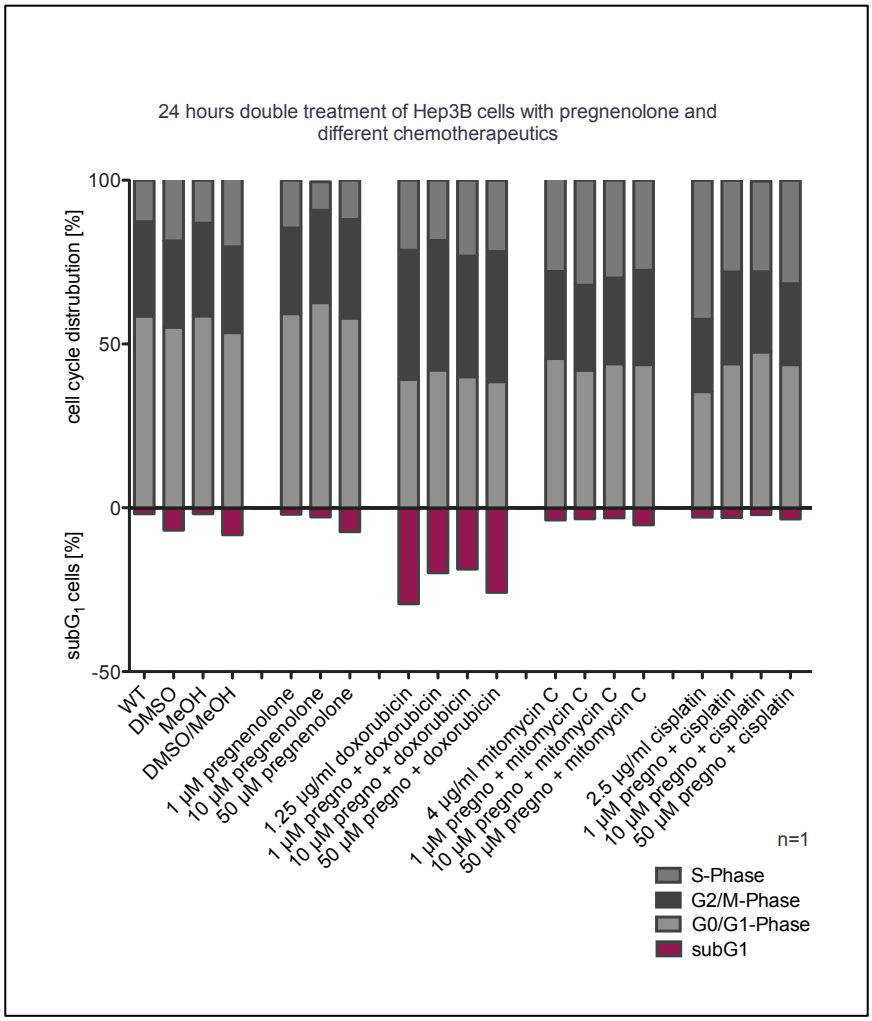

Figure 36: Cell cycle distribution and cell death rates of pregnenolone double-treated Hep3B cells with different chemotherapeutics after 24 hours. Hep3B cells were treated for 24 hours with pregnenolone or pregnenolone in combination with chemotherapeutics to evaluate possible synergistic effects of the double treatment. The cell cycle distributions of the living cells were not altered to those seen in solvent-treated or untreated wildtype cells. No synergistic effect of pregnenolone with either doxorubicin, mitomycin C or cisplatin could be determined in any given concentration. Experiments were performed once in technical duplicates. Mean values were calculated.

3.5.3.2.2 Double Treatment with Tosufloxacin and Doxorubicin Showed Minor Additional Effects on Cell Death Rates

Hep3B cells were treated with tosufloxacinin, doxorubicin, mitomycin C and cisplatin in single and combined applications (Figure 37). None of the single tosufloxacin concentrations used (1, 10, 30 µM) was sufficient to induce cell death by itself. Furthermore, no additional or synergistic effect was observed when tosufloxacin was combined with cisplatin or mitomycin C. A minor additional effect was seen upon combinational treatment with both 10 µM or 30 µM tosufloxacin and doxorubicin. Cell numbers in the $subG_1$ fraction rose from

25% in single treated cells to 30% and 40% in tosufloxacin / doxorubicin–treated cells, respectively.

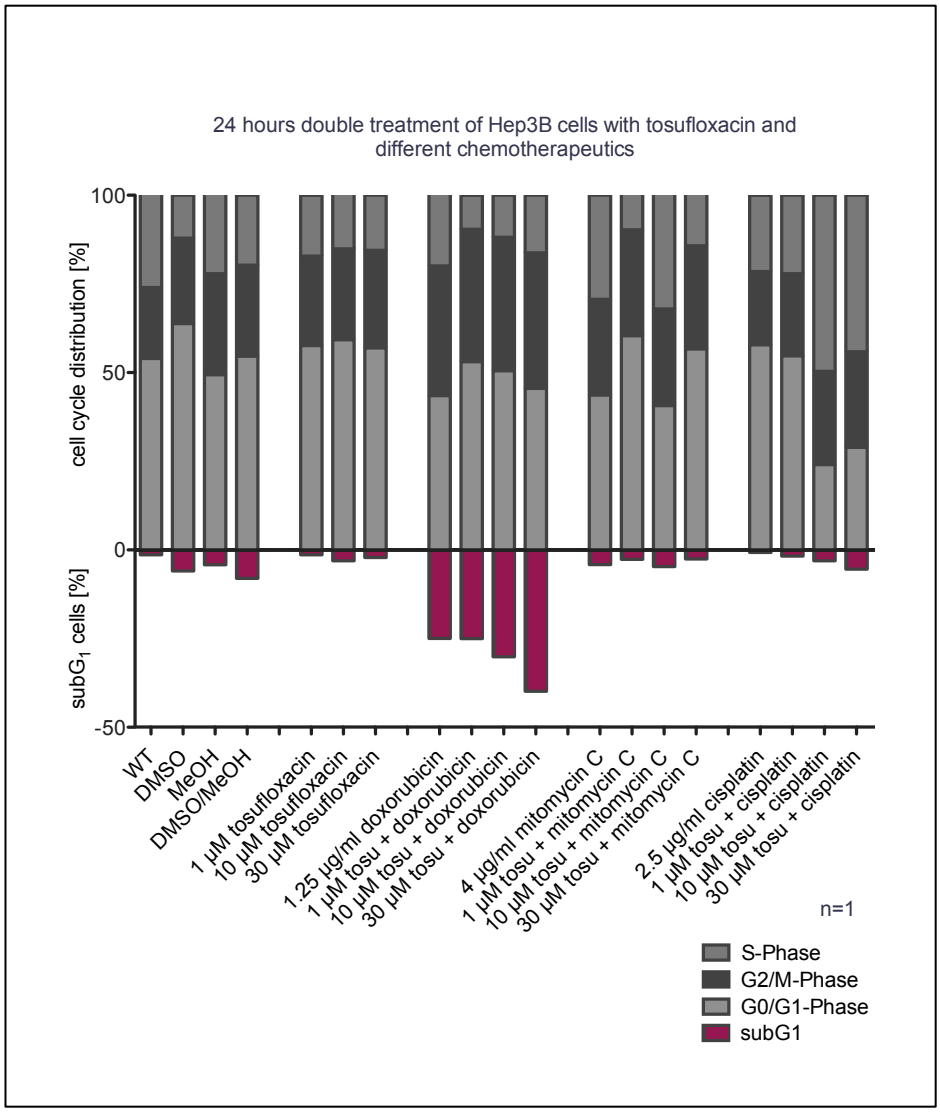

Figure 37: Cell cycle distribution and cell death rates of tosufloxacin double-treated Hep3B cells with different chemotherapeutics after 24 hours. Hep3B cells were treated for 24 hours with tosufloxacin or tosufloxacin in combination with different chemotherapeutics to evaluate possible synergistic effects of the double treatment. Combination of 10 µM and 30 µM tosufloxacin with doxorubicin led to a small synergistic increase in cell death rates, compared to the single treatments. Experiments were performed once in technical duplicates. Mean values were calculated.

3.5.3.2.3 Double Treatment with Camptothecin and Mitomycin C Resulted in Major Synergistic Effects on Cell Death Rates

Cells were treated with camptothecin, doxorubicin, mitomycin C and cisplatin in single and combined applications (Figure 38). A dose-dependent synergistic effect was seen in all combinations apart from treatment of cells with camptothecin and doxorubicin, where a minor additional effect was seen. The highest synergistic effect was seen upon combination of camptothecin and mitomycin C, leading to a significant cell death increase in all tested

concentrations. Up to 40% of the double-treated cells were in the apoptotic subG$_1$ cell fraction, compared to only 3 to 6% of the cells treated with camptothecin or mitomycin C alone.

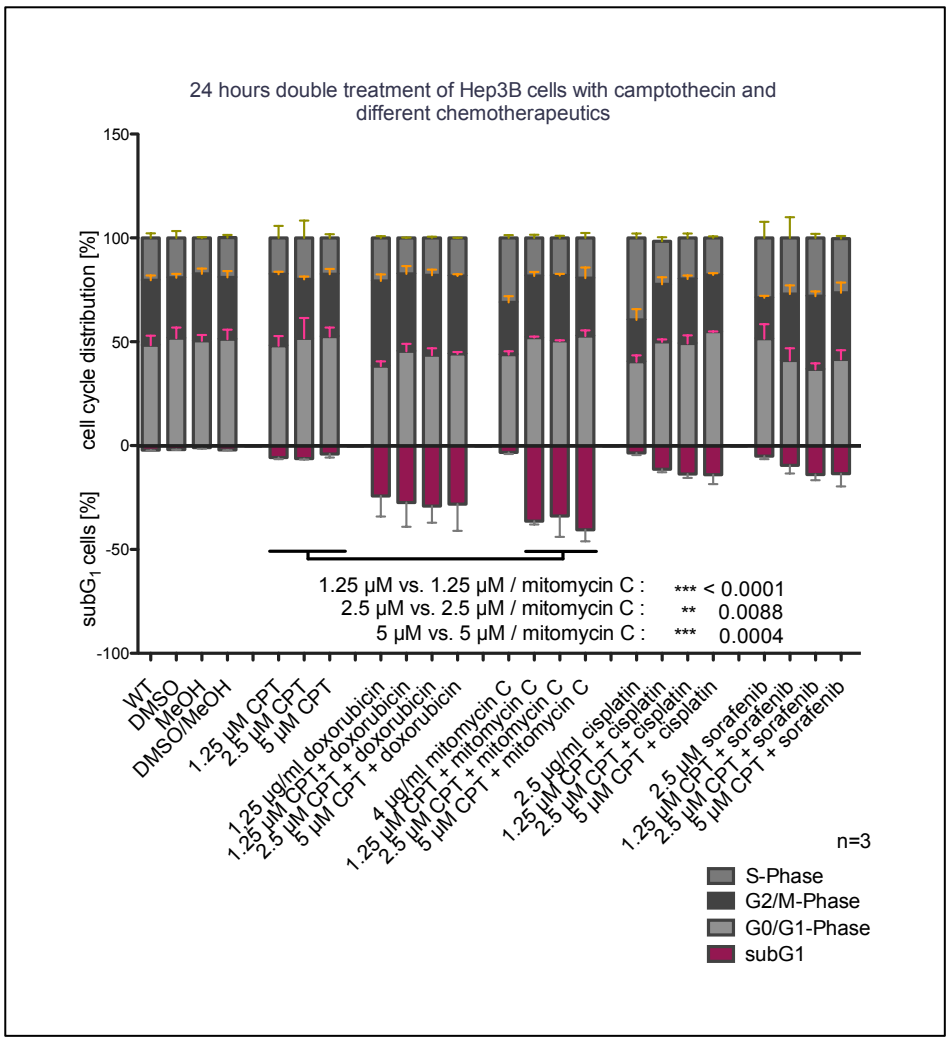

Figure 38: Cell cycle distribution and cell death rates of camptothecin double-treated Hep3B cells with different chemotherapeutics after 24 hours. The effects on cell death rates and cell cycle distribution of camptothecin (CPT)-treated cells, in single or double administration with either doxorubicin, mitomycin C, cisplatin or sorafenib, was monitored via Nicoletti staining. Solvent-treated and wildtype cells served as control. The cell cycle distribution was not altered significantly in any given treatment. Nevertheless, all double treatments led to a synergistic cell death rate increase, with a significant increase seen in all combinations of camptothecin with mitomycin C (p-values between <0.0001 and 0.0088). Experiments were performed in biological triplicates, each consisting of technical duplicates. Mean values ± SD, as well as p-values (two-tailed t-test), were calculated.

3.5.3.2.4 Double Treatment of 7-ethyl-10-hydroxycamptothecin and Mitomycin C Resulted in Synergistically Increased HCC Cell Death

Cells were treated with 7-ethyl-10-hydroxycamptothecin, doxorubicin, mitomycin C and cisplatin in single and combined applications (Figure 39). 7-ethyl-10-hydroxycamptothecin is the active part of Irinotecan, the clinically used camptothecin derivate. Almost no additive effect was seen, when 7-ethyl-10-

hydroxycamptothecin was combined with any concentration of cisplatin, leading to a cell death rate of approximately 11%. Combination of 7-ethyl-10-hydroxycamptothecin with doxorubicin led to a minor increase in the apoptotic subG$_1$ fraction of cells from 23% (single doxorubicin treatment) to 32% (double treatment). The combination of 7-ethyl-10-hydroxycamptothecin with mitomycin C led to a major synergistic effect, increasing cell death rates from 2-5% in mitomycin C single-treated cells to 23% when combined with 1.25 µM 7-ethyl-10-hydroxycamptothecin.

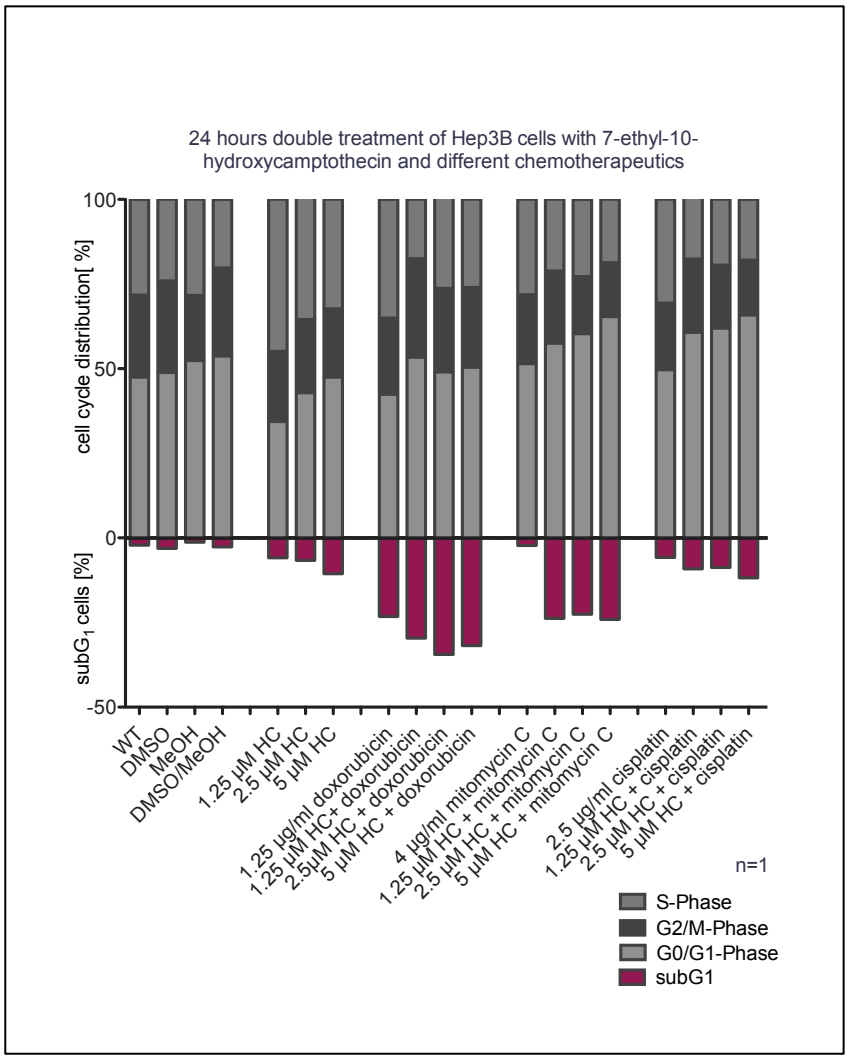

Figure 39: Cell cycle distribution and cell death rates of 7-ethyl-10-hydroxycamptothecin double-treated Hep3B cells with different chemotherapeutics after 24 hours. After treatment with 7-ethyl-10-hydroxycamptothecin without or with the addition of doxorubicin, mitomycin C or cisplatin, the cell cycle distribution was not altered significantly compared to those of the wildtype and solvent-treated cells. Nevertheless, a cell death rate increase was seen in combinations of 7-ethyl-10-hydroxycamptothecin with doxorubicin and with mitomycin C. Experiments were performed once in technical duplicates. Mean values were calculated.

3.5.3.3 Further Evaluation of the Effects on Cell Death from the Combinatorial Application of Camptothecin and other Chemotherapeutics in the HCC Cell Lines HepG2 and HuH7

To further investigate the effect of camptothecin and cisplatin, mitomycin C or doxorubicin double treatment on further HCC cells lines, HuH7 and HepG2 cells, were treated and subsequently analyzed as described before.

3.5.3.3.1 HepG2 Camptothecin Single- and Double-Treatment with Chemotherapeutics Excessively Induced Apoptosis

Cells were treated with camptothecin, doxorubicin, mitomycin C and cisplatin in single and combinatorial applications (Figure 40). HepG2 cells reacted sensitive to all substances. The solvent control (DMSO / MeOH) led to 17% dead cells. Furthermore, the cells showed a dose-dependent increase in cell death rates up to 50% upon camptothecin single treatment. Double treatment with camptothecin and either cisplatin or sorafenib also showed a dose-dependent increase in apoptotic cells, but was not significantly different from death rates seen upon camptothecin single treatment. The combination of camptothecin and mitomycin C resulted in a small additive effect with a total of approximately 72% dead cells.

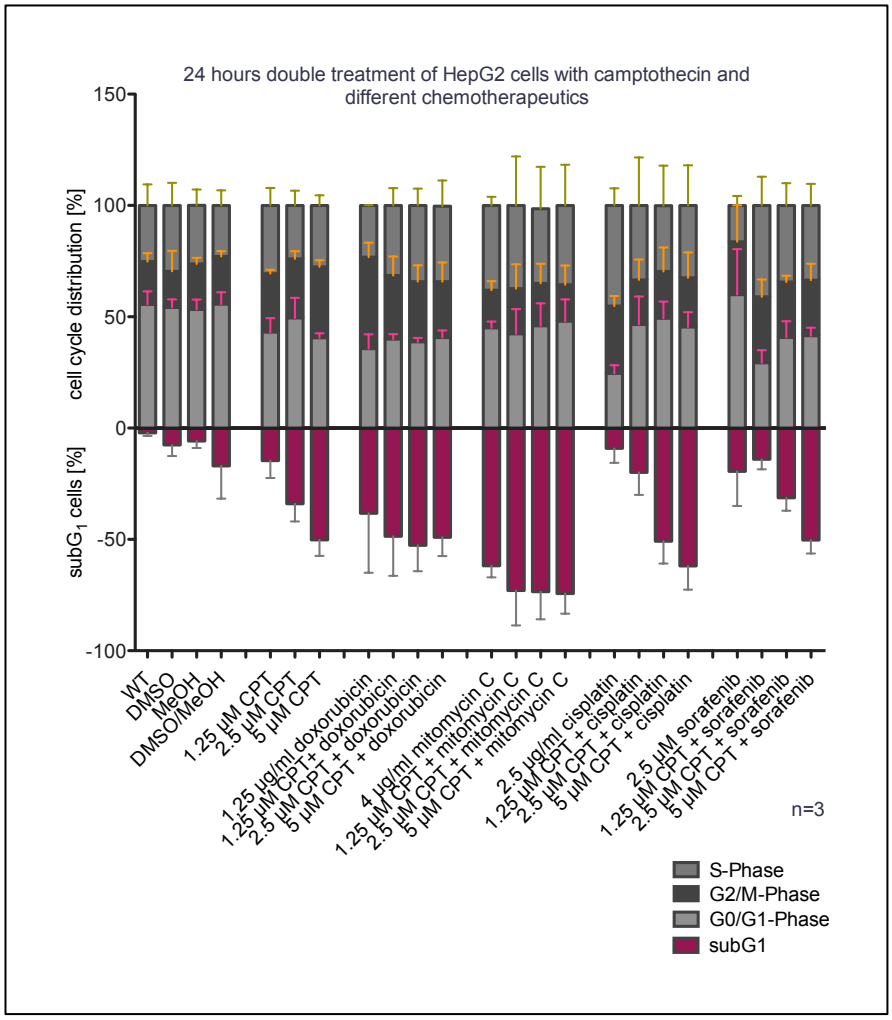

Figure 40: Cell cycle distribution and cell death rates of camptothecin double-treated HepG2 cells with different chemotherapeutics after 24 hours. HepG2 cells are sensitive to all treatment possibilities, leading to increased amounts of cells in the $subG_1$ peak. Increased cell death is seen in cells treated with 2.5 µM camptothecin and either doxorubicin, mitomycin C or cisplatin. Experiments were performed in biological triplicates, each consisting of technical duplicates. Mean values ± SD were calculated.

3.5.3.3.2 Treatment of HuH7 Cells with all Camptothecin-Combinational Applications Resulted in an Additive Increase in Cell Death Rates

Cells were treated with camptothecin, doxorubicin, mitomycin C and cisplatin in single and combinatorial applications (Figure 41). An additive effect was seen in all combinations. camptothecin single treatment led to a maximum amount of 15% dead cells. In combination with 5 µM sorafenib, a total of 21% dead cells were measured. The camptothecin double treatment with cisplatin and doxorubicin lead to a total of 21% and 41% respectively. The highest amount of apoptotic cells were measured upon mitomycin C double treatment with a maximum of 57% dead cells compared to mitomycin C single treatment with an amount of 46% cells in the $subG_1$ fractions.

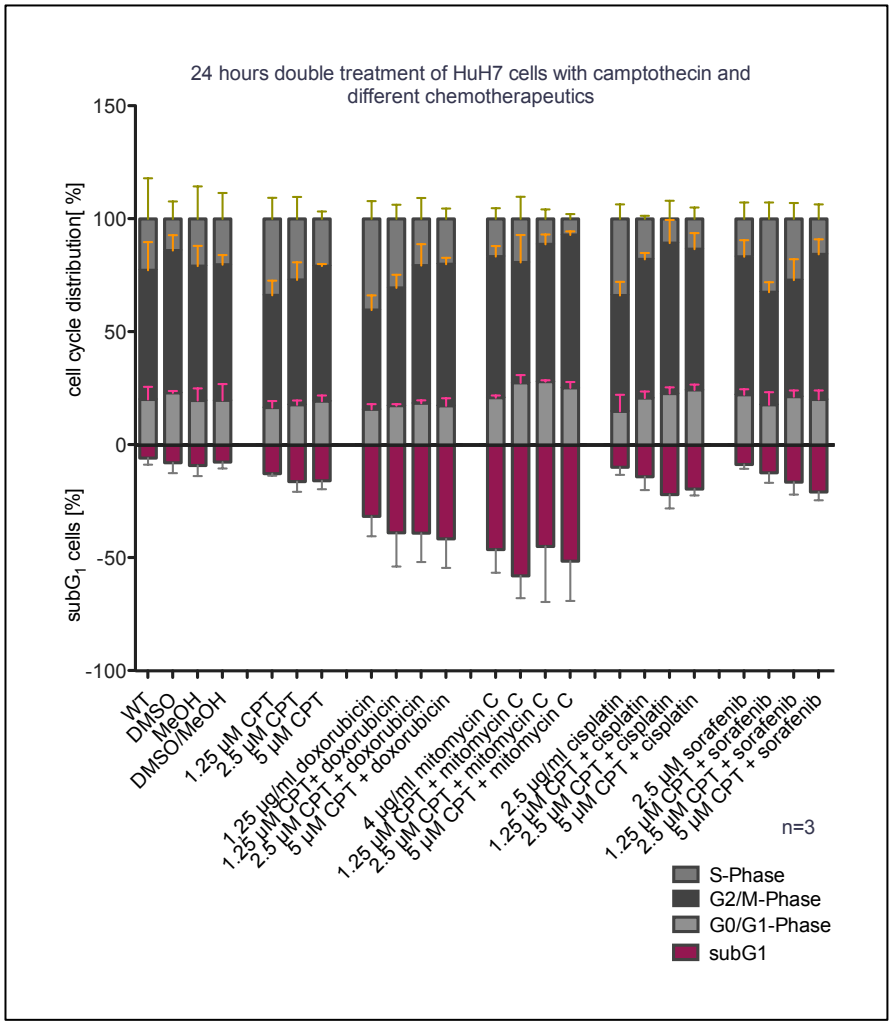

Figure 41: Cell cycle distribution and cell death rates of camptothecin double-treated HuH7 cells with different chemotherapeutics after 24 hours. The cell cycle distribution was not altered significantly under any given treatment. Furthermore, beside camptothecin / sorafenib double-treatment, all combinational treated cells showed an additive cell death effect, leading to increased numbers of cells in the $subG_1$ peak in any given concentration. Experiments were performed in biological triplicates, each consisting of technical duplicates. Mean values ± SD were calculated.

3.5.4 Influence of Camptothecin and other Topoisomerase I Inhibitors on FUBP1 Target Gene Expression

p21 is a well known direct target gene of FUBP1 [1]. To examine the effect of camptothecin, its derivate 7-ethyl-10-hydroxycamptothecin and other topoisomerase I inhibitors like NSC 725776 and NSC 724998 on FUBP1 activity in cells, target gene expression of *p21* and *c-myc* were investigated after 6 hours of treatment via qRT-PCR. Furthermore, the amount of FUBP1 protein was validated via western blot analysis.

3.5.4.1 All tested Topoisomerase I Inhibitors Induced a Dose-Dependent mRNA Expression Increase of the FUBP1 Target Gene p21 while FUBP1 Protein Level Remained Stable

All treated cells showed a significant, dose-dependent increase in *p21* levels after treatment with any of the topoisomerase I inhibitors used in this study

(camptothecin, 7-ethyl-10-hydroxycamptothecin, NSC 725776 and NSC724998) (Figure 42). Furthermore, the application of these inhibitors did not change the expression level of *c-myc* significantly. Cells treated either with camptothecin, NSC 724998 or NSC 725776 showed a dose-dependent increase in *p21* mRNA levels, with the highest alteration induced by a 10 µM compound concentration (12,9-fold, 5.4-fold and 8.5-fold *p21* mRNA expression compared to DMSO-treated control cells). Treatment with 7-ethyl-10-hydroxycamptothecin also increased the amount of *p21* mRNA, but not in a dose-dependent manner (4.2-fold compared to DMSO-treated cells). Western blot analysis showed that the protein levels of FUBP1 were not altered upon application of the inhibitors.

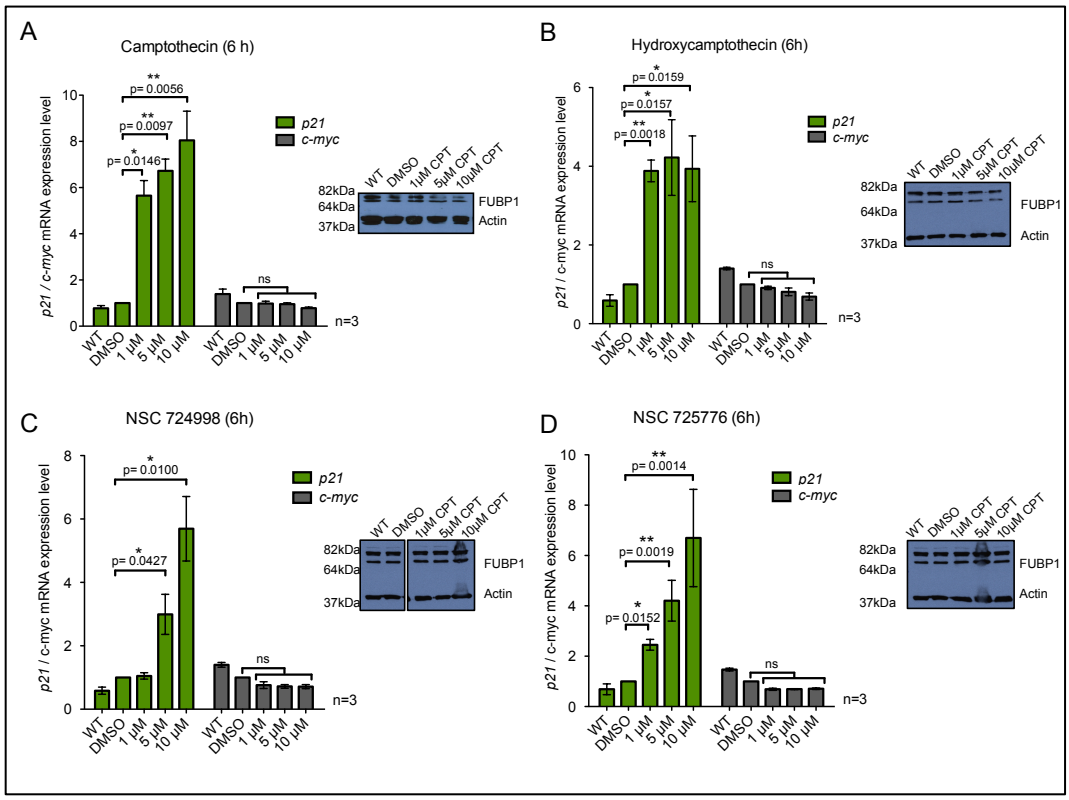

Figure 42: FUBP1 target gene expression in Hep3B cells after topoisomerase I inhibitor treatment. Cells were incubated with the inhibitors for 6 hours. Target gene expression was investigated via qRT-PCR and normalized to *GAPDH* mRNA. Protein expression was verified via western blot analysis. (A), (C), (D) Cells treated either with camptothecin, NSC 724998 or NSC 725776 showed a significant, dose-dependent increase in *p21* mRNA with a maximum of 12,9-fold, 5.4-fold and 8.5-fold expression compared to DMSO-treated control cells. (B) Treatment with 7-ethyl-10-hydroxycamptothecin increased the amount of *p21* mRNA significantly (4.2-fold), compared to DMSO-treated cells, independently of the concentration used. Western blot analysis showed that the amount of FUBP1 protein was not altered by any of the treatments. Experiments were performed in biological triplicates, each consisting of technical duplicates. Mean values ± SD as well as p-values (two-tailed t-test) were calculated.

3.5.4.2 *Treatment of HepG2 and HuH7 Cells Led to an Increase in FUBP1 Target Gene p21 mRNA Expression Levels, while FUBP1 Protein Levels Remained Stable*

HepG2 cells showed an inverted significant, dose-dependent effect of *p21* mRNA expression levels upon camptothecin treatment (Figure 43). While incubation with 1 µM camptothecin led to a 9.2-fold increase, 5 µM evoked a 4.2-fold and 10 µM only to a 2.4-fold increase compared to the DMSO-treated cells. Furthermore, *c-myc* mRNA levels were significantly decreased to a 0.3-fold expression compared to the DMSO-treated cells. FUBP1 protein levels were not altered by camptothecin application. HuH7 cells showed a significant, dose-dependent increase of *p21* mRNA levels after camptothecin treatment. The *p21* mRNA expression level rose from 5-fold (1 µM), to 10.2-fold (5 µM) and finally 12.4-fold (10 µM). During camptothecin application, expression levels of *c-myc* mRNA were slightly, but significantly decreased to 68% (5 µM) and 75% (10 µM), respectively. FUBP1 protein expression was not altered in the presence of camptothecin.

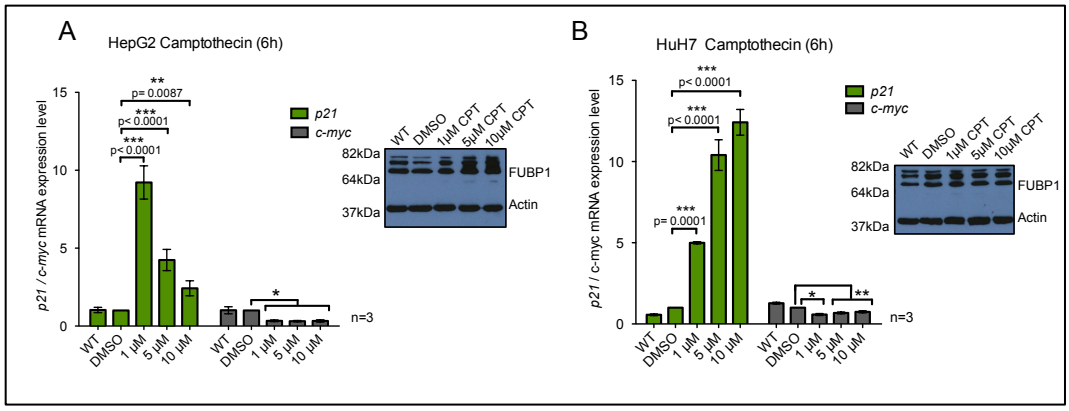

Figure 43: FUBP1 Target gene expression in HepG2 and HuH7 cells after camptothecin treatment. Cells were treated for 6 hours. Target gene expression was investigated via qPCR and normalized to *GAPDH* mRNA levels. Protein expression was verified via western blot analysis. (A) HepG2 cells showed a significant, inverted dose-dependent effect on *p21* mRNA expression levels. Furthermore, *c-myc* mRNA levels decreased significantly to 0.3-fold of the DMSO-treated control cells. (B) HuH7 cells showed a significant, dose-dependent increase in *p21* mRNA expression level following camptothecin treatment, *c-myc* mRNA levels decreased significantly to 0.5- and 0.7-fold of the DMSO-treated control cells. The amount of FUBP1 protein, confirmed by westerblot analysis, was not altered under any of the tested conditions. Experiments were performed in biological triplicates, each consisting of technical duplicates. Mean values ± SD, as well as p-values (two-tailed t-test) were calculated.

3.6 Therapeutic Treatment of Hep3B Xenograft Tumors using Irinotecan Induced Total Tumor Remission

To investigate the effect of irinotecan on established HCCs in an *in vivo* mouse model, 5×10^6 Hep3B cells were injected into the flank of NOD/SCID mice. Tumors were allowed to grow to a volume of 100 mm^3, before treatment with irinotecan started. Mice were grouped (6-8 mice per group) and treated according

to the schedule presented earlier (see page 62, paragraph 2.2.6). During the treatment period, mice were weighed daily for 21 days, and tumor volumes were measured every third day. After the treatment period, tumors and body weight were measured twice a week. Mice were sacrificed, when tumors reached a volume of 1,000 mm^3. The effects of six different treatments on tumor growth were evaluated: irinotecan, mitomycin C, irinotecan plus mitomycin C, sorafenib, i.p. control with solvent, and oral control with solvent.

3.6.1 Irinotecan Single-Treatment led to Total Tumor Remission and Significantly Increased Overall Survival in a Xenograft Mouse Model but Displayed Side Effects

Due to an unexpected rapid weight loss of more than 20%, all mice of the irinotecan / mitomycin C double treatment group were sacrificed after 7 days of treatment. Apart from the irinotecan-treated group, all others showed an increase in tumor volume during the treatment period, with no significant differences compared to the control-treated groups (Figure 44). After 3 days of treatment, tumors of the irinotecan-treated group stopped progression, and after six days, the first shrinkage of tumors was measureable. After 18 days of treatment (day 34), in all 8 mice of the irinotecan group a total tumor remission was seen. Up to day 87, these mice showed no sign of tumor recurrence. Eventually, all mice developed tumors again and were sacrificed. The life span of the irinotecan-treated mice was significantly increased compared to those of the other groups.

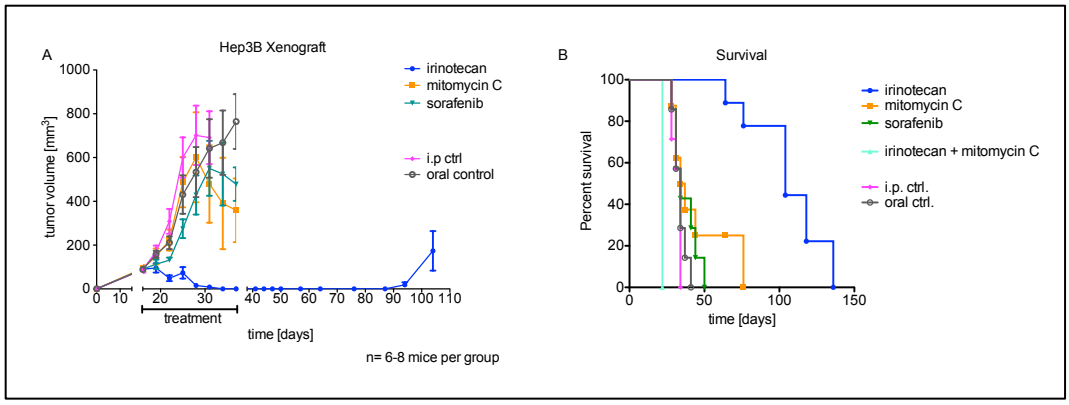

Figure 44: First Xenograft Mouse Model with Irinotecan Treatment 5 x 10^6 Hep3B cells were injected into the flank of NOD/SCID mice. The tumors were allowed to grow to a volume of 100 mm^3 before treatment started. Mice were treated with either 20 mg/kg irinotecan, 3.25 mg/kg mitomycin C, 30 mg/kg sorafenib, 20 mg/kg irinotecan plus 3.25 mg/kg mitomycin C or 0.9% NaCl-treated solvent control (i.p.- and oral-control). Due to an unexpected rapid weight loss of more than 20% in all mice of the irinotecan / mitomycin C double treatment group, the animals were sacrificed after 7 days of treatment. (A) Treatment with irinotecan led to a total tumor remission after 18 days of treatment in 100% of mice. The animals were kept remission-free for 53 days, before tumors relapsed. (B) The life span of irinotecan-treated mice was significantly increased compared to those of all other treated groups. Mean values ± SD were calculated with a size of 6 to 8 mice per group.

Minor side effects were seen in the irinotecan-treated group. All mice lost weight during the consecutive 5 days of treatment, but regained most of it in the 2 days between treatments. Mice regained their starting weight, when the treatment was stopped after 21 days (Figure 45).

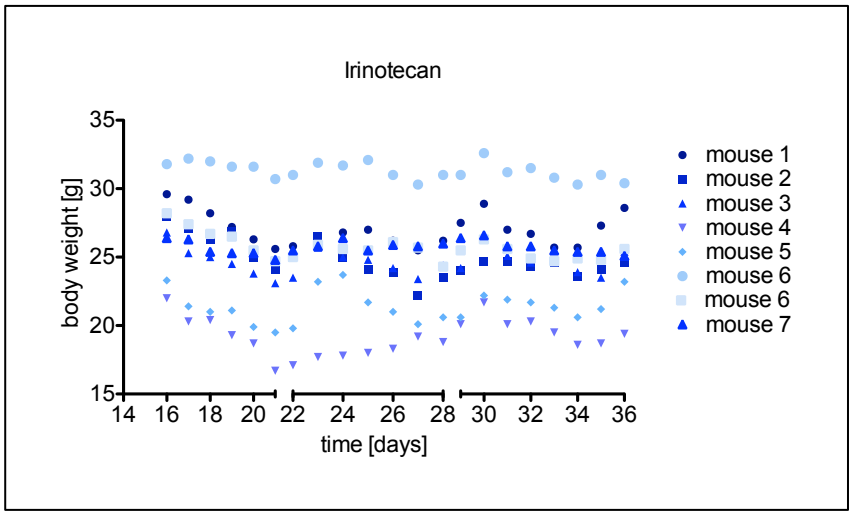

Figure 45: Body weight loss during irinotecan treatment. Mice were treated for 5 consecutive days followed by a treatment pause of two consecutive days. The cycle was repeated three times. Minor body weight losses (≤ 20%) were seen in all mice during the time of the treatment.

3.6.2 Irinotecan Single- and Double-Treatment resulted in Total Tumor Remission and Significantly Increased Overall Survival in a Xenograft Mouse Model With no Measureable Side Effects

In the second xenograft transplantation experiment, the concentrations of drugs given to the mice were reduced, based on the experience of the first experiment. Half of the dose of irinotecan (10 mg/kg) and a quarter of the mitomycin C (0.8125 mg/kg) dose were used. No unexpected side effects occurred this time. The treatment started at day 14, after injection of the Hep3B cells, when the tumors had reached an average size of 100 mm^3 (Figure 46). During the treatment period, tumors of mitomycin C single-treated mice showed almost no difference in growth compared to the control-treated group. Both groups were sacrificed after 35 days, when the xenograft tumors had reached a volume of approximately 1,000 mm^3. After 14 days of treatment, all 6 mice of the irinotecan single-treated group showed total tumor remission. The mice of the irinotecan / mitomycin C double-treated group showed a total remission already after 10 days of treatment. The single-treated animals remained tumor-recurrence free for a total of 43 days until day 71, the irinotecan / mitomycin C double-treated mice for a total of 63 days until day 91. Mice of both groups were again treated with the irinotecan / mitomycin C double treatment, when the relapsed tumors reached again a volume of 100 mm^3 (Figure 46). 100% (6/6) of

the irinotecan single-treated mouse group showed a tumor relapse (the latest after 120 days in total), which went into total remission after the second round of irinotecan / mitomycin C double treatment. Until day 120, only 50% (3/6) of the irinotecan / mitomycin C double-treated mice showed a relapse, and after the second chemotherapy with irinotecan and mitomycin C, two tumors went into total remission, while one remained stable in size. One mouse of the double-treated group had to be sacrificed after 94 days due to non-tumor related injuries.

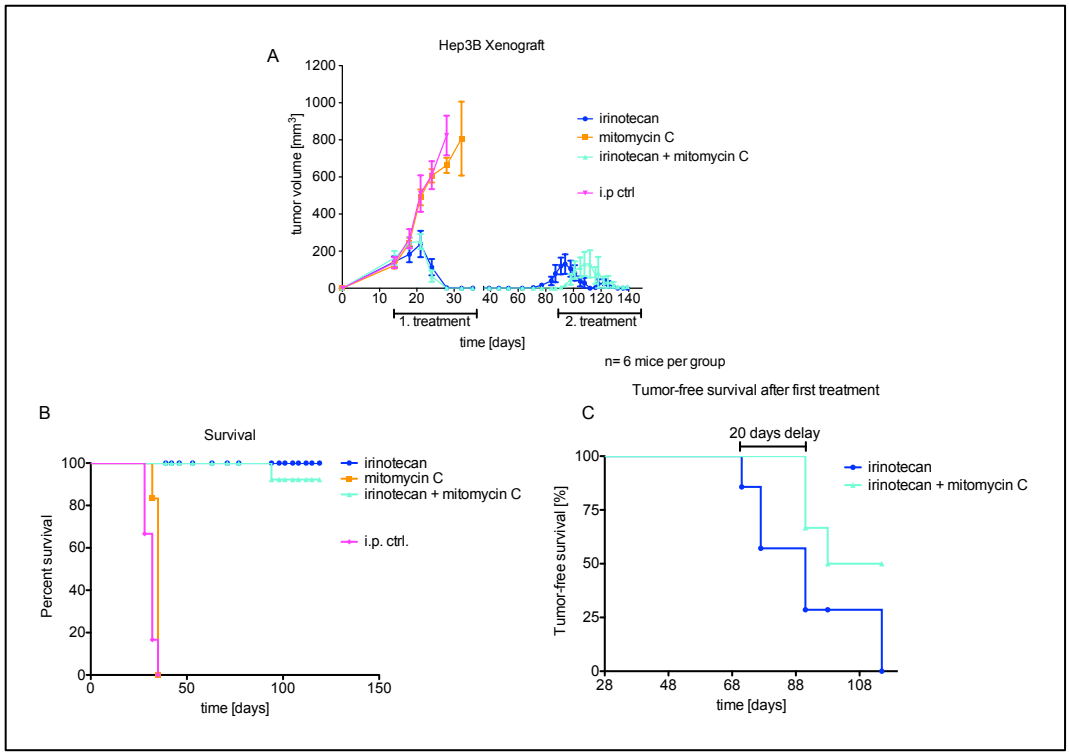

Figure 46: Second xenograft mouse model with irinotecan treatment. 5 x 10^6 Hep3B cells were injected into the flank of NOD/SCID mice. The tumors were allowed to grow to a volume of 100 mm^3 before the treatment started. Mean values ± SD were calculated with a size of 6 mice per group. Mice were treated with either 10 mg/kg irinotecan, 0.8125 mg/kg mitomycin C, 10 mg/kg irinotecan plus 0.8125 mg/kg mitomycin C or 0.9% NaCl solvent oral-control. (A) Irinotecan-treated animals showed a total tumor remission after 14 days of treatment and remained recurrence-free for a total of 43 days. The double-treated mice showed a total tumor remission after 10 days of treatment and remained relapse-free for a total of 63 days. (B) Mitomycin C single-treated mice had no survival benefit compared to the control-treated mice. The life span of irinotecan and irinotecan plus mitomycin C treated mice was significantly increased during the period of this experiment compared to those of the control mice. (C) After 120 days, 100% (6 / 6) of the irinotecan single-treated mice showed a tumor relapse. Nevertheless, only 50% (3 / 6) mice of the irinotecan / mitomycin C double-treated group relapsed. The earliest relapse in this group occurred 20 days after the earliest relapse in the single-treated group.

No side effects were seen in the group of irinotecan-treated animals. None of the mice dropped weight during the consecutive 5 days of treatment. The irinotecan / mitomycin C double-treated mice showed only minor effects of approximately 7% maximum weight loss (Figure 47).

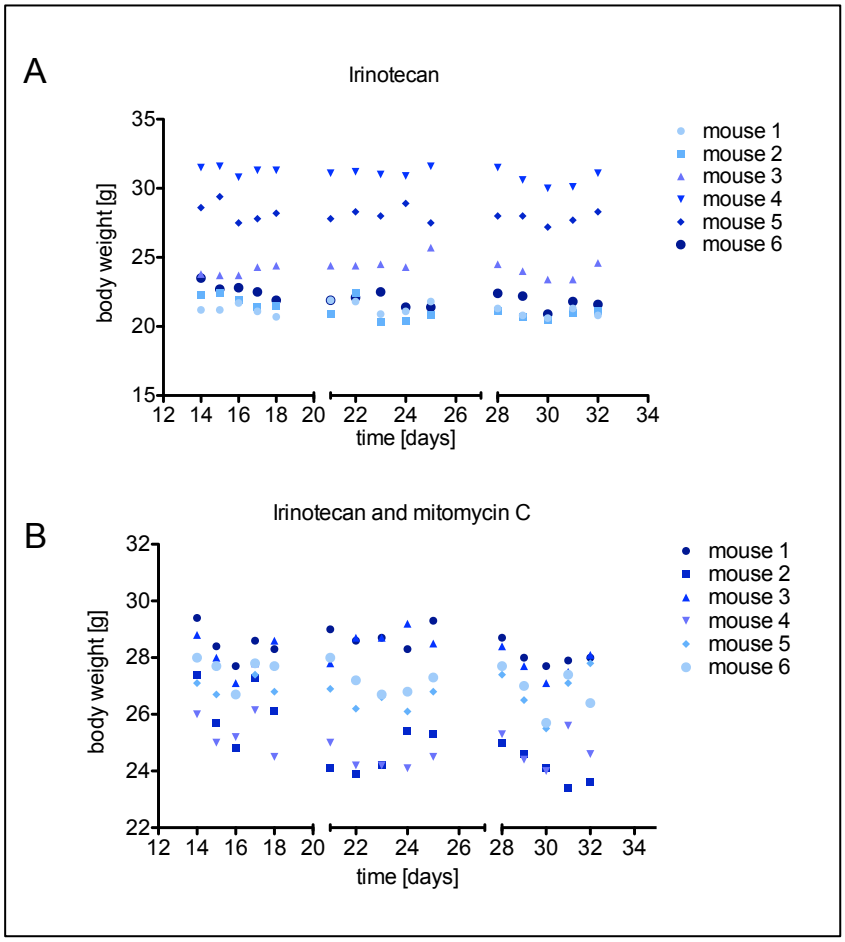

Figure 47: Body weight loss during the second irinotecan treatment xenograft experiment. Mice were treated for 5 consecutive days, followed by a treatment pause of two days. The cycle was repeated three times. (A) 10 mg/kg Irinotecan single treatment had no effect on the body weight of the mice. (B) 10 mg/kg irinotecan/ 0.8125 mg/kg mitomycin C double treatment had only minor effects on the body weight of the treated mice.

4 Discussion

The aim of this project was the identification of novel FUBP1 inhibitors to target FUBP1 activity in hepatocellular carcinoma (HCC). Until today, treatment options for late stage HCC (stage B and C) are restricted to TACE (transcatheter aterial chemoembolization) or the application of the multi-kinase inhibitor sorafenib, and both are only used as palliative treatments [79].

In our laboratory, the transcriptional regulator FUBP1 was found to be highly overexpressed in HCC compared to normal liver tissue [80]. In the same study, target genes of FUBP1 in HCC could be identified, which play important roles in the intrinsic and extrinsic apoptosis pathway as well as in the regulation of the cell cycle. The cyclin-dependent inhibitor p21 (WAF1/CIP1), an important cell cycle inhibitor [81], was identified as a direct target of FUBP1 in HCC. Furthermore, we could show that the constitutive knockdown of *FUBP1* in a HCC xenograft transplantation experiment resulted in a significantly decreased tumor formation compared to the injected control tumor cells (see page 12, Figure 5).

These finding led us to the assumption that FUBP1 might serve as a novel target in HCC therapy.

4.1 Expression and Purification of Codon-Optimized FUBP1

4.1.1 Expression of coFUBP1

Expression of human FUBP1 was performed using the *pET28b* vector in BL21 *E. coli*. To efficiently express functional protein in the heterologous host, the codon sequence was optimized for bacterial cells. It was shown that redesigning the entire gene sequence dramatically improved the likelihood of high protein expression in general [82]. Furthermore, the protein was expressed using an auto-induction system in a 10 l fermenter at 22°C. Auto-induction was developed for proteins whose expression might be harmful to the host cells. In addition, the high-density cultures obtained by auto-induction produce more target protein per volume unit, than IPTG-induced expression systems [74]. We were able to express the full-length human FUBP1 protein in BL21 bacteria and purify it using a three-step protocol. However, only minor amounts of full-length protein were obtained, in total 0.27 mg of purified coFUBP1 from 5 l culture media. The low amounts of protein could be due to significant protein degradation. In her diploma thesis, Stefanie Hauck could show that degradation of recombinantly expressed full-length FUBP1 occurs at defined sequences, and the degradation pattern suggested that proteolysis takes place at the C-terminal region of FUBP1 [78].

Until today, the structure of FUBP1 remains unsolved. In 1994, Duncan et al. could show that the carboxy-terminal domain of FUBP1 is separated from the central domain by a highly flexible proline/glycine rich linker. Furthermore, this domain is glutamine- as well as tyrosine-rich and is described as mostly unstructured [3]. Unstructured domains, as for example, glycin-rich-regions (GRR), are prone to be degraded by proteases [83]. Furthermore, in a proteome analysis of *S. cerevisiae*, Gsponer et al. could show that mRNA encoding highly unstructured proteins are less abundant and exhibit a shorter half-life than structured proteins. Additionally, highly unstructured proteins are less abundant, the rate of synthesis is significantly lower and their half-life is shorter compared to the structured proteins. According to their grouping, highly unstructured proteins contain between 30-100% of unstructured regions [84]. If the amount of unstructured regions can negatively influence the protein synthesis rate as well as the protein half-life, these effects could contribute to the low amount of recombinantly expressed FUBP1, which inherits 32.5% of unstructured regions, if the C-terminus is accepted as such one. Ms. Hauck could furthermore demonstrate the influence of the unstructured C-terminus on the protein expression and degradation. The expression of a truncated FUBP1 missing the c-terminal region (FUBP1ΔC) led to the isolation of significantly higher protein amounts, as well as significantly lowers protein degradation products [78].

To further enhance the amount of full-length protein, different strategies could be pursued, e.g. the use of different host strains, as well as the co-production of chaperones [85]. In the engineered *E. coli* host strain “Artic Express” (Agilent Technologies) the mRNA is stabilized by attenuation of RNase activity. The co-production of chaperones supports the initial protein folding, leading to less protein aggregation. Additionally, the change of the expression system could also lead to superior results. We therefore expressed full-length FUBP1 in mammalian, as well as in insect cells. Both systems were suitable for FUBP1 expression, but nevertheless, the protein yield was comparable to the one achieved by the bacterial expression system (data not shown).

4.1.2 Recombinant Protein Purification

To purify recombinant FUBP1, a three-step protocol was established. First, IMAC purification using Ni-NTA columns was performed. Afterwards, a heparin column was used, exploiting the FUBP1 DNA-binding capacity. Finally, size exclusion using a Superdex 16/60 200 column was used. In contrast to the experience from Hsiao et al. 2010, no nonspecific interaction of the protein with the superdex

column was observed [17]. To analyze the protein fractions, samples for SDS-PAGE electrophoresis were collected, before protein sample fractions were pooled and subsequently stored at -80°C. Although only low total protein amounts of coFUBP1 were obtained, the samples were pure and, according to the size exclusion chromatogram, monomeric.

To verify the identity of the recombinant protein, Western blot analysis and mass spectrometry were performed, and confirmed the identity of human FUBP1.

4.2 Functional Analyses of recombinant FUBP1

To ensure the functionality of the recombinant protein, binding studies with a 53-mer *p21-FUSE* oligonucleotide were performed. The binding affinity between *FUSEp21* and FUBP1 could be determined in a nanomolar range in SPR as well as in MST measurements.

To guarantee the specificity of the binding between FUBP1 and *FUSEp21*, the oligonucleotides *p31* and *p39* were used as negative controls. These oligonucleotides were previously found not to bind to FUBP1 in electro mobility shift (EMSA) assays [80]. Furthermore, MBP (maltose binding protein) protein was used as a protein not binding to *FUSE* DNA, to show the specificity of the *p21* oligonucleotide. In two independent experiments, a binding constant of 12.9 nM for the interaction of FUBP1 and *FUSEp21* could be determined.

During MST measurements with the same *FUSEp21* oligonucleotide and recombinant FUBP1, a binding constant of 12.31 nM was measured. In an additional, independent MST experiment, a binding constant of 8.8 nM could be calculated (data not shown).

In summary, the K_D values of all experiments suggest a specific, high affinity binding between recombinant FUBP1 and *FUSEp21*.

In 2010, Hsiao et al. purified a FUBP1 full-length variant, which inherited cloning artifacts of 69 additionally included amino acids at the N-terminus, expressed in a baculovirus expression system. Furthermore, the cysteines 132, 148 and 332 were replaced with alanines in this FUBP1 variant. To determine a binding constant between FUBP1 and *FUSE*, a synthetic 53-mer oligo of the non-coding *c-myc-FUSE* was used as the binding partner [17]. FUBP1 *FUSE* binding was quantified using fluorescence anisotropy measurement and fluorescence correlation spectroscopy measurements. Fluorescence anisotropy measurement resulted in a K_D determination of 415.8 ± 137.78 nM, in the fluorescence correlation spectroscopy measurements a K_D of 168.6 ± 36.6 nM could be

calculated. In 2002, Braddock et al. measured a K_D of 10 nM between a FUBP1 variant (consisting of only KH3 and KH4) and a 29-mer *c-myc FUSE* [86].

The independent experiments performed by different groups show that FUBP1 and *FUSE* form a high-affinity complex. Differences in K_D values can be explained by multiple factors. As described before, the full-length protein used by Hsiao et al. 2010 inherited several cloning artifacts, which could have affected the binding capacity of the protein. Furthermore, the *FUSE* oligonucleotide used by this group was derived from the *c-myc*, not the *p21 FUSE* element. FUBP1 can bind to different *FUSE* motifs with varying affinities; therefore it is likely that the binding affinities of FUBP1 towards *c-myc* and *p21 FUSE* differ from each other. Although Braddock et al. in 2002 also used the *c-myc FUSE* motif, the measured K_D is almost similar to the one we measured [86]. However, in contrast to our study, they used only the DNA binding-domains KH3 and KH4 of FUBP1, not the full-length protein, which could explain the similar high affinity binding, despite the different *FUSE* motifs.

4.3 AlphaScreen® Interaction Studies

To identify small molecule inhibitors of the FUBP1 and *FUSEp21* interaction, an AlphaScreen® assay procedure was established. The assay system was used to subsequently screen two different libraries, one small molecule library with 14,400 substances (Maybridge Hit Finder™ library) and one FDA-approved drug library with 1,600 substances (Prestwick Chemical library). Hits were defined as substances, which diminished the signal intensity to 30% or less and were subsequently re-screened using the same assay. After the second screen, all hits were bioinformatically evaluated by the use of a SOM (self-organizing-map), established and performed by Janosch Achenbach (AG Proschak, University of Frankfurt). A total of 103 compounds of the Maybridge Hit Finder™ library (<1%) and 55 compounds of the Prestwick Chemical library (3.43%) were defined as hits.

In 2004, Huth et al. already screened for FUBP1 inhibitors using three approaches: HTS-NMR, Virtual Ligand Binding (VLB) and affinity selection/mass spectrometry (ASMS) [87]. In contrast to the project pursued during this thesis, they only used the KH3/KH4 DNA-binding domain as described in 2002 [86]. Nevertheless, they only found four compounds, which bound with rather low affinities between 0.35 mM and >4 mM to the recombinant FUBP1 DNA-binding

domain. None of these compounds have been further investigated as FUBP1 inhibitors.

To estimate the quality of the established AlphaScreen® assay, the statistical effect size (z-factor) was calculated. The z-factor is a dimensionless, simple statistical characteristic for high throughput screenings (HTS). A value of 1 defines an ideal assay, a factor between 0.5 and 1 defines an excellent assay, values between 0 and 0.5 a marginal assay [88]. The values of the competitive assay (see page 75, paragraph 3.3.2) are used to determine the statistical effect size. 0 nM unbound free *FUSEp21* were used as the negative control, 100 nM unbound *FUSEp21* as the positive control. The AlphaScreen® assay established in this study was classified as an excellent assay with a z-factor of 0.74.

Equation 8:

$$Z - factor: 1 - \frac{3(\sigma_p - \sigma_n)}{|\mu_p - \mu_n|}$$

σ_p: *standard deviation positive control*

σ_n: *standard deviation negative control*

μ_p: mean positive control

μ_n: mean negative control

To identify further FUBP1 inhibitors in the future, an additional, already established screening approach could be used. In 2014, Mahapatra et al. described a HTS fluorescence anisotropy screen for the oncogenic mRNA binding protein IMP-I [89]. They used purified protein and a 93-nucleotide fluorescently labeled *c-myc* mRNA binding site. The advantage of this assay system compared to the Alpha® technology is the cost efficacy, because no additional dye or bead system need to be purchased. Furthermore, the assay functions as a real time assay measuring the steady state binding conditions, thereby decreasing the amount of incubation time to the time needed to for the binding between both partners until the equilibrium phase is reached.

4.4 Re-Screening of Potential FUBP1 Inhibitors using SPR Technology

Re-screening of potential FUBP1 inhibitors, which I found in the AlphaScreen® assay, was performed using SPR measurements. The *FUSEp21* oligonucleotide was used as the ligand, whereas recombinant coFUBP1 protein served as the analyte. Immediately prior to measurement, a dilution series of each compound (0 µM, 0.1 µM, 1 µM, 10 µM, 50 µM and 100 µM) was added to the analyte samples. The decrease of the association of both components was measured, thereby evaluating the potential of the compound as a FUBP1 inhibitor.

17 hit compounds of the Maybridge Hit Finder™ library, representing at least one compound from every group organized by the SOM, were tested, and four promising candidates were identified. The molecule HTS 06795 showed the best dose-dependent inhibition with a decrease in signal intensity of 75% at 10 µM concentration (Figure 28).

13 hit compounds isolated from the Prestwick Chemical library were re-tested, leading to the validation of 3 hit compounds: tosufloxacin, pregnenolone and camptothecin.

As camptothecin is known as a potent inhibitor of the topoisomerase I (TOP1) [60], the additional TOP1 inhibitors NSC 725776, NSC 724998 as well as 7-ethyl-10-hydroxy-camptothecin (active part of the clinically used irinotecan) were also tested in SPR measurements. All tested TOP1 inhibitors provoked a dose-dependent decrease of the FUBP1-*FUSEp21* interaction (see page 80, paragraph 3.4.2.1). Furthermore, they all act as interfacial inhibitors, targeting protein/ssDNA complexes [59]. This suggested, that the mechanism responsible for the FUBP1 inhibition might be identical: As the topoisomerase also binds to single stranded DNA, the compounds might also function as interfacial inhibitors, when inhibiting the FUBP1/*FUSE* interaction. Nevertheless, the SPR results would argue against this hypothesis, as pre-mixed protein/compound samples show a dose-dependent reduction of FUBP1/*FUSEp21* binding, and not a trapping of the binding complex. Of note, no experiment was performed, during which preformed FUBP1/*FUSEp21* complexes where incubated with the inhibitors, showing the effect of the inhibitors on the already formed DNA/protein complex. The crystallization of the FUBP1/*FUSEp21* complex together with the identified inhibitors might reveal the molecular mechanism how the inhibitors interfere with the FUBP1 function.

Interestingly, tosufloxacin, another hit compound, is also known as an interfacial topoisomerase inhibitor. In contrast to camptothecin, tosufloxacin selectively targets the bacterial topoisomerase type IIA enzyme (gyrase) [90].

As two out of three of the inhibitors isolated in the AlphaScreen® work with a comparable inhibitory mechanism, these findings would support the hypothesis that the FUBP1/*FUSEp21* complex inhibition by camptothecin and tosufloxacin could also be mediated by an interfacial mechanism.

4.5 Functional Analyses of FUBP1 Inhibitors

To monitor the effects of the inhibitory substances camptothecin, pregnenolone and tosufloxacin on hepatocellular carcinoma cell lines, cell expansion and cell activity as well as cell death assays were performed. Interestingly, in all of these tests, only camptothecin induced significant cellular effects. To further monitor the extent of FUBP1 inhbition by camptothecin, expression of the FUBP1 direct target gene (*p21*) was monitored in treated and untreated cells.

4.5.1 Tosufloxacin and Pregnenolone Treatment Showed no Effect on Cell Expansion or Cell Death in Hep3B Cells

Cell expansion assays were performed over a period of 72 hours (see page 82, paragraph 3.5.1). Cells treated with tosufloxacin or pregnenolone showed almost no alteration in cell expansion. Furthermore, WST assays performed with tosufloxacin- and pregnenolone-treated cells displayed no specific effect on cell activity (see page 83, paragraph 3.5.2.1). In Nicoletti experiments, no cell death induction could be observed after single treatment with tosufloxacin or pregnenolone, regardless whether the cells were treated for 24 or 72 hours. To apply an additional apoptotic trigger, double treatments with the known chemotherapeutics doxorubicin, mitomycin C and cisplatin were performed for 24 hours. Although double treatments with pregnenolone and chemotherapeutics had no additional effect on cell death rates, a minor additional effect was seen when combining tosufloxacin and mitomycin C (see page 88, paragraph 3.5.3.2.2).

The fact that tosufloxacin and pregnenolone interacted with recombinant FUBP1 protein in biochemical binding studies, but showed no effects in cellular assays, needs to be further elucidated. To address this problem, it is necessary to map the binding-sites of these substances to FUBP1 (see page 106, paragraph 4.4). If the binding concept is elucidated *in vitro*, it is important to verify this process in the cell. Throughout the binding of FUBP1 to *FUSE*, FUBP1 does not only interact with the single stranded *FUSE* DNA, but also with the p89 subunit of

TFIIH, and with FIR, the FUBP1 interaction repressor [4]. These interactions were not possible in the biochemical *in vitro* binding studies, where only FUBP1 and a 53 bp ssDNA oligonucleotide were present. These additional intracellular interactions are likely to lead to conformational changes of FUBP1, which could result in a “loss” of the inhibitor binding motifs, explaining the negative results of the cellular assays. However, if pregnenolone and tosufloxacin indeed interact with FUBP1 intra-cellularly, the relevance of FUBP1 as a therapeutically target in HCC therapy needs to be reconsidered. To address this question, ChIP experiments with treated HCC cell lines could be performed to compare the prevalence of FUBP1 on different transcriptionally active sites within the genome, as for example on the *p21 FUSE* locus, before and after treatment of the cells. Furthermore, luciferase reporter assays with the *FUSEp21* sequence could be performed to investigate the effects of the substances on the transcriptional activity of FUBP1.

4.5.2 Camptothecin Treatment decreases Cell Proliferation and Increases Cell Death in Hepatocellular Carcinoma Cell Lines

In contrast, however, camptothecin treatment influenced the cell behavior significantly. Hep3B cell expansion was diminished to the same extent as in cells treated with the HCC gold standard therapy Sorafenib (see page 82, paragraph 3.5.1). WST assays, displaying the mitochondrial activity and revealed that treatment with camptothecin led to a sigmoidal, dose-dependent cell activity decrease. 100 nM camptothecin were sufficient to decrease the Hep3B cell activity to ≤ 50% (see page 83, paragraph 3.5.2.1). In a second approach, combinations of the camptothecin derivate 7-ethyl-10-hydroxycamptothecin with either mitomycin C or sorafenib were applied. Both combinations showed synergistic effects. When combining 0.3 µM 7-ethyl-10-hydroxycamptothecin with either 0.3 µM mitomycin C or 0.3 µM Sorafenib, a reduction of mitochondrial activity down to 13.5% and 12% of the original (untreated) value was seen (see page 83, paragraph 3.5.2.2). As cell expansion and WST assays do not allow to discriminate between cell death and reduced cell proliferation (and vice versa), additional tests were performed. To further elucidate the role of camptothecin in cell death induction in HCC tumor cells, Nicoletti assays were performed in Hep3B cells. In both setups, single and double treatment, camptothecin positively influenced the amount of dead cells. Camptothecin single-treated cells showed enhanced killing after 72 hours, and additionally, an alteration in the cell cycle distribution of the remaining cells, e.g. G2/M arrest and sustained S-phase. Furthermore, the mitomycin C / camptothecin double treatment revealed a

significant, synergistic cell killing effect after 24 hours. To validate these results, double treatment experiments were also performed in HuH7 and HepG2 cell lines, also resulting in increased cell death rates (see paragraph 3.5.3.1 - 3.5.3.3.2).

4.5.3 The Influence of Camptothecin on Cell Death

Camptothecin induces DNA damage, which activates the checkpoint kinases 1 (CHK1) and 2 (CHK2). CHK1 is phosphorylated by ATR (ataxia telangiectasia and Rad3-related protein) on serine 345 and phosphorylates in turn Cdc25A, leading to the proteasomal degradation of Cdc25A and resulting in a subsequent S-phase and G2/M-phase arrest [91, 92]. CHK 2 is primarily phosphorylated by ATM (Ataxia telangiectasia mutated) on threonine 68, which leads to its dimerization and subsequent auto-phosphorylation which are required for its complete activation [93]. Although both kinases seem to be activated after exposure to camptothecin, as indicated by the activation of the ATM and ATR pathway, the ATM pathway does not seem to be predominantly activated one after camptothecin application [92, 94] (see Figure 48).

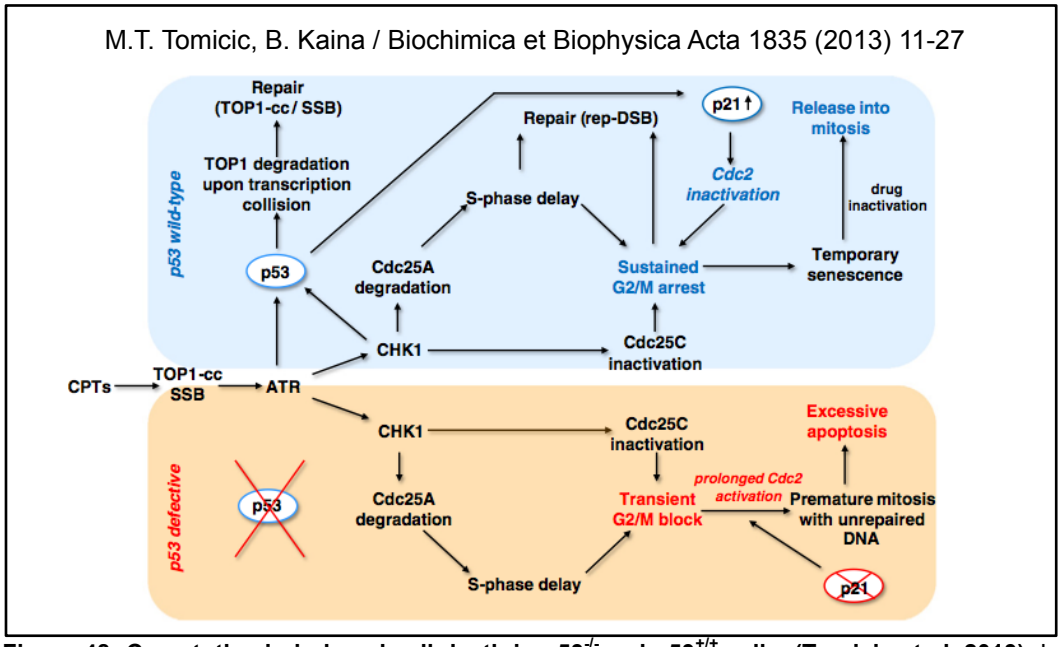

Figure 48: Camptothecin-induced cell death in $p53^{-/-}$ and $p53^{+/+}$ cells. (Tomicic et al. 2013). In $p53^{+/+}$ cells, camptothecin treatment leads to p21 activation followed by sustained G_2/M arrest, and temporary senescence. After drug inactivation the cells are released into mitosis. In $p53^{-/-}$ cells, p21 is not activated, leading to a transient G_2/M block followed by a premature mitosis and subsequent excessive apoptosis

4.5.4 Camptothecin Induces Excessive Apoptosis in p53-Negative Cells

As checkpoint pathways are often connected to apoptosis, Tomicic et al. proposed a model in 2013, describing the ATR-CHK1-triggered signaling to cell cycle arrest and apoptosis [64] (see Figure 48). They claim that camptothecin

triggers the ATR pathway, which leads to G2/M arrest and S-phase delay phenotype, which we also observed in our 72 hours Nicoletti assay. However, they propose that in p53-wildtype cells the G2/M arrest should be sustained through inactivation and subsequent degradation of Cdc2, which is a result of sustained p21 expression in those cells [95, 96]. In contrast, p53-deficient cells should lack p21 expression, which leads to a long-lasting activation of Cdc2, a transient G2/M arrest and finally to excessive apoptosis (see Figure 48).

Interestingly, our cell death data with treated $p53^{+/+}$ and $p53^{-/-}$ cells showed the opposite result. HepG2 cells ($p53^{+/+}$), treated for 24 hours with either camptothecin or camptothecin combined with mitomycin C, doxorubicin, cisplatin or sorafenib, showed higher cell death rates as similarly treated Hep3B cell ($p53^{-/-}$).

In our laboratory, we could show that p21 is not only a target of p53 but also of FUBP1 [80]. Therefore inhibition of FUBP1 through camptothecin in *p53*-deficient cells should also lead to elevated *p21* mRNA and protein levels, strengthening the hypothesis that camptothecin also targets FUBP1.

4.5.5 Camptothecin Treatment of Hepatocellular Carcinoma Cell Lines Increases p21 mRNA Expression Levels

We performed *p21* mRNA expression studies with Hep3B cells ($p53^{-/-}$) after 6 hours of treatment with 1 µM, 5 µM and 10 µM camptothecin. We could show that indeed a dose-dependent increase in *p21* mRNA expression can be observed after camptothecin treatment. To validate that this effect is not due to FUBP1 degradation, we performed Western blot analysis, showing stable FUBP1 protein levels after treatment (see page 94, paragraph 3.5.4.1). Additionally, we performed the same experiment with the topoisomerase I inhibitors NSC 725776, NSC 724998 and 7-ethyl-10-hydroxy-camptothecin. All treatments resulted in increased *p21* expression levels in $p53^{-/-}$ cells, whereas FUBP1 protein expression remained stable, strengthening the hypothesis of a possible influence of FUBP1 in camptothecin-induced apoptosis.

FUBP1 inhibition does not alter the expression of *c-myc* in HCC cell lines [80]. Therefore, as an additional control, mRNA expression levels of *c-myc* were monitored, and they remained stable in $p53^{-/-}$ cells during treatment. Repetition of these experiments in $p53^{mutant}$ (HuH7) and $p53^{+/+}$ (HepG2) cells again resulted in increased *p21* mRNA expression levels (see page 96, paragraph 3.5.4.2).

4.5.6 Bi-Functional Activity of FUBP1 in Glioblastoma Cell Lines Correlates with Therapeutic Function of Topotecan in Those Cells

Another hint that FUBP1 inhibition might be involved in cellular effects upon camptothecin treatment is seen when comparing apoptosis induction in different glioblastoma cell lines.

U87 and LN-229 are both expressing $p53^{+/+}$; nevertheless, U87 cells are resistant to topotecan and SN-38 treatment (both camptothecin derivates) [97, 98], whereas LN-229 cells are moderately sensitive [99]. As both cell lines express $p53^{+/+}$, its p53 downstream signaling should not be responsible for the different apoptosis sensitivity upon topotecan treatment. Interestingly, FUBP1 does have different roles in these cells. While the knockdown of FUBP1 does lead to more apoptosis and less proliferation in LN-229, it does works in the opposite direction in U87 cells (Venkatesh Kolluru, GSH, unpublished data). If camptothecin inhibits the anti-apoptotic and pro-proliferative function of FUBP1, this could explain why its derivate works in LN-229 but not in U87 cells.

4.5.7 The Camptothecin Derivate Irinotecan is Therapeutically Effective in Colorectal Cancer, a Tumor Known for its Frequently Mutated FIR Molecule

FIR, the FUBP1 interacting repressor, was found to be frequently mutated in primary colorectal cancers, but not in the adjacent normal tissue. The mutation produces an alternative splicing variant, in which the N-terminal repression domain is deleted. Co-expression of this splicing variant with the repressor-competent FIR in HeLa and SW480 cells abrogated the suppression of *c-myc* gene expression and inhibited apoptosis in these cells, indicating a dominant negative, oncogenic effect of the mutated splicing variant, which leads to an enhanced FUBP1 activity [21, 22]. Irinotecan, another camptothecin derivate, is frequently and successfully used in metastatic colorectal-cancer first-line therapy in combination with 5-Fluorouracil and Folin acid [100]. Furthermore, the treatment of colorectal cancer liver metastasis with a combination of irinotecan and mitomycin C administered via DEB-TACE led to a partial response in 4/4 patients [101]. The molecular findings suggest, that irinotecan efficacy in colorectal cancer is not only due to topoisomerase I inhibition but also to FUBP1 inhibition.

4.5.8 Discrimination between FUBP1 and TOP1 Inhibition by Camptothecin

As camptothecin is a known inhibitor of topoisomerase I, it is important to discriminate between the effects caused by the topoisomerase I inhibition and the

consequences of FUBP1 inhibition. As both molecules are expressed in the nucleus of the same cell, the separation of both effects is rather difficult to do.

Although many findings hint into the direction, that camptothecin inhibits FUBP1 function intracellularly, a direct proof is still missing. The fact that the FUBP1 direct target gene *p21* is regulated by camptothecin in $p53^{-/-}$ cells proofs that the assumed camptothecin-induced apoptosis mechanism, summarized by Tomicic et al. 2013, is at least incomplete. However, it is also not a direct proof for the involvement of FUBP1 in these processes.

If the attempt to solve the structure of FUBP1/*FUSE* is successful, this information could be used for an in-silico screening with camptothecin. Furthermore, if a crystallography protocol is established, one could also try to crystallize a complex of FUBP1/*FUSE*/camptothecin.

Additionally to the effort of ChIP analysis and luciferase assays with camptothecin-treated cells (see paragraph 4.5.1), MS-analysis of the proteasome of camptothecin-treated HCC cells will be performed and compared with an analysis of *FUBP1* knockdown and untreated HCC cells. If camptothecin inhibits not only TOP1 but also FUBP1, a similarity in the protein expression pattern of the *FUBP1* knockdown and camptothecin-treated cells should be apparent.

4.6 Irinotecan Treatment Led to Total Tumor Remission in Hep3B Xenograft Transplantation Experiments

As camptothecin displays significant effects on HCC cell survival *in cell culture* in single and combinational treatments with mitomycin C, xenograft experiments were performed to monitor its effect on an already established tumor *in vivo*.

The mouse xenograft tumor model with human tumor cells is frequently used in pre-clinical studies and its development was a major step towards clinically useful tumor models [102, 103]. Furthermore, in 2001 a retrospective study of the US NCI could show that in at least one third of all substances tested in human xenografts it was likely that the substances would achieve activity in a phase II clinical trial [104].

Two studies were performed to monitor the effect of irinotecan and mitomycin C single and double treatment on established tumors in mice, compared to the effect of sorafenib in the same setting. Hep3B cells were injected into the flank of immune-compromised NOD/SCID mice, and afterwards, the tumor was allowed to reach a volume of approximately 100 mm^3, before the appropriate treatment was started.

In the first experiment, a total tumor remission could be observed in 100% of the irinotecan-treated mice, representing a significant survival benefit compared to the mice of all other treatment groups (see page 97, Figure 44). The treatment schedule and substance concentrations, as well as application procedures were adopted as published by Cohen et al. 2010, who performed a peritoneally disseminated colorectal cancer xenograft experiment [105]. In the single treatment experiment, Cohen et al. found mitomycin C and irinotecan as the most potent substances, which was also the case in our experiment. Irinotecan-treated mice showed tumor-free survival for at least 53 days, resulting in an overall survival time of 136 days, which resembles the data from Cohen et al. with a time frame of 135 days survival after irinotecan treatment. They also tried different combinational treatments, among them a combination of irinotecan and mitomycin C. As this combination showed the best synergistic effect in our cell culture experiments, I decided to apply this double treatment. Unfortunately, an unexpected rapid weight loss of more than 20% in all mice of the irinotecan / mitomycin C double treatment group could be observed, and as a consequence, these mice were sacrificed after 7 days of treatment.

In the following experiment, only half of the irinotecan dose (10 mg/kg) and a quarter of the mitomycin C concentration (0.8125 mg/kg) were used in the double- and the single-treated groups. The mitomycin C single-treated group showed no enhanced survival compared to the control group receiving solvent. 100% of the irinotecan single- and irinotecan / mitomycin C double-treated mice showed a total tumor remission. Interestingly, tumor-free survival was 20 days shorter in irinotecan single-treated than in the double-treated mice. Furthermore, 100% (6/6) of the single-treated mice experienced a tumor relapse, compared to only 50% (3/6) of the double-treated mice, with one double-treated mouse showing no progression at all until at least day 120. This statistic demonstrates a clear advantage of the irinotecan / mitomycin C double treatment compared to the single treatment.

All mice were again treated with the double combination, when tumors relapsed and reached a volume of approximately 100 mm^3, regardless of the first treatment. Again, all tumors responded to the double treatment, leading to a total tumor remission in all cases. These results show that a tumor HCC grown from human cells can be successfully treated in a xenograft transplantation model using a combination of irinotecan and mitomycin C.

In 2002, the group of Prewitt et al. also tested a combinational treatment in a xenograft transplantation model, investigating the effect of irinotecan combined with cetuximab in irinotecan-refractory-colorectal tumors [106]. The double-treated tumors grew significantly slower than those receiving single treatment. This study represents an interesting example for a successful translation of a preclinical drug screening in xenografts into a clinical trial. In 2004, a phase II study with 329 patients with metastatic colorectal cancer, whose disease had progressed during or after irinotecan treatment was started, resembling the results of the xenograft model. Furthermore, the results of this study formed the basis of the approval by several regulatory agencies worldwide, to use a combination of cetuximab and irinotecan in irinotecan-refractory metastatic colon cancer patients [107].

As our xenograft transplantation experiments resulted in a 100% response rate in already established HCC tumors towards an irinotecan / mitomycin C double treatment, a potential clinical use of this combination is of great interest. In cooperation with Prof. Zeuzem and Prof. Tojan, “Zentrum der inneren Medizin” at the University Hospital Frankfurt, two HCC patients are currently treated in Frankfurt in an investigator-initiated trial with camptothecin and mitomycin C.

4.7 Conclusions about FUBP1 as a Potential New Target of Camptothecin and the Resulting New Treatment Options in HCC Therapy

The results of this study strengthen the role of FUBP1 as a therapeutic target in hepatocellular carcinoma therapy.

For the first time I, could show that camptothecin might display an additional mechanism of action for its cytotoxic activity, namely the inhibition of FUBP1. Unfortunately, through the lack of structural informations about FUBP1, a direct proof of the interaction between FUBP1 and camptothecin, such as co-crystallization, is still missing.

Nevertheless, the data collected during this study form the basis for the concept of a FUBP1-inhibitory effect of camptothecin.

Two independent binding experiments showed that camptothecin was able to interfere with the binding between FUBP1 and *FUSEp21*. Furthermore, additionally tested interfacial TOP1 inhibitors, i.e. 7-ethyl-10-hydroxycamptothecin, the active part of the camptothecin-derivate irinotecan, or indenoisoquinoles like NSC 725776 and NSC 724998, were also able to interfere with FUBP1/*FUSEp21* binding in a dose-dependent manner.

In cellular assays performed in HCC cells, the effect of all TOP1 inhibitors on *p21*, the direct target gene of FUBP1, was elucidated via qRT-PCR experiments. Cells treated with the TOP1 inhibitors displayed significantly increased *p21* mRNA levels when compared to control-treated cells, while protein levels of FUBP1 were not altered, hence suggesting an inhibitory effect on FUBP1 protein function in HCC cells.

A final proof for the direct interaction is still missing, but with the results obtained during this study, there is growing evidence for the inhibitory effect of camptothecin on FUBP1 activity. The results could be supported by further experiments such as CHIP analysis, luciferase-assays and MS-analysis, as discussed in paragraph 4.

Although the molecular mechanism is not yet fully understood, the treatment with camptothecin with and without the addition of other chemotherapeutics like mitomycin C showed significant effects on HCC cell expansion (see paragraph 3.5.1, page 82), cell activity (see paragraph 3.5.2, page 83) and apoptosis (see paragraph 3.5.3, page 84-93). These results finally led to the establishment of a mouse xenograft experiment, during which tumors derived from human HCC cells were treated with irinotecan. The treatments with irinotecan and irinotecan plus mitomycin C led to a total tumor remission and a significantly increased overall survival of the mice compared to the control-treated groups. These findings show that HCC tumors derived from human cells are treatable by camptothecin in a mouse xenograft experiment.

Although additional HCC mouse xenograft experiments with different HCC cells need to be performed to confirm the results from the first two HCC xenograft experiments, the results of this study appear promising for HCC patients and have led to the initiation of a pilot study with two patients suffering from intermediate stage HCC, using transarterial chemoembolisation with a combination of CPT and mitomycin C. In case of a successful conclusion of the preclinical studies, the preparation of a clinical HCC-study with the combinational treatment of camptothecin and mitomycin C is planned in collaborations with the physicians of the university hospital Frankfurt

Taken together, the results of this study propose a new role for camptothecin as an inhibitor of FUBP1 and led to the preparation of a new, promising therapeutic treatment option for HCC patients.

5 Ehrenwörtliche Erklärung

Ich erkläre hiermit ehrenwörtlich, dass ich die vorliegende Arbeit entsprechend den Regeln guter wissenschaftlicher Praxis selbstständig und ohne unzulässige Hilfe Dritter angefertigt habe.

Sämtliche aus fremden Quellen direkt oder indirekt übernommenen Gedanken sowie sämtliche von Anderen direkt oder indirekt übernommenen Daten, Techniken und Materialien sind als solche kenntlich gemacht. Die Arbeit wurde bisher bei keiner anderen Hochschule zu Prüfungszwecken eingereicht.

Darmstadt, den ……

.....

6 Abbreviations

ALPHA	amplified luminescent proximity homogenous assay
APS	ammonium persulfate
ASMS	affinity selection/mass spectrometry
BCLC	Barcelona Clinic Liver Cancer
C-terminal	carboxy-terminal
ccRCC	clear cell renal cell carcinoma
ChIP	chromatin immunoprecipitation
CIP	alkaline phosphatase
co	codon-optimized
CPT	camptothecin
dATP	desoxyadenosine triphosphate
DCS	double colony selection
dCTP	desoxycytosine triphosphate
dGTP	desoxyguanosine triphosphate
DNA	desoxyribonucleic acid
dNTP	desoxynucleoside triphosphate
ds	double strand
DTT	dithiothreitol
dTTP	desoxytyrosine triphosphate
E.coli	*Escherichia coli*
EALS	European Association for the Study of Liver Disease
ECL	enhanced chemiluminescence
EDTA	ethylenethylenediaminetetraacetic acid
EORTC	European Organization for Research and Treatment of Cancer
EpCAM	epithelial cell adhesion molecule
EtBr	ethidium bromide
EtOH	ethanol
FDA	food and drug approved
FGFR	fibroblast growth factor receptor
FIR	FUBP1 interacting repressor
fl	full length
FUBP1	FUSE element binding protein 1
FUSE	far upstream element
GFP	green fluorescent protein
HAI	hepatic aterial infusion
HC	7-ethyl-10-hydroxycamptothecin
HCC	hepatocellular carcinoma
HIF1α	hypoxia inducible factor 1α
His-tag	hexahistidine-tag
HRP	horseradish-peroxidase
HTS-NMR	high-throughput screening - nuclear magnetic resonance
HVB	hepatitis virus B
HVC	hepatitis virus C
i.p.	intra-peritoneal
IMAC	immobilized metal ion affinity chromatography

KCl	potassium chloride
K_D	dissociation constant
kDa	kilo Dalton
KH_2PO_4	potassium-dihydrogenphosphate
KHSRP	KH-type splicing regulatory protein
l	liter
LB-medium	Luria-Bertani medium
M	molar
MCS	multiple cloning site
MeOH	methanol
$MgCl_2$	magnesium chloride
$MgSO_4$	magnesium sulfate
min	minute(s)
ml	milliliter
mM	millimolar
MST	microscale thermophoresis
MVI	major vascular invasion
N-terminal	amino-terminal
NA	not available
NCI	National Cancer Institute
Ni-NTA	nickel-nitrilotriacetic acid
NIH	National Institutes of Health
nM	nanomolar
NOD/SCID	non-obese diabetic / severe combined Immunodeficiency
NT	N-terminal
O/N	over night
OD	optical density
OS	overall survival
p-value	probability-value
PAGE	polyacrylamide gel electrophoresis
PAGE	polyacrylamide gel electrophoresis
PCR	polymerase chain reaction
PEI	percutaneous ethanol injection
pH	pondus Hydrogenii
PI	propidium iodide
PMSF	phenylmethylsulfonylfluorid
poly dIdC	poly (2′-deoxyinosinic-2′-deoxycytidylic acid) sodium salt
PST	performance status
qRT-PCR	quantitative real-time pcr
RF	radiofrequency ablation
RGG	arginine-glycine-glycine
RNAse	ribonuclease
rpm	rounds per minute
RU	response unit
s	second(s)
SD	standard deviation
SDS	sodium dodecyl sulfate
SEC	size exclusion chromatography
SELEX	systematic evolution of ligands by exponential enrichment
SHARP	sorafenib HCC assessment randomized protocol

SOM	self-organizing map
SPR	surface plasmone resonance
ss	single strand
ssDNA	single stranded DNA
TACE	transcatheter aterial chemoembolization
TACE	transcatheter aterial chemoembolization
TBE	tris-borate-EDTA buffer
TEMED	tetramethylethylenediamine
TFIIH	transcriptional factor II H
TOP1	topoisomerase I
TOP1cc	topoisomerase I cleavage complex
Tris	2-Amino-2-hydroxymethyl-propane-1,3-diol
U2AF	U2 auxiliary factor
UHM	U2AF homology motif
VEGF	vascular endothelial growth factor
VLB	virtual ligand binding
WAF1/CIP1	cyclin-dependent inhibitor p21
WST	water soluble tetrazolium
µg	microgram
µl	microliter
µM	micromolar

7 Literature

1. Rabenhorst, U., et al., *Overexpression of the far upstream element binding protein 1 in hepatocellular carcinoma is required for tumor growth.* Hepatology, 2009. **50**(4): p. 1121-9.
2. Avigan, M.I., B. Strober, and D. Levens, *A far upstream element stimulates c-myc expression in undifferentiated leukemia cells.* J Biol Chem, 1990. **265**(30): p. 18538-45.
3. Duncan, R., et al., *A sequence-specific, single-strand binding protein activates the far upstream element of c-myc and defines a new DNA-binding motif.* Genes Dev, 1994. **8**(4): p. 465-80.
4. Liu, J., et al., *Defective interplay of activators and repressors with TFIH in xeroderma pigmentosum.* Cell, 2001. **104**(3): p. 353-63.
5. Duncan, R., et al., *A unique transactivation sequence motif is found in the carboxyl-terminal domain of the single-strand-binding protein FBP.* Mol Cell Biol, 1996. **16**(5): p. 2274-82.
6. Braddock, D.T., et al., *Molecular basis of sequence-specific single-stranded DNA recognition by KH domains: solution structure of a complex between hnRNP K KH3 and single-stranded DNA.* EMBO J, 2002. **21**(13): p. 3476-85.
7. Benjamin, L.R., et al., *Hierarchical mechanisms build the DNA-binding specificity of FUSE binding protein.* Proc Natl Acad Sci U S A, 2008. **105**(47): p. 18296-301.
8. Costa, M., et al., *Human DNA helicase VIII: a DNA and RNA helicase corresponding to the G3BP protein, an element of the ras transduction pathway.* Nucleic Acids Res, 1999. **27**(3): p. 817-21.
9. Vindigni, A., et al., *Identification of human DNA helicase V with the far upstream element-binding protein.* Nucleic Acids Res, 2001. **29**(5): p. 1061-7.
10. Jang, M., et al., *Far upstream element-binding protein-1, a novel caspase substrate, acts as a cross-talker between apoptosis and the c-myc oncogene.* Oncogene, 2009. **28**(12): p. 1529-36.
11. Zhang, J. and Q.M. Chen, *Far upstream element binding protein 1: a commander of transcription, translation and beyond.* Oncogene, 2013. **32**(24): p. 2907-16.
12. Davis-Smyth, T., et al., *The far upstream element-binding proteins comprise an ancient family of single-strand DNA-binding transactivators.* J Biol Chem, 1996. **271**(49): p. 31679-87.
13. Bouchireb, N. and M.S. Clark, *Human FUSE binding protein 3 gene (FBP3). Map position 9q33-34.1.* Chromosome Res, 1999. **7**(7): p. 577.
14. Gherzi, R., et al., *The role of KSRP in mRNA decay and microRNA precursor maturation.* Wiley Interdiscip Rev RNA, 2010. **1**(2): p. 230-9.
15. Danckwardt, S., et al., *p38 MAPK controls prothrombin expression by regulated RNA 3' end processing.* Mol Cell, 2011. **41**(3): p. 298-310.
16. Liu, J., et al., *The FBP interacting repressor targets TFIIH to inhibit activated transcription.* Mol Cell, 2000. **5**(2): p. 331-41.
17. Hsiao, H.H., et al., *Quantitative characterization of the interactions among c-myc transcriptional regulators FUSE, FBP, and FIR.* Biochemistry, 2010. **49**(22): p. 4620-34.
18. Levens, D., *How the c-myc promoter works and why it sometimes does not.* J Natl Cancer Inst Monogr, 2008(39): p. 41-3.

19. Zhang, Z., D. Harris, and V.N. Pandey, *The FUSE binding protein is a cellular factor required for efficient replication of hepatitis C virus.* J Virol, 2008. **82**(12): p. 5761-73.
20. Weber, A., et al., *The FUSE binding proteins FBP1 and FBP3 are potential c-myc regulators in renal, but not in prostate and bladder cancer.* BMC Cancer, 2008. **8**: p. 369.
21. Matsushita, K., et al., *An essential role of alternative splicing of c-myc suppressor FUSE-binding protein-interacting repressor in carcinogenesis.* Cancer Res, 2006. **66**(3): p. 1409-17.
22. Matsushita, K., et al., *[Clinical application of alternative splicing form of c-myc suppressor FUSE-binding protein-interacting repressor for cancer detection and treatment].* Rinsho Byori, 2009. **57**(12): p. 1151-8.
23. Bettegowda, C., et al., *Mutations in CIC and FUBP1 contribute to human oligodendroglioma.* Science, 2011. **333**(6048): p. 1453-5.
24. Singer, S., et al., *Coordinated expression of stathmin family members by far upstream sequence element-binding protein-1 increases motility in non-small cell lung cancer.* Cancer Res, 2009. **69**(6): p. 2234-43.
25. Lasserre, J.P., et al., *Effects of the endocrine disruptors atrazine and PCB 153 on the protein expression of MCF-7 human cells.* J Proteome Res, 2009. **8**(12): p. 5485-96.
26. Xu, S.G., P.J. Yan, and Z.M. Shao, *Differential proteomic analysis of a highly metastatic variant of human breast cancer cells using two-dimensional differential gel electrophoresis.* J Cancer Res Clin Oncol, 2010. **136**(10): p. 1545-56.
27. Zubaidah, R.M., et al., *2-D DIGE profiling of hepatocellular carcinoma tissues identified isoforms of far upstream binding protein (FUBP) as novel candidates in liver carcinogenesis.* Proteomics, 2008. **8**(23-24): p. 5086-96.
28. Malz, M., et al., *Overexpression of far upstream element binding proteins: a mechanism regulating proliferation and migration in liver cancer cells.* Hepatology, 2009. **50**(4): p. 1130-9.
29. El-Serag, H.B. and K.L. Rudolph, *Hepatocellular carcinoma: epidemiology and molecular carcinogenesis.* Gastroenterology, 2007. **132**(7): p. 2557-76.
30. Llovet, J.M., C. Bru, and J. Bruix, *Prognosis of hepatocellular carcinoma: the BCLC staging classification.* Semin Liver Dis, 1999. **19**(3): p. 329-38.
31. European Association for Study of, L., R. European Organisation for, and C. Treatment of, *EASL-EORTC clinical practice guidelines: management of hepatocellular carcinoma.* Eur J Cancer, 2012. **48**(5): p. 599-641.
32. European Association For The Study Of The, L., R. European Organisation For, and C. Treatment Of, *EASL-EORTC clinical practice guidelines: management of hepatocellular carcinoma.* J Hepatol, 2012. **56**(4): p. 908-43.
33. Llovet, J.M., et al., *Sorafenib in advanced hepatocellular carcinoma.* N Engl J Med, 2008. **359**(4): p. 378-90.
34. A.Cheng, Y.K., D.Lin, J.Park, M.Kudo, S.Qin, M.Omata, S.W. Pitman Lowenthal, S. Lanzalone, L.Yang, M. Lechuga, E. Raymond and SUN1170 HCC Study Group, *Phase III trial of sunitinib (Su) versus sorafenib (So) in advanced hepatocellular carcinoma (HCC).* Journal of Clinical Oncology, 2011. **29**(No.15).
35. Llovet, J.M. and J. Bruix, *Systematic review of randomized trials for unresectable hepatocellular carcinoma: Chemoembolization improves survival.* Hepatology, 2003. **37**(2): p. 429-42.

36. Villanueva, A., V. Hernandez-Gea, and J.M. Llovet, *Medical therapies for hepatocellular carcinoma: a critical view of the evidence.* Nat Rev Gastroenterol Hepatol, 2013. **10**(1): p. 34-42.
37. Page, A.J., et al., *Hepatocellular Carcinoma: Diagnosis, Management, and Prognosis.* Surg Oncol Clin N Am, 2014. **23**(2): p. 289-311.
38. Arzumanyan, A., H.M. Reis, and M.A. Feitelson, *Pathogenic mechanisms in HBV- and HCV-associated hepatocellular carcinoma.* Nat Rev Cancer, 2013. **13**(2): p. 123-35.
39. Yamashita, T., et al., *Activation of hepatic stem cell marker EpCAM by Wnt-beta-catenin signaling in hepatocellular carcinoma.* Cancer Res, 2007. **67**(22): p. 10831-9.
40. Vrancken, K., J. Paeshuyse, and S. Liekens, *Angiogenic activity of hepatitis B and C viruses.* Antivir Chem Chemother, 2012. **22**(4): p. 159-70.
41. Sanz-Cameno, P., et al., *Hepatitis B virus promotes angiopoietin-2 expression in liver tissue: role of HBV x protein.* Am J Pathol, 2006. **169**(4): p. 1215-22.
42. Abe, M., et al., *Hepatitis C virus core protein upregulates the expression of vascular endothelial growth factor via the nuclear factor-kappaB/hypoxia-inducible factor-1alpha axis under hypoxic conditions.* Hepatol Res, 2012. **42**(6): p. 591-600.
43. Poon, R.T., et al., *Long-term survival and pattern of recurrence after resection of small hepatocellular carcinoma in patients with preserved liver function: implications for a strategy of salvage transplantation.* Ann Surg, 2002. **235**(3): p. 373-82.
44. Shi, M., et al., *Partial hepatectomy with wide versus narrow resection margin for solitary hepatocellular carcinoma: a prospective randomized trial.* Ann Surg, 2007. **245**(1): p. 36-43.
45. Livraghi, T., et al., *Sustained complete response and complications rates after radiofrequency ablation of very early hepatocellular carcinoma in cirrhosis: Is resection still the treatment of choice?* Hepatology, 2008. **47**(1): p. 82-9.
46. Sherman, M., *Serological surveillance for hepatocellular carcinoma: time to quit.* J Hepatol, 2010. **52**(4): p. 614-5.
47. Llovet, J.M., M. Schwartz, and V. Mazzaferro, *Resection and liver transplantation for hepatocellular carcinoma.* Semin Liver Dis, 2005. **25**(2): p. 181-200.
48. Llovet, J.M., J. Fuster, and J. Bruix, *Intention-to-treat analysis of surgical treatment for early hepatocellular carcinoma: resection versus transplantation.* Hepatology, 1999. **30**(6): p. 1434-40.
49. Yao, F.Y., et al., *A follow-up analysis of the pattern and predictors of dropout from the waiting list for liver transplantation in patients with hepatocellular carcinoma: implications for the current organ allocation policy.* Liver Transpl, 2003. **9**(7): p. 684-92.
50. Bruix, J., M. Sherman, and D. American Association for the Study of Liver, *Management of hepatocellular carcinoma: an update.* Hepatology, 2011. **53**(3): p. 1020-2.
51. Meza-Junco, J., et al., *Locoregional radiological treatment for hepatocellular carcinoma; Which, when and how?* Cancer Treat Rev, 2012. **38**(1): p. 54-62.
52. Brown, D.B., et al., *Transcatheter therapy for hepatic malignancy: standardization of terminology and reporting criteria.* J Vasc Interv Radiol, 2009. **20**(7 Suppl): p. S425-34.
53. Burrel, M., et al., *Survival of patients with hepatocellular carcinoma treated by transarterial chemoembolisation (TACE) using Drug Eluting*

Beads. Implications for clinical practice and trial design. J Hepatol, 2012. **56**(6): p. 1330-5.
54. Cheng, A.L., et al., *Efficacy and safety of sorafenib in patients in the Asia-Pacific region with advanced hepatocellular carcinoma: a phase III randomised, double-blind, placebo-controlled trial.* Lancet Oncol, 2009. **10**(1): p. 25-34.
55. Furuse, J., et al., *Phase I study of sorafenib in Japanese patients with hepatocellular carcinoma.* Cancer Sci, 2008. **99**(1): p. 159-65.
56. Lencioni, R., et al., *First interim analysis of the GIDEON (Global Investigation of therapeutic decisions in hepatocellular carcinoma and of its treatment with sorafeNib) non-interventional study.* Int J Clin Pract, 2012. **66**(7): p. 675-83.
57. Llovet, J.M., et al., *Brivanib in patients with advanced hepatocellular carcinoma who were intolerant to sorafenib or for whom sorafenib failed: results from the randomized phase III BRISK-PS study.* J Clin Oncol, 2013. **31**(28): p. 3509-16.
58. http://www.investor.bayer.de/en/nc/news/archive/investor-news-2012/investor-news-2012/phase-iii-trial-evaluating-the-addition-of-tarcevaR-erlotinib-to-nexavarR-sorafenib-did-not-pr/, *Phase III Trial Evaluating the Addition of Tarceva® (erlotinib) to Nexavar® (sorafenib) Did Not Provide Additional Benefit to Patients with Liver Cancer versus Nexavar Alone.* 2012.
59. Pommier, Y. and C. Marchand, *Interfacial inhibitors: targeting macromolecular complexes.* Nat Rev Drug Discov, 2012. **11**(1): p. 25-36.
60. Pommier, Y., *Topoisomerase I inhibitors: camptothecins and beyond.* Nat Rev Cancer, 2006. **6**(10): p. 789-802.
61. Staker, B.L., et al., *The mechanism of topoisomerase I poisoning by a camptothecin analog.* Proc Natl Acad Sci U S A, 2002. **99**(24): p. 15387-92.
62. Staker, B.L., et al., *Structures of three classes of anticancer agents bound to the human topoisomerase I-DNA covalent complex.* J Med Chem, 2005. **48**(7): p. 2336-45.
63. Marchand, C., et al., *A novel norindenoisoquinoline structure reveals a common interfacial inhibitor paradigm for ternary trapping of the topoisomerase I-DNA covalent complex.* Mol Cancer Ther, 2006. **5**(2): p. 287-95.
64. Tomicic, M.T. and B. Kaina, *Topoisomerase degradation, DSB repair, p53 and IAPs in cancer cell resistance to camptothecin-like topoisomerase I inhibitors.* Biochim Biophys Acta, 2013. **1835**(1): p. 11-27.
65. Catimel, G., et al., *Phase I and pharmacokinetic study of irinotecan (CPT-11) administered daily for three consecutive days every three weeks in patients with advanced solid tumors.* Ann Oncol, 1995. **6**(2): p. 133-40.
66. Boige, V., et al., *Irinotecan as first-line chemotherapy in patients with advanced hepatocellular carcinoma: a multicenter phase II study with dose adjustment according to baseline serum bilirubin level.* Eur J Cancer, 2006. **42**(4): p. 456-9.
67. Ang, C., et al., *A Nonrandomized, Phase II Study of Sequential Irinotecan and Flavopiridol in Patients With Advanced Hepatocellular Carcinoma.* Gastrointest Cancer Res, 2012. **5**(6): p. 185-9.
68. Tony MOK1, Tsai-Shen YANG2, Yee CHAO3, Cheng-Hsu WANG4, Mei-Ching LIU5, Yoon Koo KANG6, Won Ki KANG7, Jun Suk KIM8, Yajie WANG9 andThomas LEUNG1, *Phase II study of irinotecan in combination with capecitabine as a first-line chemotherapy in Asian patients with inoperable hepatocellular carcinoma.* Asia-Pacific Journal of Clinical Oncology, 2009. **5**(2): p. 95-100.

69. Ohtsubo, K., et al., *Advanced hepatocellular carcinoma treated effectively with irinotecan via hepatic arterial infusion followed by proton beam therapy.* J Infect Chemother, 2009. **15**(5): p. 316-21.
70. Brandi, G., et al., *A phase I study of continuous hepatic arterial infusion of Irinotecan in patients with locally advanced hepatocellular carcinoma.* Dig Liver Dis, 2011. **43**(12): p. 1015-21.
71. Mühlhardt, C., *Der Experimentator: Molekularbiologie/Genomics.* 2003. **4**.
72. Riccardi, C. and I. Nicoletti, *Analysis of apoptosis by propidium iodide staining and flow cytometry.* Nat Protoc, 2006. **1**(3): p. 1458-61.
73. Knippers, R., *Molekulare Genetik.* Thieme Verlag, 2006.
74. Studier, F.W., *Protein production by auto-induction in high density shaking cultures.* Protein Expr Purif, 2005. **41**(1): p. 207-34.
75. Rehm, H., *Der Experimentator: Proteinbiochemie/Proteomics.* Spektrum Akademischer Verlag, Gustav Fischer, 2002. **4**.
76. Farooqui, A.A. and L.A. Horrocks, *Purification of lipases and phospholipases by heparin-sepharose chromatography.* Methods Mol Biol, 1999. **109**: p. 133-43.
77. Lottspeich, F.E., J.W., *Bioanalytik.* Spektrum, Akademischer Verlag, 2006. **2**.
78. Hauck, S., *Expression and Purification of FUSE Element Binding Protein 1 and Testing of Potential Inhibitors.* Diploma Thesis, AG Zörnig, Georg-Speyer-Haus, 2013.
79. Talenfeld, A.D., A.K. Sista, and D.C. Madoff, *Transarterial Therapies for Primary Liver Tumors.* Surg Oncol Clin N Am, 2014. **23**(2): p. 323-351.
80. Rabenhorst, U. and R. Beinoraviciute-Kellner, *Overexpression of the Far Upstream Element Binding Protein 1 in Hepatocellular Carcinoma Is Required for Tumor Growth.* Hepatology, 2009. **50**(4): p. 1121-1129.
81. Gartel, A.L. and S.K. Radhakrishnan, *Lost in transcription: p21 repression, mechanisms, and consequences.* Cancer Res, 2005. **65**(10): p. 3980-5.
82. Elena, C., et al., *Expression of codon optimized genes in microbial systems: current industrial applications and perspectives.* Front Microbiol, 2014. **5**: p. 21.
83. Kraut, D.A., *Slippery substrates impair ATP-dependent protease function by slowing unfolding.* J Biol Chem, 2013. **288**(48): p. 34729-35.
84. Gsponer, J., et al., *Tight regulation of unstructured proteins: from transcript synthesis to protein degradation.* Science, 2008. **322**(5906): p. 1365-8.
85. Costa, S., et al., *Fusion tags for protein solubility, purification and immunogenicity in : the novel Fh8 system.* Front Microbiol, 2014. **5**: p. 63.
86. Braddock, D.T., et al., *Structure and dynamics of KH domains from FBP bound to single-stranded DNA.* Nature, 2002. **415**(6875): p. 1051-6.
87. Huth, J.R., et al., *NMR-driven discovery of benzoylanthranilic acid inhibitors of far upstream element binding protein binding to the human oncogene c-myc promoter.* J Med Chem, 2004. **47**(20): p. 4851-7.
88. Zhang, J.H., T.D. Chung, and K.R. Oldenburg, *A Simple Statistical Parameter for Use in Evaluation and Validation of High Throughput Screening Assays.* J Biomol Screen, 1999. **4**(2): p. 67-73.
89. Mahapatra, L., et al., *High-Throughput Fluorescence Anisotropy Screen for Inhibitors of the Oncogenic mRNA Binding Protein, IMP-1.* J Biomol Screen, 2014. **19**(3): p. 427-36.
90. Arguedas, A.G., et al., *In vitro activity of tosufloxacin, a new quinolone, against respiratory pathogens derived from cystic fibrosis sputum.* Antimicrob Agents Chemother, 1990. **34**(11): p. 2223-7.

91. Xiao, Z., et al., *Chk1 mediates S and G2 arrests through Cdc25A degradation in response to DNA-damaging agents.* J Biol Chem, 2003. **278**(24): p. 21767-73.
92. Flatten, K., et al., *The role of checkpoint kinase 1 in sensitivity to topoisomerase I poisons.* J Biol Chem, 2005. **280**(14): p. 14349-55.
93. Schwarz, J.K., C.M. Lovly, and H. Piwnica-Worms, *Regulation of the Chk2 protein kinase by oligomerization-mediated cis- and trans-phosphorylation.* Mol Cancer Res, 2003. **1**(8): p. 598-609.
94. Zuco, V., V. Benedetti, and F. Zunino, *ATM- and ATR-mediated response to DNA damage induced by a novel camptothecin, ST1968.* Cancer Lett, 2010. **292**(2): p. 186-96.
95. Flatt, P.M., et al., *p53 regulation of G(2) checkpoint is retinoblastoma protein dependent.* Mol Cell Biol, 2000. **20**(12): p. 4210-23.
96. Furuta, T., et al., *p21CDKN1A allows the repair of replication-mediated DNA double-strand breaks induced by topoisomerase I and is inactivated by the checkpoint kinase inhibitor 7-hydroxystaurosporine.* Oncogene, 2006. **25**(20): p. 2839-49.
97. Tomicic, M.T., M. Christmann, and B. Kaina, *Topotecan-triggered degradation of topoisomerase I is p53-dependent and impacts cell survival.* Cancer Res, 2005. **65**(19): p. 8920-6.
98. Wang, Y., et al., *p53 disruption profoundly alters the response of human glioblastoma cells to DNA topoisomerase I inhibition.* Oncogene, 2004. **23**(6): p. 1283-90.
99. Winter, S. and M. Weller, *Potentiation of CD95L-induced apoptosis of human malignant glioma cells by topotecan involves inhibition of RNA synthesis but not changes in CD95 or CD95L protein expression.* J Pharmacol Exp Ther, 1998. **286**(3): p. 1374-82.
100. Stein, A. and C. Bokemeyer, *How to select the optimal treatment for first line metastatic colorectal cancer.* World J Gastroenterol, 2014. **20**(4): p. 899-907.
101. Morise, Z., et al., *Transarterial chemoembolization with degradable starch microspheres, irinotecan, and mitomycin-C in patients with liver metastases.* J Gastrointest Surg, 2006. **10**(2): p. 249-58.
102. Kelland, L.R., *Of mice and men: values and liabilities of the athymic nude mouse model in anticancer drug development.* Eur J Cancer, 2004. **40**(6): p. 827-36.
103. Peterson, J.K. and P.J. Houghton, *Integrating pharmacology and in vivo cancer models in preclinical and clinical drug development.* Eur J Cancer, 2004. **40**(6): p. 837-44.
104. Johnson, J.I., et al., *Relationships between drug activity in NCI preclinical in vitro and in vivo models and early clinical trials.* Br J Cancer, 2001. **84**(10): p. 1424-31.
105. Cohen, M.S., et al., *Combination intraperitoneal chemotherapy is superior to mitomycin C or oxaliplatin for colorectal carcinomatosis in vivo.* Ann Surg Oncol, 2010. **17**(1): p. 296-303.
106. Prewett, M.C., et al., *Enhanced antitumor activity of anti-epidermal growth factor receptor monoclonal antibody IMC-C225 in combination with irinotecan (CPT-11) against human colorectal tumor xenografts.* Clin Cancer Res, 2002. **8**(5): p. 994-1003.
107. Cunningham, D., et al., *Cetuximab monotherapy and cetuximab plus irinotecan in irinotecan-refractory metastatic colorectal cancer.* N Engl J Med, 2004. **351**(4): p. 337-45.

8 Curriculum Vitae

Name	Sabrina Khageh Hosseini, geb. Ploog
Geburtsdatum	22. Mai 1982
Geburtsort	Hamburg, Deutschland
Staatsangehörigkeit	Deutsch

Schulausbildung

1988-1990	Grundschule Mendelsohnstraße, Hamburg
1990-1992	Grundschule Handewitt
1992-1998	Zentralschule Harrislee, Realschulabschluss
1998-2001	IGS Flensburg
2001	Schulabschluß: Abitur

Berufserfahrung

2001-2004	Ausbildung zur Biologielaborantin im Institut für Pharmakologie, Universitätsklinikum Homburg Saar
2004-2006	Biologielaborantin im Institut für Pharmakologie, Universitätsklinikum Homburg Saar

Studium

2006-2008	Studium der Molekularen Biologie, Johannes Gutenberg-Universität, Mainz. Studienabschluss: Bachelor of Science (Note: 1,6)
2008-2010	Studium der Bio-Medizin, Johannes Gutenberg-Universität, Mainz. Studienabschluss: Master of Science (Note: 1,1)

Doktorarbeit

Nov. 2010 – Sept. 2014	Arbeitsgruppe Prof. Dr. Martin Zörnig, Georg-Speyer-Haus, Frankfurt / TU Darmstadt; Titel: „Targeting FUBP1 in Hepatocellular“ Carcinoma Mitglied des Graduiertenkollegs 1172 „Biologicals“ der deutschen Forschungsgemeinschaft

Stipendien

Nov. 2010 – Juli 2013	Promotionsstipendium des Graduiertenkollegs 1172 „Biologicals“ der deutschen Forschungsgemeinschaft
Juli 2013 – Dez. 2013	Promotionsstipendium des CGT der Landesoffensive zur Entwicklung Wissenschaftlich-Ökonomischer Exzellenz (LOEWE)
Jan. 2014-Aug. 2014	Promotionsstipendium im Rahmen des Deutschen Konsortium für Translationale Krebsforschung (DKTK), Deutsches Krebsforschungszentrum (DKFZ)

Vorträge

Sep. 2012	4. UCT science day, Universitätskrankenhaus, Frankfurt am Main, „Targeting FUBP1 in Hepatocellular Carcinoma“
Sep. 2013	5. UCT science day, Universitätskrankenhaus, Frankfurt am Main, „Targeting FUBP1 in Hepatocellular Carcinoma”
Juni 2014	DKTK Meeting: Drug development platform, „Targeting FUBP1 in hepatocellular Carcinoma“

Ergänzende Qualifikationen

Sept. 2009	Zertifizierte Teilnahme an dem Kurs: „Sicherheit in der Gentechnik“ Fortbildungsveranstaltung zur Vermittlung der nach §15 Abs. 2 Satz 1 Nr. 3 i.V. Abs. 4 Satz 1 Gentechnik-Sicherheitsverordnung geforderten Kenntnisse, Johannes Gutenberg-Universität Mainz
Juni 2011	Zertifizierte Teilnahme an: „Grundkurs Durchflusszytometrie“ BD, Heidelberg
Okt. 2013	Zertifizierte Teilnahme an: Versuchstierkundekurs nach „FELASA, Kategorie B“, Ruprecht-Karls-Universität Heidelberg

9 Danksagung

Die vorliegende Arbeit wurde im Institut für Tumorbiologie und Experimentelle Therapie Georg-Speyer-Haus in Frankfurt am Main in der Arbeitsgruppe von Prof. Dr. Martin Zörnig angefertigt. Bei ihm bedanke ich mich herzlich für die Möglichkeit, an diesem spannenden Thema arbeiten zu können, sowie für das Vertrauen, das es mir ermöglichte, meine eigenen Ideen zu entwickeln und umzusetzen.

Prof. Dr. Beatrix Süß danke ich herzlich für ihre Betreuung dieser Doktorarbeit im Fachbereich Biologie der TU Darmstadt, sowie für die andauernde Betreuung als Co-Supervisorin im Rahmen des Graduiertenkollegs „Biologicals“.

Bei Prof. Dr. Cardoso bedanke ich mich für ihre Bereitschaft, die Aufgabe meiner 2. Gutachterin im Fachbereich Biologie an der TU Darmstadt zu übernehmen.

Ein weiterer Dank geht an Prof. Dr. Thiel für seine Bereitschaft, sich als Prüfer meiner Dissertation zur Verfügung zu stellen.

Bei Prof. Dr. Eugen Proschak und Dr. Ricardo Biondi möchte ich mich für die anregenden Diskussionen und neuen Ideen im Zuge unserer Kollaboration bedanken. Danke auch an deren Mitarbeiter Steffen, Janosch und Evi.

Des Weiteren gilt mein Dank Prof. Dr. Dieter Steinhilber, Fachbereich Biochemie, Chemie und Pharmazie der Johann Wolfgang Goethe-Universität, der mir während meiner gesamten Doktorarbeit als Co-Supervisor im Rahmen des Graduiertenkollegs „Biologicals“ stets mit konstruktiven Rat zur Seite stand.

Ein besonderer Dank gilt den aktuellen und ehemaligen Arbeitskollegen der AG Zörnig. Es war toll, in dieser freundlichen und familiären Atmosphäre arbeiten zu können.

Im Speziellen danke ich Josi für die großartige Hilfe bei den Xenograft Experimenten.

Ein weiterer großer Dank geht an Uta Rabenhorst: Danke für die tolle Einarbeitung und die ersten 1 ½ Jahre, in denen Du mir immer ohne zu zögern mit Rat und Tat beiseite standest.

Susanne, Du bist wunderbar! Vielen Dank für die große Hilfe und das immer offene Ohr. Katha danke ich für Ihr unfassbares Gedächtnis und das schier unendliche Fachwissen, welches mir bei manchen Diskussionen sehr geholfen hat. Steffis unermüdlicher Arbeitseinsatz ist schon jetzt legendär und ich danke ihr für all das, was sie für diese Arbeit getan hat. Vor allem möchte ich mich aber bei allen dreien für ihre Freundschaft bedanken, die mir die Arbeit noch mehr erleichtert hat.